GROWTH AND PROPERTIES OF $In_{1-x}Ga_xAs$ ON InP

AND

ITS APPLICATION TO DEVICES

BY

YOSHIKAZU TAKEDA

NOVEMBER 1979

DEPARTMENT OF ELECTRICAL ENGINEERING

KYOTO UNIVERSITY

KYOTO, JAPAN

GROWTH AND PROPERTIES OF $In_{1-x}Ga_xAs$ ON InP AND ITS APPLICATION TO DEVICES

BY
YOSHIKAZU TAKEDA

NOVEMBER 1979

DEPARTMENT OF ELECTRICAL ENGINEERING
KYOTO UNIVERSITY
KYOTO, JAPAN

ABSTRACT

Lattice mismatch in the epitaxially grown $In_{1-x}Ga_xAs$ layer on GaAs substrate degrades the crystal quality of the alloy and prevents it from applying to devices. However, in this study the quality of $In_{1-x}Ga_xAs$($x \simeq 0.5$) has been greatly improved by growing it on InP substrate where the lattice mismatch can be avoided. The mobility, for example, has been found to jump from $\sim 2\,500$ $cm^2/Vsec$ in $In_{1-x}Ga_xAs$($x \simeq 0.5$) on GaAs substrate to $8\,500$ $cm^2/Vsec$ in $In_{0.53}Ga_{0.47}As$ on InP substrate. The high mobility has stimulated again the theoretical arguments on scattering mechanisms in alloys. The high quality $In_{0.53}Ga_{0.47}As$ has enabled us to apply a high electric field to this material and to apply to devices such as field-effect transistors and avalanche photodiodes.

The growth system and procedures for liquid phase epitaxial $In_{1-x}Ga_xAs$ on InP substrate are shown, and physical, chemical and optical characterizations are conducted on the grown layers to find the optimum growth conditions. The effects of the incomplete removal of melt on the LPE layers are pointed out. The growth of the alloy over a wide range of composition is carried out, and the composition latching phenomenon and the effects of the lattice mismatch on the grown layers are described.

The energy gap of the high quality $In_{0.53}Ga_{0.47}As$ is determined accurately. The Hall and drift mobility and the Hall factors of ternary alloys are calculated theoretically, and the Hall mobility of n-type $In_{0.53}Ga_{0.47}As$ is investigated experimentally. A high electric field is applied to the coplanar devices made of this alloy and high-field transport properties such as velocity - field characteristics and transferred-electron oscillation are observed.

Zn-doped p-type $In_{0.53}Ga_{0.47}As$ layers are grown and their electrical and optical properties are examined. An $In_{0.53}Ga_{0.47}As$ p-n junction is formed utilizing the Zn-doping. The results are

used for the fabrication of infrared photodetectors with this alloy, and their electrical and optoelectronic characteristics are studied. The avalanche multiplication is obtained in this photodetector. Finally, conclusions and suggestions for further study are summarized.

ACKNOWLEDGMENTS

The author wishes to express his deep gratitude and appreciation to Professor Akio Sasaki for his continuous guidance, invaluable advice and encouragement throughout the present work. The author wishes to thank Professor Toshinori Takagi for his continuous encouragement, stimulating discussion and criticism on the manuscript. The author is grateful to Professor Akira Kawabata for his useful suggestions and criticism on the manuscript.

Appreciation is due to Professor Isao Yamada and Dr. Junzo Ishikawa for their continuous encouragement and experimental facilities. Appreciation is also due to Dr. Shigeo Fujita for his constant discussion and experimental facilities, and to Professor Hiroyuki Matsunami, Dr. Junji Saraie, Dr. Akira Suzuki, and Mr. Shigehiro Nishino for their discussion and experimental facilities.

Thanks are due to Mr. Yujiro Imamura and Mr. Naoto Shikagawa for their work in the experiments as master course students. Thanks are also due to Satoru Shiono, Yukio Naito, Kuniyasu Asada, Masaaki Kuzuhara, Kiyoshi Takeuchi, and Konosuke Noda for their help in the experiments and calculations as senior students.

Chapters II and III were supported in part by the Grant-in-Aid for the specified subject "Crystal Growth" from the Scientific Research of the Ministry of Education. Chapters X and XI were also supported in part by the Grant-in-Aid from the Scientific Research of the Ministry of Education.

TABLE OF CONTENTS

TABLE OF CONTENTS

TABLE OF CONTENTS

LIST OF FIGURES

LIST OF TABLES

I. INTRODUCTION

It is well known that semiconductor research has been stimulated by the discovery of triode action in germanium[1], and the properties of germanium and silicon have been applied to a great number of devices in industrial and daily use. Although the importance of these two materials is unrivalled in the semiconductor field, there has been great interest in III-V compound semiconductors since the early 1950's[2,3]. They have unique properties which silicon and germanium do not possess, and applications have been widely extended utilizing their properties under well-controlled conditions.

Although the compound semiconductors provide a wide range of material parameters, they do not all have the optimum or desirable properties for device applications. Since the 1950's and early 60's many ternary alloys between III-V binary compounds have been grown and investigated to extend further the range of material parameters [4-11]. However, very few could be applied to devices, since most of them were bulk-grown or low in crystal quality with a large lattice mismatch. $GaAs_{1-x}P_x$ and $Al_{1-x}Ga_xAs$ are the two exceptions and have been applied to optoelectronic devices.

Among the III-V ternary alloys, $In_{1-x}Ga_xAs$ is one of the most interesting materials in the electrical and optical properties.

$In_{1-x}Ga_xAs$ can be designed to have a wider band gap than InAs and higher mobility than GaAs. Near middle composition, the band gap, E_g, is about 0.75 eV at which the extrinsic carrier concentration ($>10^{15}$ cm^{-3}) is not affected by the temperature variations of the intrinsic carrier concentration ($\sim 10^{11}$ cm^{-3}) around room temperature. Further, the energy separation, ΔE, between the central and satellite valleys in the conduction band becomes wider with the increase of the InAs mole fraction. Near $x \simeq 0.5$, E_g is expected to equal ΔE. This does not cause the electron velocity to decrease

by the transferred-electron effect. Thus, $In_{1-x}Ga_xAs$($x \simeq 0.5$) can be considered better suited for high frequency field-effect transistors and high speed switching devices than GaAs or InP[12,13].

Recent development of optical fibers has shown that at $\sim$ 1.3 μm wavelength the material dispersion is zero[14] and the transmission loss is as low as 0.47 dB/km in the P_2O_5-doped silica fiber [15], and that in the Ge_2O_3-doped silica fiber the transmission is extremely low, 0.20 dB/km at 1.55 μm wavelength[16]. At 1.55 μm, optical transmission longer than 100 km is possible without any repeater. $In_{1-x}Ga_xAs$($x \simeq 0.5$) is expected to be best suited for the detector at this wavelength.

The $In_{1-x}Ga_xAs$ epitaxial films of around middle composition ($x \simeq 0.5$) have been grown by vapor phase epitaxy on GaAs[17,18] and Al_2O_3[19] substrates. Fairly high electron mobility and electron scattering analyses have been reported by Glicksman *et al.*[20] for $In_{1-x}Ga_xAs$($0.75 \leqq x \leqq 1.0$). However, the mobility values around 6 000 $cm^2/Vsec$ are not higher than those of GaAs. Bulk $In_{1-x}Ga_xAs$ crystals have shown very high mobility[21-23] compared with epitaxial alloys of around middle compositions, but it is difficult to grow single crystals uniform in composition. Crystals with non-uniform composition are not suitable for most device applications.

Uniform and good crystal $In_{1-x}Ga_xAs$ can be grown on GaAs using stepwise[24] or continuous[25-26] composition grading to take up the lattice mismatch between the substrate and the desired composition layers. However, with the grading process it is not easy to reach $In_{1-x}Ga_xAs$($x \simeq 0.5$) from GaAs substrate nor is it suitable for mass production.

We took an important step of using a material other than the constituent binary compounds for the substrate. Since we were interested in the properties and applications of $In_{1-x}Ga_xAs$ with $x \simeq 0.5$, InP has been selected as the substrate which matches the

lattice constant of $In_{0.53}Ga_{0.47}As$[27,28].

With the InP substrate, the quality of epitaxially grown $In_{1-x}Ga_xAs$($x \simeq 0.5$) has been greatly improved using no buffer layer or composition grading. The mobility, for example, has jumped from $\sim$2 500 cm^2/Vsec in $In_{1-x}Ga_xAs$($x \simeq 0.5$) on GaAs substrate to 8 500 cm^2/Vsec in $In_{0.53}Ga_{0.47}As$ on InP substrate[29,30]. The high mobility has stimulated again the theoretical arguments on the scattering mechanisms in the alloy[31]. The high quality $In_{0.53}Ga_{0.47}As$ enabled us to apply a high electric field[13] and to fabricate avalanche photodiodes with this material[32].

In this thesis, the liquid phase epitaxial growth and properties of $In_{1-x}Ga_xAs$ on InP substrate, and the fundamental device properties and characteristics are described. In Chapter II, the growth system and procedures, and the calculation of the In-Ga-As ternary phase diagram are studied and presented. Chapter III contains many physical, chemical and optical characteristics of the $In_{1-x}Ga_xAs$($x \simeq 0.5$) layers grown on InP substrates. In Chapter IV, the quasi-grown layers in the LPE growth after incomplete removal of melt, and in Chapter V, growth of the alloy over a wide composition range, composition latching phenomenon, and effects of the lattice mismatch on the grown layers are described. In Chapter VI, the energy gap of high quality $In_{0.53}Ga_{0.47}As$ is determined accurately. Chapter VII concerns the theoretical calculation of the Hall and drift mobility and the Hall factors of ternary alloys, and Chapter VIII is devoted to the experimental results of the Hall mobility of n-$In_{0.53}Ga_{0.47}As$. In Chapter IX, high-field transport properties such as velocity - field ($v - E$) characteristics and transferred-electron oscillation in n-$In_{0.53}Ga_{0.47}As$ are investigated and applied to model field-effect transistors (FET's). In Chapter X, growth and properties of Zn-doped p-type $In_{0.53}Ga_{0.47}As$ layers and p-n junction are described. The results are employed in Chapter XI which focuses on the fabrication and characteristics

of the $In_{0.53}Ga_{0.47}As/InP$ infrared photodetectors. Finally, conclusions and suggestions for further study are summarized in Chapter XII.

References

[1] J. Bardeen and W. H. Brattain, Phys. Rev., 74, 230 (1948)

[2] H. Welker, Z. Naturforsch. 7a, 744 (1952)

[3] For reviews in the 50's and early 60's, see for example, F. A. Cunnel and E. W. Saker, "Properties of the III-V Compound Semiconductors," in *Progress in Semiconductors,* edited by A. F. Gibson, P. Aigrain, and R. E. Burgess (John Wiley & Sons, New York, 1957) Vol. 2,
C. Hilsum and A. C. Rose-Innes, *Semiconducting III-V Compounds* (Pergamon Press, Oxford, 1961),
O. Maledung, *Physics of III-V Compounds* (John Wiley & Sons, New York, 1964), and
C. Hilsum, "Gallium Arsenide," in *Progress in Semiconductors,* edited by A. F. Gibson and R. E. Burgess (A Heywood Book, London, 1965) Vol. 9.

[4] F. Herman, M. Glicksman, and R. H. Parmenter, "Semiconductor Alloys," in *Progress in Semiconductors,* edited by A. F. Gibson, P. Aigrain, and R. E. Burgess (John Wiley & Sons, New York, 1957) Vol. 2

[5] J. C. Woolley, "Solid Solutions of III-V Compounds," in *Compound Semiconductors,* Vol. 1 - *Preparation of III-V Compounds,* edited by R. K. Willardson and H. I. Goering (Reinhold, New York, 1962)

[6] J. C. Woolley, "Alloy Semiconductors," in *Progress in Solid-State Chemistry,* edited by Howard Reiss (Pergamon Press, Oxford, 1964) Vol. 1

[7] O. Madelung, *Physics of III-V Compounds* (John Wiley & Sons, New York, 1964)

[8] N. A. Goryunova, F. P. Kesamanly, and D. N. Nasledov, "Phenomena in Solid Solutions," in *Semiconductors and Semimetals,* edited by R. K. Willardson and A. C. Beer (Academic Press, New York, 1968) Vol. 4

[9] T. F. Connolly (editor), *Semiconductors - Preparation, Crystal Growth, and Selected Properties,* Solid State Physics Literature Guides (IFI/Plenum, New York, 1972) Vol. 2

[10] M. Neuberger, *III-V Ternary Semiconducting Compounds - Data Table, Handbook of Electronic Materials* (IFI/Plenum, New York, 1972) Vol. 7

[11] H. Kressel and H. Nelson, "Properties and Applications of III-V Compound Films Deposited by Liquid Phase Epitaxy," in *Physics of Thin Films*, edited by G. Hass, M. H. Francombe, and R. W. Hoffman (Academic Press, New York, 1973) Vol. 7

For recent developments in ternary and quaternary III-V compounds see for example,
M. B. Panish and I. Hayashi, "Heterostructure Junction Lasers," in *Applied Solid State Science*, edited by R. Wolfe (Academic Press, New York, 1974) Vol. 4,
H. Kressel and J. K. Butler, *Semiconductor Lasers and Heterojunction LEDs* (Academic Press, New York, 1977),
H. C. Casey, Jr., and M. B. Panish, *Heterostructure Lasers*, Part A and B (Academic Press, New York, 1978),
and the bienial conference series since 1966, *Gallium Arsenide and Related Compounds* (Institute of Physics, London, 1967∿)

[12] W. Fawcett, C. Hilsum, and H. D. Rees, Electron Lett., 5, 313 (1969)

[13] A. Sasaki, Y. Takeda, N. Shikagawa, and T. Takagi, Proc. 8th Conf. (1976 International) on Solid State Devices, Tokyo, 1976; Japan. J. Appl. Phys., 16 (1977) Suppl. 16-1, p. 239

[14] D. N. Payne and W. A. Gambling, Electron. Lett., 11, 176 (1975)

[15] M. Horiguchi and H. Osanai, Electron. Lett., 12, 310 (1976)

[16] T. Miya, Y. Terunuma, T. Hosaka, and T. Miyashita, Electron. Lett., 15, 106 (1979)

[17] R. W. Conrad, P. L. Hoyt, and D. D. Martin, J. Electrochem. Soc., 114, 164 (1967)

[18] B. J. Baliga and S. K. Ghandhi, J. Electrochem. Soc., 122, 683 (1975)

[19] H. M. Manasevit and W. I. Simpson, J. Electrochem. Soc., 120, 135 (1973)

[20] M. Glicksman, R. E. Enstrom, S. A. Mittleman, and J. R. Appert, Phys. Rev., B9, 1621 (1974)

[21] M. S. Abrahams, R. Braunstein, and F. D. Rosi, J. Phys. Chem. Solids, 10, 204 (1959)

[22] J. W. Wagner, J. Electrochem. Soc., 117, 1193 (1970)

[23] T. V. Dzhakhutashvili, A. A. Mirtskhulava, L. G. Sakvarelidze, A. L. Shkol'nik, and M. S. Matinova, Sov. Phys. - Semicond., 5, 190 (1971)

[24] R. E. Nahory, M. A. Pollack, and J. C. DeWinter, Appl. Phys. Lett., 25, 146 (1974)

[25] R. E. Enstrom, D. Richman, M. S. Abrahams, J. R. Appert, D. G. Fisher, A. H. Sommer, and B. F. Williams, in *Gallium Arsenide and Related Compounds*, 1970 Conference, Series 9 (Institute of Physics, London, 1971) p. 30

[26] H. Nagai and Y. Noguchi, Appl. Phys. Lett., 26, 108 (1975)

[27] A. Sasaki, M. Mohri, T. Takagi, and T. Tanaka, Abstracts of the 4th International Conf. on Cryst. Growth, Tokyo, 1974, p. 237

[28] Y. Takeda, A. Sasaki, T. Takagi, and Y. Imamura, "Liquid Phase Epitaxial Growth of $In_{1-x}Ga_xAs$ on InP substrate," 22nd Meet. Japan. Soc. Appl. Phys. and Related Socs., 1975 April, Chiba Univ., 2a-E-9

[29] Y. Takeda, A. Sasaki, Y. Imamura, and T. Takagi, J. Appl. Phys., 47, 5405 (1976)

[30] Y. Takeda, A. Sasaki, Y. Imamura, and T. Takagi, J. Electrochem. Soc., 125, 130 (1978)

[31] For example, M. A. Littlejohn, J. R. Hauser, T. H. Glisson, D. K. Ferry, and J. W. Harrison, Solid-State Electron., 21, 107 (1978)
M. A. Littlejohn, R. A. Sadler, T. H. Glisson, and J. R. Hauser, in *Gallium Arsenide and Related Compounds*, 1978 Conference, Series 45 (Institute of Physics, London, 1979) p. 239

[32] Y. Takeda and A. Sasaki, "$In_{0.53}Ga_{0.47}As$ Avalanche Photodiode on InP(111)B Substrate," 1979 Nat. Conv. Rec., IECE Japan, April, S3-19 (in Japanese)

II. LPE GROWTH PROCEDURES

2-1. INTRODUCTION

In this study, liquid phase epitaxy (LPE) is used to grow $In_{1-x}Ga_xAs$ on InP substrates.

Beginning with the preparation of Ge for tunnel diodes by H. Nelson[1], the growth of semiconductor films by LPE has rapidly been developed into a general useful technique for the preparation of films of many III-V and II- VI compounds and other materials. For the growth of III-V compound films, LPE has, in general, the following major advantages over vapor phase epitaxy (VPE) : 1) simplicity of equipment, 2) generally higher growth rates, 3) elimination of hazards due to use of reactive gases and their reactive products which are often toxic, explosive, or corrosive, and 4) larger selection of dopants that can be readily incorporated into the layer[2]. Moreover, the multi-layer structure is easily formed by the multi-well sliding boat and the composition of each layer is accurately controlled in the growth of ternary and quaternary alloys. Because of these advantages, LPE has been chosen for the author's experiments on the growth of $In_{1-x}Ga_xAs$ on InP substrates.

The LPE growth system, growth procedures, and phase diagram of In-Ga-As are described in this chapter.

2-2. LPE GROWTH SYSTEM

A schematic diagram of the growth system is shown in Fig. 2-1. Pd-diffused hydrogen[i)] is flowing at a rate of 100∿200 cc/min through the quartz tube. The dew point of the hydrogen is measured to be below - 75°C at the gas outlet. The quartz tube[ii)] is 1 250 mm in

---

i) Hydrogen purifier is Model LW-06SC, Japan Pure Hydrogen Co. Inc..

ii) Toshiba Ceramics Co. LTD.

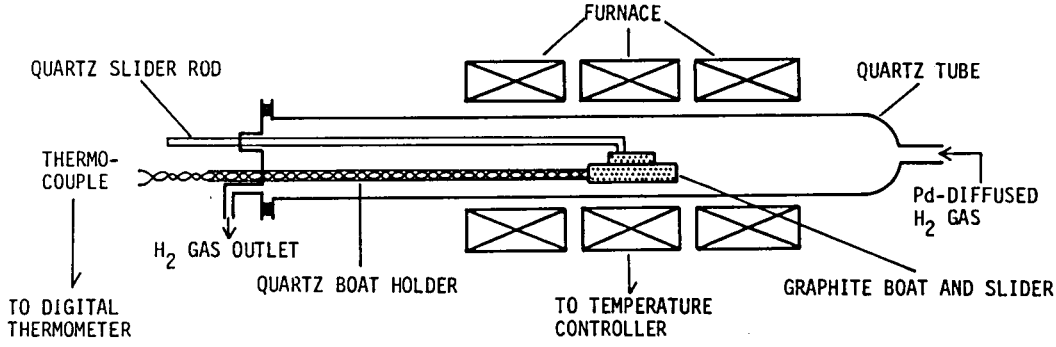

Fig. 2-1 Schematic diagram of the LPE growth system used in the experiments. The furnace is composed of three zones and only the central zone is controlled by the PID-temperature controller unit.

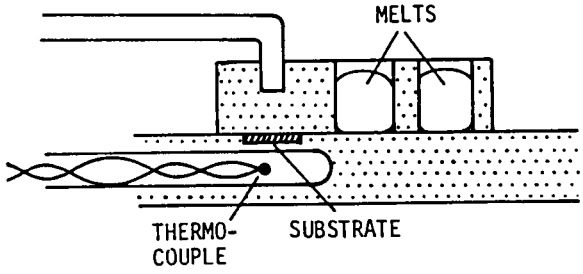

Fig. 2-2 Original structure of the boat and slider. The InP substrate is covered by the slider during the saturation period of the melts.

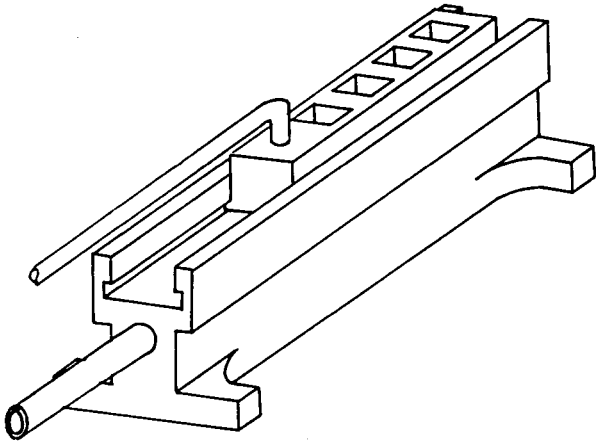

Fig. 2-3 The improved structure of the boat and slider. The bottom corner of the slider is extended to keep the tolerance constant.

length and 52 mm in diameter. A resistance heated furnace[i)] and a PID-temperature controller unit[i)] are used in the growth system. Cooling rates between 0.05 and 8°C/min are obtained. The temperature just below the substrate is detected by a C-A (chromel-alumel) thermocouple and monitored by a digital thermometer[ii)] with 0.1°C accuracy.

The boat and slider are made of high purity graphite[iii)]. The original structure is shown in Fig. 2-2. The slider has only two wells and is put on the boat. The substrate is covered with the slider to minimize thermal etching of the substrate during the saturation period of the melts. The improved structure is shown in Fig. 2-3. It has four wells and the bottom corner of the slider is extended and fitted to the boat. The tolerance between the slider and the substrate surface is kept constant during the slide by the extended bottom corner. The results of the improved structure will be discussed in Chapter IV.

2-3. MATERIAL PREPARATION

All of the glassware is degreased and cleaned ultrasonically in trichloroethylene[iv)], acetone[iv)], and deionized water. Then, they are kept in aqua regia for 12 h and rinsed in deionized water and methanol[iv)]. The graphite boats are cleaned in the same way as the glassware and baked in a vacuum ($\sim 5\times10^{-6}$ Torr) for several hours at 1000°C. The rinsed quartz tubes and the baked boats are set up in the furnace and baked at 950°C for 24 $\sim$ 50 h in a flowing hydrogen atmosphere (at a rate of $\sim$500 cc/min).

---

i) Kokusai Electric Co. LTD.

ii) Type 2572, Yokogawa Electric Works, LTD.

iii) SMG Grade, Showa Denko Co. LTD.

iv) Electronics Grade, Nakarai Chemicals, LTD.

Starting materials are six 9's pure In[i], seven 9's pure Ga[i], and undoped polycrystalline InAs ($n = 1 \sim 3 \times 10^{16}$ cm^{-3} and $\mu = 20{,}000 \sim 23{,}000$ $cm^2/Vsec$)[ii]. In, Ga, and InAs are ultrasonically cleaned in trichloroethylene, aceton, and methanol of the same grade as used in cleaning the glassware. Ga is not etched, but In is etched with a 5% HCl:H_2O_2 solution for 1 min and InAs with a 1% Br:methanol solution for 2 min at RT. Then, In is rinsed in deionized water and methanol, and InAs in methanol.

Polished InP substrates[iii] are degreased in hot trichloroethylene for $10 \sim 30$ min, ultrasonically cleaned in acetone and methanol, etched with the 1% Br:methanol solution for 2 min, and finally rinsed in methanol. The melts are about 2 g, and a slight excess of InAs is added to ensure As saturation in the melts. The substrate dimensions are $10 \times 5 \times 0.4$ mm^3.

The melt materials are weighed by the balance[iv] with the accuracy of 0.1 mg. Since the smallest amount of Ga is ~ 20 mg, the weighing accuracy will be about 5×10^{-3} at worst. The influence of the weighing accuracy will be discussed in § 3-3-6.

2-4. TEMPERATURE CYCLE

An example of the temperature cycle for the growth is shown in Fig. 2-4. Prior to the growth, In and Ga are baked in a flowing hydrogen atmosphere (at a rate of 500 cc/min) at 800°C for 3 h. In order to minimize the thermal etching of the InP substrate (which will be discussed in § 3-3-1) and to avoid the deviation of the melt compositions due to the loss of As during the baking treatment at a high temperature, the substrate and InAs are intro-

---

i) Mitsubishi Metal Mining Co. LTD.

ii) Sumitomo Electric Industries, LTD.

iii) MCP Electronics LTD. and Sumitomo Electric Industruies, LTD.

iv) Type GL-2, Shimadzu Corp.

duced to the furnace after cooling the melts to room temperature. The substrate is placed in a recess of the boat and covered with the slider to minimize thermal etching during the saturation period of the melts, as described in § 2-2. The growth temperature (T_G) (the initial temperature at which the melt is brought over the substrate is called the growth temperature in the thesis, since the temperature is lowered in this growth process) is varied from 500 to 800°C. The cooling rate is ranged from 0.05 to 0.3°C/min. It takes 1.5 h from the start of heating to the sliding, including 30 ∿ 40 min saturation period.

Every time the end cap of the quartz tube is opened, high purity nitrogen is continuously flown through the tube. After the loading of the materials and/or the substrate, the tube is flushed by Pd-diffused hydrogen at a rate of 500 cc/min for 30 min and then started to heat up the furnace.

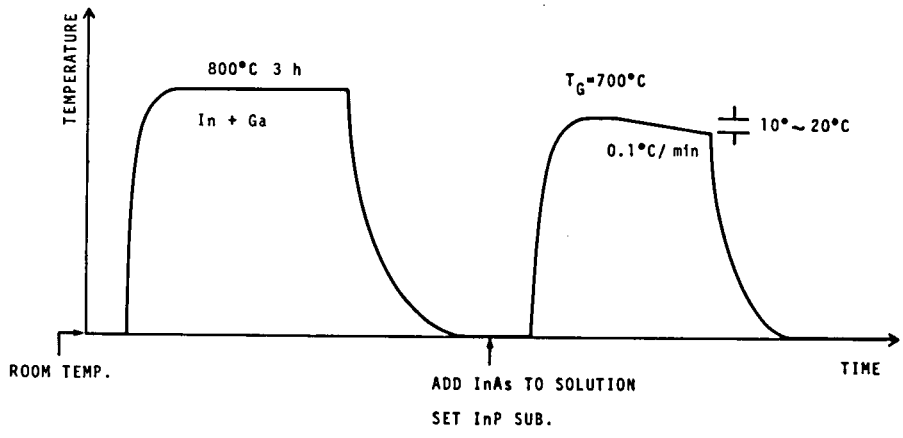

Fig. 2-4 An example of the temperature cycle for the growth. In and Ga are baked at 800°C for 3 h. The InP substrate and InAs are introduced after baking In and Ga.

2-5. PHASE DIAGRAM

2-5-1. Introduction

The ternary phase diagram which gives the liquidus temperature and solidus composition of a given ternary system must be known to grow a ternary alloy with a specific solidus composition by liquid phase epitaxy.

The In-Ga-As ternary phase diagrams have been calculated by G. B. Stringfellow and P. E. Greene using a quasi-chemical model[3], by G. A. Antypas using Darken's quadratic formalism[4], by T. Y. Wu and G. L. Pearson using a quasi-regular solution model[5], and by M. B. Panish and M. Ilegems using a regular solution model[6]. Wu and Pearson's model was based on the experimental data extending to the low temperature of 600°C. Their model is simple and detailed in description[7]. Thus, the author decided to use their phase diagram in the experiments.

Although in Wu and Pearson's phase diagram the number of the experimental data at the lower temperatures are limited and the substrate they used is GaAs, their phase diagram has been a good guidance for the present author's experiments. His epitaxial growth has been carried out in most cases at temperatures lower than 700°C and on InP substrates.

Theoretical model of the phase diagram[5], the calculation at lower temperatures are described in this section.

2-5-2. Theoretical Model

Ilegems and Pearson[8] developed a theoretical model for ternary phase diagram calculation. They investigated the chemical equilibrium conditions between the alloy crystal and the ternary melt and derived two equations. When applied to the In-Ga-As system

they can be written as:

$$\left.\begin{aligned} \gamma_{InAs}(1-x) &= \frac{4\gamma_{In}\gamma_{As}}{\gamma_{In}^{s\ell}\gamma_{As}^{s\ell}} N_{In}N_{As} \exp\left[\frac{\Delta S_{InAs}^{F}}{RT}\left(T_{InAs}^{F} - T\right)\right] \\ \gamma_{GaAs}\, x &= \frac{4\gamma_{Ga}\gamma_{As}}{\gamma_{Ga}^{s\ell}\gamma_{As}^{s\ell}} N_{Ga}N_{As} \exp\left[\frac{\Delta S_{GaAs}^{F}}{RT}\left(T_{GaAs}^{F} - T\right)\right] \end{aligned}\right\} \quad (1)$$

where N, ΔS^F, T^F, and γ denote the atomic fraction of the constituent in the ternary melt, the entropy of fusion, the melting point, and the activity coefficient, respectively. The superscript $s\ell$ represents the stoichiometric liquid. In their derivation, no explicit assumptions about the thermodynamic behavior of liquid and solid solutions were made except that the difference of the specific heat between the binary compound and its stoichiometric liquid is negligible. These two equations can be used to determine a ternary phase diagram quite accurately if reliable information for ΔS^F, T^F, and γ is available.

Reliable ΔS^F and T^F data have been obtained for GaAs and InAs [9], but all the γ's have to be estimated using semi-empirical techniques. With different thermodynamic approximations for the behavior of the solutions, different expressions of γ must be adopted. The most commonly used assumptions are ideal solution, regular solution, and athermal solution models.

In the regular solution model, the activity coefficient γ is expressed in terms of the interaction parameter $\alpha_{X\text{-}As}$ which is determined empirically to fit the binary liquidus data. Since the solubility lines calculated by the regular solution model fit Hall's[10] data almost perfectly, Wu and Pearson decided to adopt the regular solution assumption for the In-Ga-As system[5, 7].

With the regular solution approximation , the activity coefficients in the liquid phase are given by Prigogine and Defey[11] as:

$$\left.\begin{aligned} RT\ln\gamma_{In} &= \alpha_{In-As}N_{As}^{2} + \alpha_{In-Ga}N_{Ga}^{2} + (\alpha_{In-As} + \alpha_{In-Ga} - \alpha_{Ga-As})N_{Ga}N_{As} \\ RT\ln\gamma_{Ga} &= \alpha_{Ga-As}N_{As}^{2} + \alpha_{In-Ga}N_{In}^{2} + (\alpha_{Ga-As} + \alpha_{In-Ga} - \alpha_{In-As})N_{In}N_{As} \\ RT\ln\gamma_{As} &= \alpha_{In-As}N_{In}^{2} + \alpha_{Ga-As}N_{Ga}^{2} + (\alpha_{In-As} + \alpha_{Ga-As} - \alpha_{In-Ga})N_{In}N_{Ga} \end{aligned}\right] \quad (2)$$

and in the solid phase as:

$$\left.\begin{aligned} RT\ln\gamma_{InAs} &= \beta\, x^{2} \\ RT\ln\gamma_{GaAs} &= \beta(1-x)^{2} \end{aligned}\right] \quad (3)$$

where α is the interaction parameter between the two liquid constituents and β is the interaction parameter between the two binary compounds.

Once all of the interaction parameters are established, we can substitute Eqs. (2) and (3) into Eq. (1) and solve for the liquidus temperature T and solidus composition x at any given ternary liquidus composition. This procedure thus establishes the ternary phase diagram.

2-5-3. Calculated Results of Wu and Pearson's Model

The thermodynamic parameters used in Wu and Pearson's model are listed in Table 2-1. The In-Ga-As ternary phase diagram at the In-rich corner is shown in Fig. 2-5. The author's experiments on crystal growth have been carried out at temperatures between 500 and 850°C and at solidus compositions between 0.3 and 0.7. The In-rich corner covers all of these temperatures and compositions because the distribution coefficients of As and Ga are much greater than

	GaAs	InAs
T^F (K)	1515	1210
ΔS^F (e.u./mole)	16.64	14.52
	Ga-As	In-As
α_{X-As} (cal/mole)	-9.9T + 5900	-10.16T + 4030
α_{In-Ga} (cal/mole)	1100 + 0.16T + 9.8TN_{Ga} ($N_{In} > 0.65$)	
β (cal/mole)	2.83T - 1130	

Table 2-1 Thermodynamic parameters used in Wu and Pearson's model.

that of In.

The liquidus compositions which give the solidus composition $x = 0.5$ at several temperatures are listed in Table 2-2-a. Since the elemental As is very volatile and poisonous, either InAs or GaAs are often used as an As source. InAs was chosen since at some temperatures and compositions the atomic fraction of Ga in the liquidus is higher than that of As and GaAs (which has the atomic fraction ratio 1 : 1) cannot be used.

Since the author uses In, Ga, and InAs as the melt materials, the atomic fractions N_{In}, N_{Ga}, and N_{As} are transformed into weight ratios W_{InAs}/W_{In} and W_{Ga}/W_{In} through the relations:

$$\frac{W_{InAs}}{W_{In}} = \frac{189.74\, N_{As}}{114.82(N_{In} - N_{As})}, \quad \frac{W_{Ga}}{W_{In}} = \frac{69.72\, N_{Ga}}{114.82(N_{In} - N_{As})}$$

and some of them are listed in Table 2-2-b. Specific compositions are listed in each relevant chapter.

The melt compositions calculated here have been used as a guidance since they did not give the predicted solidus compositions in the LPE growth on InP substrates and were not so accurate as the author expected. The discrepancy between the calculated and experimental results will be discussed in Chapter III, §3-3-6.

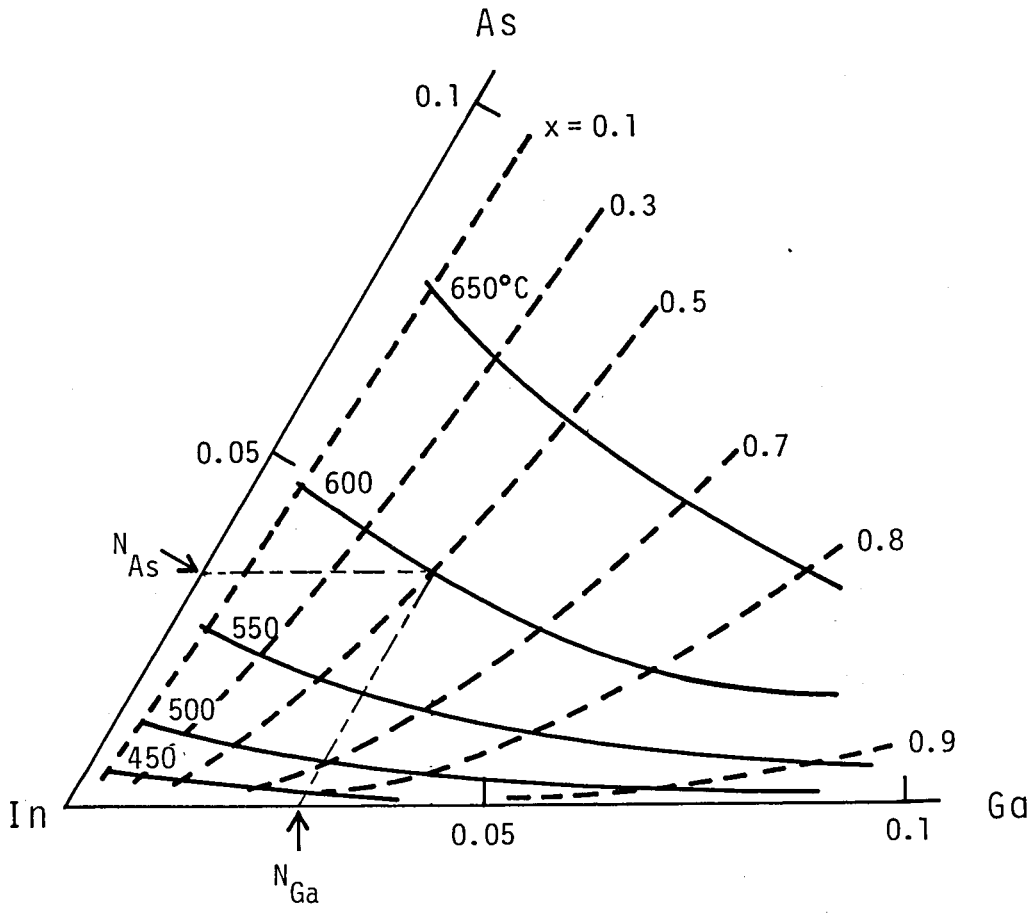

Fig. 2-5 The In-rich corner of the calculated In-Ga-As ternary phase diagram. The solid line is the liquidus and the dashed line is the solidus. The liquidus composition, N_{Ga} and N_{As}, which gives a solidus composition 0.5 at 600°C is indicated in the figure.

T (°C)	N_{In}	N_{Ga}	N_{As}
800	0.79037	0.04825	0.16137
750	0.83697	0.04350	0.11953
700	0.87804	0.03826	0.08370
650	0.91291	0.03271	0.05438
600	0.94075	0.02706	0.03219
550	0.96137	0.02152	0.01711

(a)

T (°C)	In (g)	Ga (mg)	InAs (mg)
800	1.000	46.58	423.96
750	1.000	36.82	275.32
700	1.000	29.25	174.12
650	1.000	23.14	104.67
600	1.000	18.08	58.55
550	1.000	13.84	29.94

(b)

Table 2-2 (a) Some of the calculated atomic fractions in the liquidus which are expected to give the solidus composition 0.5 at each temperature. (b) Weight ratios of solid In, Ga, and InAs which are calculated from the values in Table (a).

2-6. SUMMARY

1) The growth system used in the experiments have been described and shown schematically.

2) Careful procedures for material preparation have been described.

3) The temperature cycle for the growth and pre-baking has been shown.

4) The phase diagram has been calculated for the lower temperature using Wu and Pearson's model.

References

[1] H. Nelson, RCA Rev., 24, 603 (1963)

[2] H. Kressel and H. Nelson in *Physics of Thin Films*, edited by G. Hass, M. H. Francombe, and R. W. Hoffman (Academic Press, New York and London, 1973) Vol. 7, p. 115

[3] G. B. Stringfellow and P. E. Greene, J. Phys. Chem. Solids, 30, 1779 (1969)

[4] G. A. Antypas, J. Electrochem. Soc., 117, 1393 (1970)

[5] T. Y. Wu and G. L. Pearson, J. Phys. Chem. Solids, 33, 409 (1972)

[6] M. B. Panish and M. Ilegems in *Progress in Solid State-Chemistry*, edited by H. Reiss and J. O. McCaldin (Pergamon Press, Oxford, 1972) Vol. 7, p. 39

[7] T. Y. Wu, Ph. D. Thesis, Stanford University, Stanford, 1971

[8] M. Ilegems and G. L. Pearson in *Gallium Arsenide and Related Compounds*, 1968 Conference (Institute of Physics and Physical Society, London, 1969) p. 3

[9] B. D. Lichter and P. Sommelet, Trans. Met. Soc. AIME, 245, 1021 (1969)

[10] R. N. Hall, J. Electrochem. Soc., 110, 385 (1963)

[11] I. Prigogine and R. Defey, *Chemical Thermodynamics* (Longmans, London, 1965)

III. CHARACTERIZATION OF $In_{1-x}Ga_xAs(x \cong 0.5)$ ON InP*

3-1. INTRODUCTION

At the early stage of the investigation there was no experiment on the growth of $In_{1-x}Ga_xAs$ on InP substrate. In order to be aware of the importance of the close lattice matching between the alloy and the substrate and to have a whole scope of the properties of $In_{1-x}Ga_xAs(x \cong 0.5)$ on InP, many characterizations have been carried out on the alloy layers which were grown at temperatures between 500 and 800°C. Other conditions such as the melt baking, cooling rate and interval, and substrate orientation were kept the same.

In this chapter, characteristics such as surface morphology, film thickness, etch pit density, x-ray transmission Laue pattern, composition and composition homogeneity, and photoluminescence are examined on the grown alloys. The experimental methods for the characterizations are described. Since the InP substrate is thermally etched before growth, the thermal etching characteristics are also described.

3-2. EXPERIMENTS

3-2-1. Growth Procedures

The growth conditions are essentially the same as described in Chapter II. The growth temperature is varied at 50°C interval from 500 to 800°C. The cooling rate is 0.15°C/min, and the cooling interval is about 10°C at each growth temperature. The phase diagram is calculated according to Wu and Pearson's model[1], and the ternary

---

* Y. Takeda, A. Sasaki, Y. Imamura, and T. Takagi, J. Electrochem. Soc., 125, 130 (1978)

melt having a solidus composition of $In_{0.50}Ga_{0.50}As$ is used at each growth temperature. The melt compositions are given in Chapter II, Table 2-2-a and b.

3-2-2. Film Thickness

The thickness of the grown layer is observed by cleaving the wafer along (110) plane which is perpendicular to the (111) plane. Since the refractive indices of the two layers (InGaAs and InP) at visible light is different enough to see a delineation of the grown layer without staining the cleaved edge. The wafer is easily cleaved after lapping the substrate to the thickness $\sim$200 μm.

3-2-3. Etching

Etch pits in the grown layers are revealed by etching with the A-B solution[2] for 30 $\sim$ 60 sec at room temperature or several sec at 50°C. The A-B solution or A-B etchant is composed of an A solution (40 cc H_2O + 0.3 g $AgNO_3$ + 40 cc HF) and a B solution (40 g CrO_3 + 40 cc H_2O) after G. H. Olsen and M. Ettenberg[3]. The A-B etchant was originally named after the author's name of reference[2], *i.e.*, Abrahams and Buiocchi. Olsen and Ettenberg reported that the etchant was stored in two separate solutions (the A and B solutions) indefinitely as long as they were not mixed[3]. In the present author's experience he feels it is true if HF is kept from evaporating. InP is also etched with the A-B solution at 60 $\sim$ 70°C for 10 min. The R-C solution[4] can be also used for etching InP at the same condition, but it gives very tiny pits.

3-2-4. X-Ray Transmission Laue Method

The well-known x-ray method to study the crystal structure is applied to InGaAs. To observe the Laue pattern from the InGaAs layer

alone, the InP substrate is selectively etched out by hot HCl. The schematic drawing of the sample is shown in Fig. 3-1.

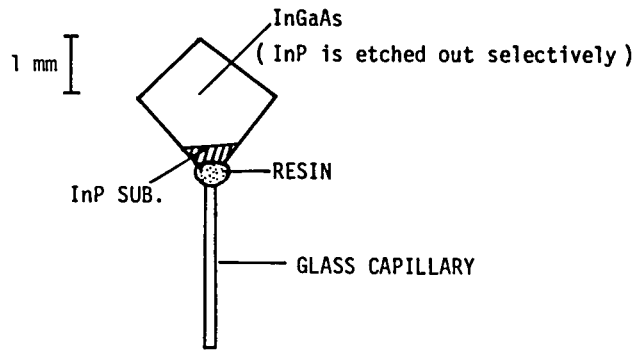

Fig. 3-1 The sample for the transmission Laue method.

3-2-5. X-Ray Diffraction

The composition is determined by x-ray diffraction of Cu-$K\alpha_1$ and $K\alpha_2$ radiation using Vegard's law which can be applied to this alloy[5]. At high diffraction angles such as for (333) or (444) reflections, both reflections from the epitaxial layer and the substrate are detected. The higher the angle is, the deeper the x-ray penetrates into the materials. Since the diffraction angle of the InP substrate is known, the precise diffraction angle of the alloy is determined from (333) or (444) reflections using the substrate as an internal standard.

3-2-6. EPMA

The EPMA(electron probe microanalysis) is very often used for the characterization of the chemical composition of a solid specimen. By this method a quantitative analysis of a specimen of very small size (< 1 μm) can be obtained. For a description of the EPMA, see, *e.g.*, *Characterization of Solid Surfaces* edited by P. F.

Kane and G. B. Larrabee[6]. The instrument used in the experiments is Shimadzu ARL-EMX. The specimen is held by the epoxy resin, angle-lapped by 3°, and polished to obtain a mirror surface. The angle-lapped surface is perpendicular to the electron beam, but the original surface is not. See Fig. 3-2.

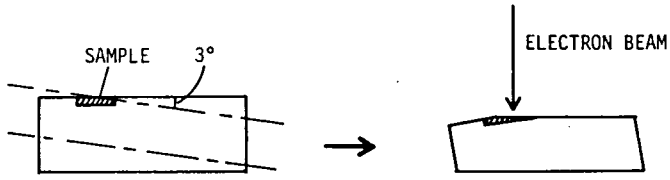

Fig. 3-2 The sample for the EPMA is held by the epoxy resin and angle-lapped. The angle-lapped surface is perpendicular to the electron beam, but the original surface is not.

3-2-7. Photoluminescence

The photoluminescence is excited by a He-Ne laser (6328 Å) and detected by a PbS photoconductive diode cooled with a Dry Ice: methanol solution. A conventional lock-in technique is used. The spectral response of the total system is in the range from 1.4 to 2.3 μm (at half-responses). After being lightly etched with a 1% Br:methanol solution, the sample is attached to a copper jig and immersed in liquid nitrogen contained in a double wall Dewar. Photoluminescence is measured mainly at 77 K, since at the lower temperature a finer structure of the spectra is observed. At room temperature the spectra tend to become broader due to the thermal excitation of carriers. For the measurement at RT the samples are set in the empty Dewar. All the samples are angle-lapped by 3° to examine the spectral variations along the thickness of the grown layers. The sample is moved parallel to the angle-lapped surface by a manipulator to which the copper jig is attached. The schematic diagram of

the photoluminescence measurements apparatus is shown in Fig. 3-3.

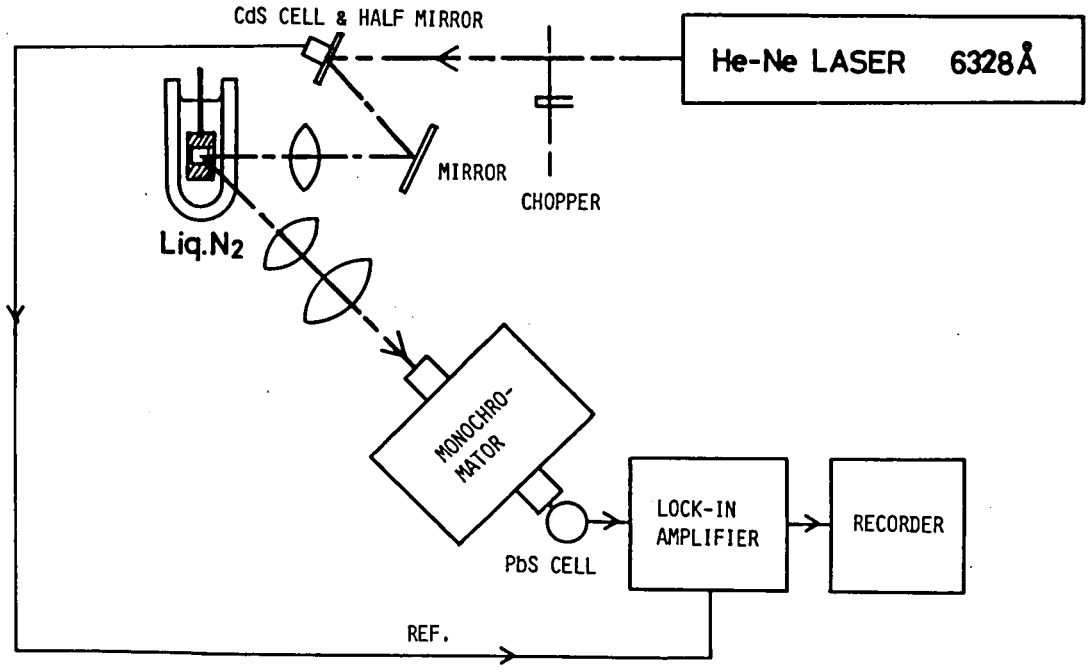

Fig. 3-3 Schematic diagram of the photoluminescence measurements apparatus.

3-3. RESULTS AND DISCUSSION

3-3-1. Thermal Etching of InP Substrate Surface

Examples of the InP (111)B-surface baked at 500° and 700°C for 1 h in a flowing hydrogen gas (at a rate of 100 cc/min) are shown in Figs. 3-4-a and b, respectively, and cleaved cross section

in c . The substrate is placed in a recess of the boat and covered with the slider during the heat-treatment as shown in Fig. 2-2. The substrate surface shows evidence of thermal etching. Small droplets remain on the surface at a lower temperature, and larger droplets at a higher temperature. A large droplet is seen to be due to the coalescence of small droplets. The droplets are identified to be In by the EPMA, and by observing the droplets to melt at around 160°C. Thus, this thermal etching is due to the thermal decomposition of InP at a high temperature. Similar observations have been reported by Pak *et al.*[7]. This etching effect influences the thickness and the surface morphology of the grown layer as shown next.

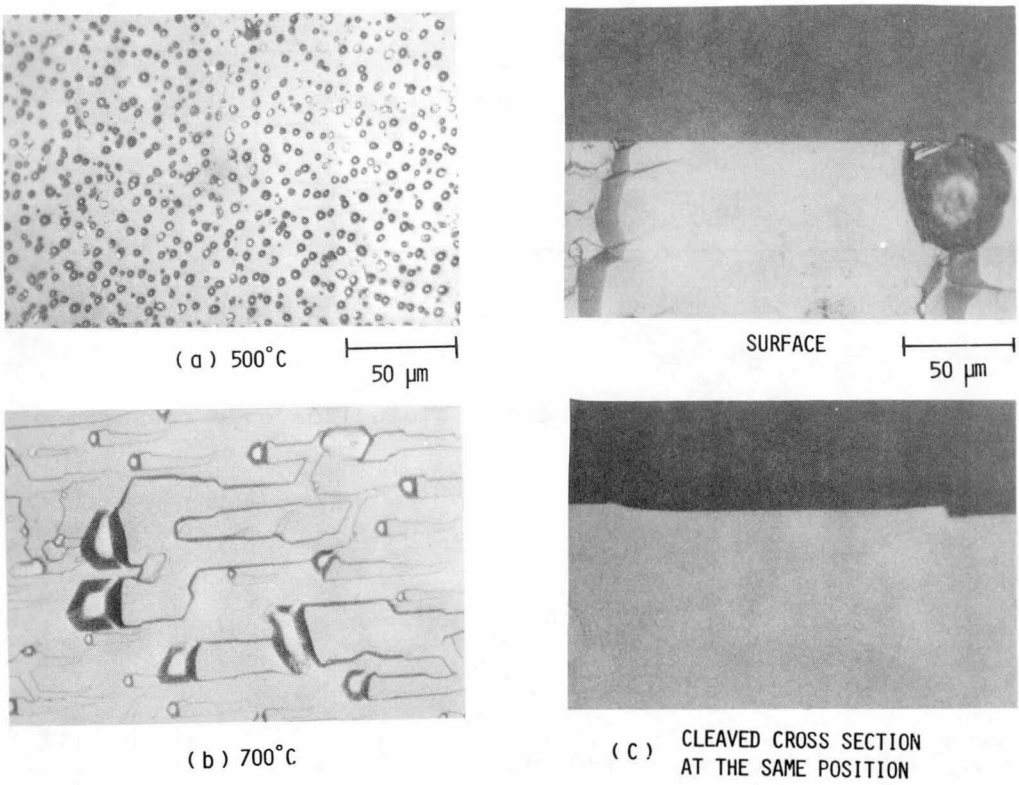

Fig. 3-4 Examples of the thermal etching of the InP substrate surface after 1 h baking at 500°C (a) and 700°C (b) in a flowing hydrogen gas. (c) is the surface and cleaved edge of InP baked at 700°C.

3-3-2. Surface Morphology

As-grown surfaces and cleaved cross sections of the epilayers grown at 550°C and 700°C are shown in Figs. 3-5 (a) and (b), respectively. The as-grown surface at 700°C is the smoothest among those grown in the range from 500 to 800°C. At temperatures below 650°C, the surface becomes rough. Melt droplets are left on the as-grown surface during wiping due to the surface roughness. At temperatures

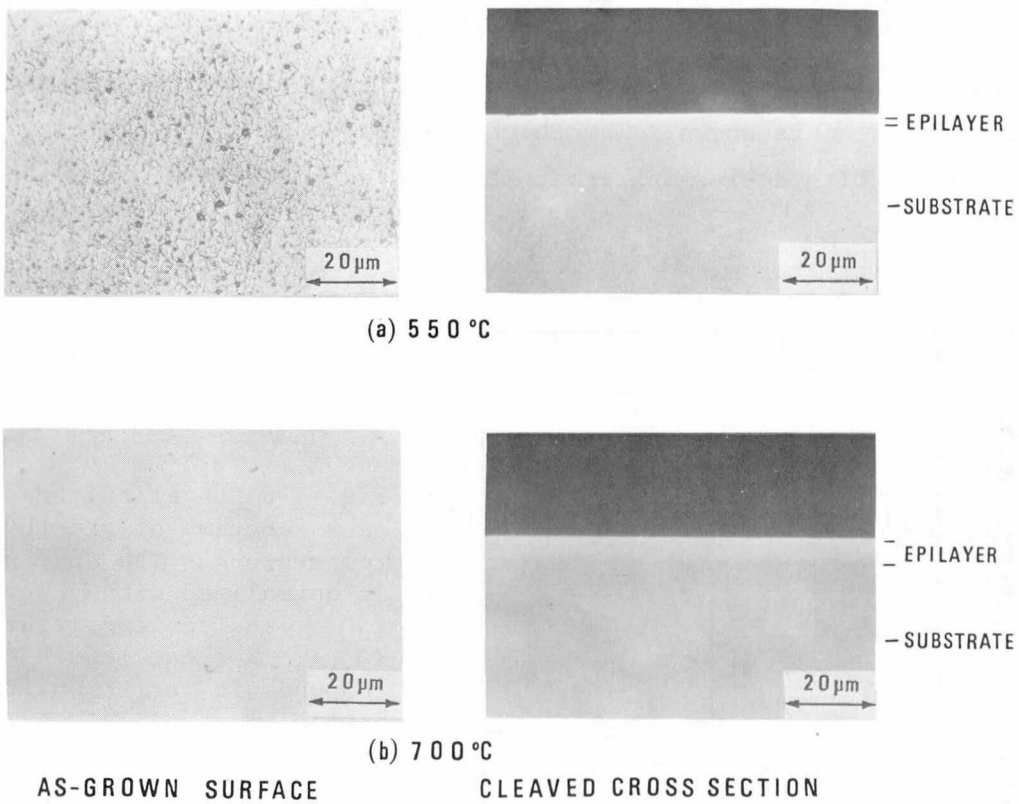

Fig. 3-5 As-grown surfaces and cleaved cross sections of the epitaxial layers grown at 550°C (a) and 700°C (b). Small spots are droplets of melt remaining on the rough surface. No inclusions are found in cleaved cross sections.

above 750°C, the as-grown surface is also rough. This is confirmed to be caused by the roughness of the substrate surface as a result of the thermal etching. At 800°C the melt remains almost over the entire surface after wiping. However, a uniform layer would be grown if the problem of the thermal etching is overcome by keeping the phosphorus over-pressure or by etching back the InP surface. The etching-back will be discussed in §3-3-8. In the experiments all the alloys grown at 800°C are excluded from the measurements.

3-3-3. Layer Thickness

In Fig. 3-6, the temperature dependence of the layer thickness normalized with the In weight in the melt (W_{In}) and the cooling interval (T_C) is shown. The thickness decreases approximately exponential with decreasing growth temperature. Between 550°C and

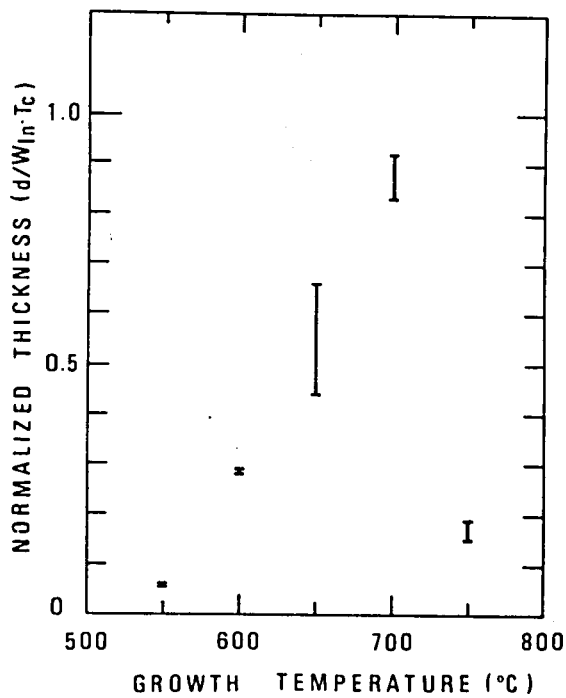

Fig. 3-6 Layer thickness as a function of growth temperature. The thickness is normalized with In weight (W_{In}) and cooling interval (T_C). The bar length corresponds to variation from sample to sample.

700°C, the curve follows qualitatively the temperature dependence of the As fraction in the melt. The calculated As fraction (using the phase diagram described in Chapter II) normalized with the In fraction is shown in Fig. 3-7. At 500°C no continuous layer is grown, and this can be attributed to the low solubility of As at 500°C. The abrupt decrease at 750°C could be explained as follows. A fair amount of In remains on the substrate surface due to the thermal etching, as shown in Fig. 3-4. The melt when contacted with the substrate is diluted by this In and undersaturated at the interface. Therefore, the initial cooling period is spent in re-equilibration and resaturation, and the layer thickness is small. No In inclusions are found at the interface of the layers, indicating that all the In droplets are taken into the contacted melt before the growth begins.

The thickness of the grown layer should be considered more

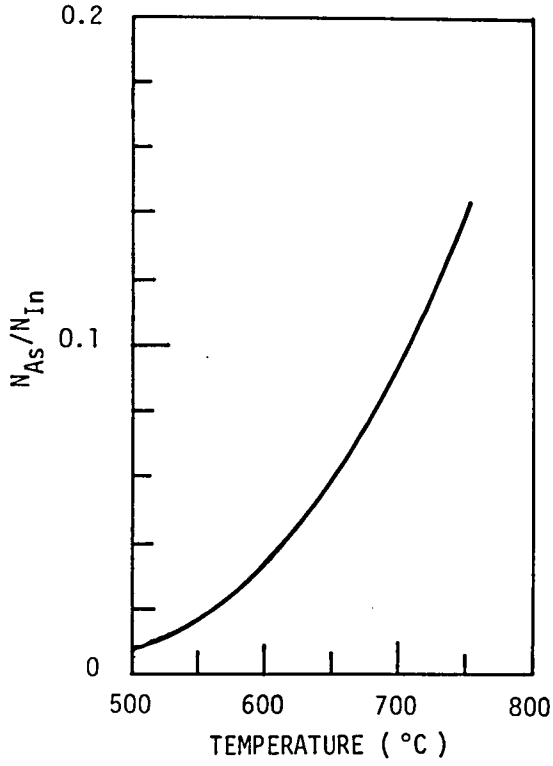

Fig. 3-7 Growth temperature dependence of the calculated As fraction normalized with the In fraction in the melt.

precisely both experimentally and theoretically. The experiments must be carried out on a larger area of the substrate to eliminate the influence of the edge growth[8], and with flat and thin melt materials[9]. The edge growth will be discussed in Chapter IV, §4-6-2. The layer thickness of ternary alloy is calculated by solving the diffusion equation with a more precise model[9,10]. These problems for InGaAs are left for the further study.

3-3-4. X-Ray Transmission Laue Pattern

At the very early stage of the research on the crystal growth of InGaAs on InP (1974), there was a question whether the grown alloy layer is really epitaxial or not. Although the author was sure from the etching pattern and the cleavage direction that it is the epitaxy of the strict definition, *i.e.*, the grown layer has the same crystal structure and orientation as the substrate, the x-ray transmission Laue (T-Laue) method is applied to the grown layer with and without the InP substrate.

Figure 3-8-a is the T-Laue pattern of (111)-oriented InP and Fig. 3-8-b shows that of $In_{1-x}Ga_xAs$($x \cong 0.5$) (# 137) whose substrate is etched out. The two patterns of (a) and (b) are superimposed in Fig. 3-8-c. From the figure it is clear that the alloy layer has the same crystal structure. In addition, the InGaAs layer with the InP substrate is cleaved perfectly along (110), and this means that the grown layer has the same crystal orientation as the substrate. Thus, the alloy layer grows epitaxially in the strict sense of the definition.

It can be seen that the spots in Fig. 3-8-b is different from those in Fig. 3-8-a. The elongated spots in Fig. 3-8-b are due to distortion of the lattice after the lattice-mismatch being relieved with the substrate etched out selectively. Somewhat starlike spots in Fig. 3-8-b would be resulted from polygonization[11] due to micro-

cracks, which will be shown in Chapter V, §5-3. More pronounced distortion is observed in Fig. 3-8-d. These samples have lattice-mismatch larger than 0.3 % .

In the samples where the lattice is closely matched (*e.g.*, 0.03 %) there should be no such distortion or polygonization.

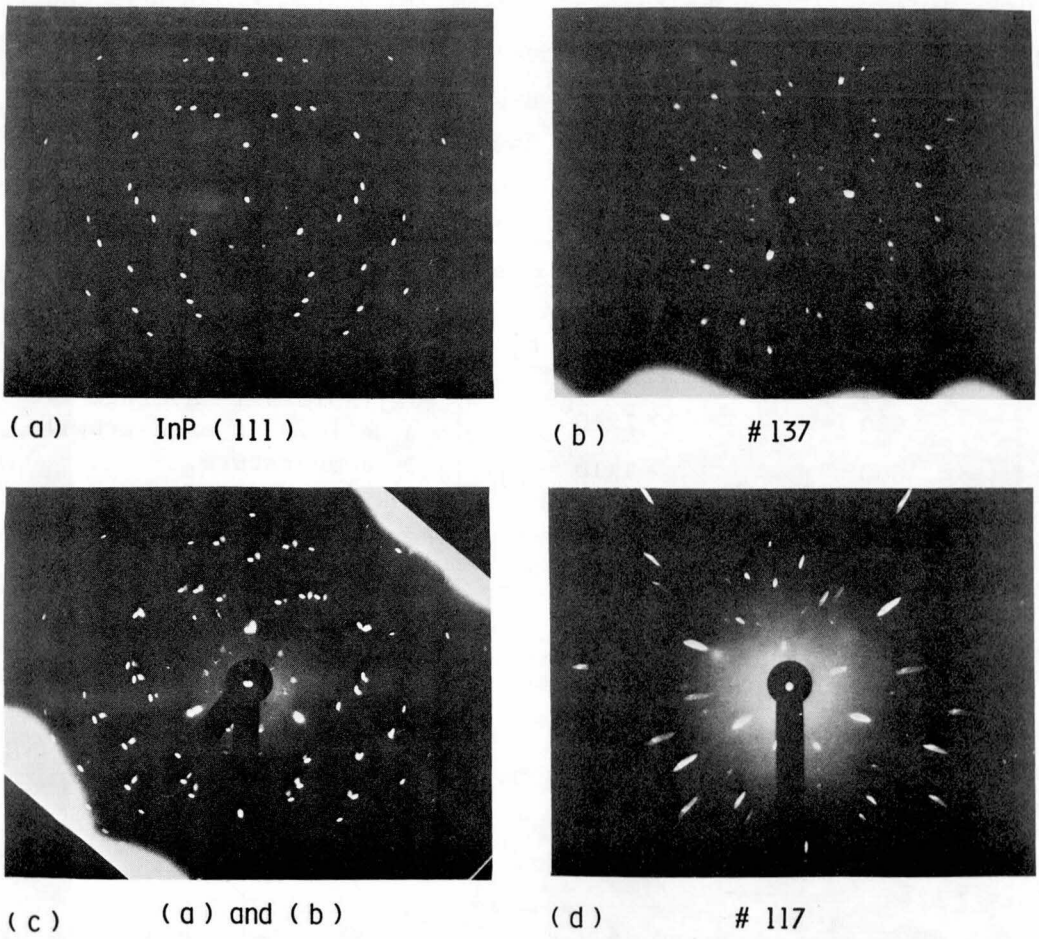

Fig. 3-8 Transmission Laue patterns: (a) for (111)-oriented InP, (b) for (111)-oriented InGaAs. In (c) the patterns in (a) and (b) are superimposed to confirm the identical spot arrangement. (d) shows elongated spots due to lattice distortion.

3-3-5. Etch Pit Density

The average etch pit density at each growth temperature is listed in Table 3-1. In the sample at 550°C the EPD is too high to count, far beyond 10^6 cm^{-2}. This high EPD may be in part due to the relatively large lattice mismatch between the substrate and the layer as will be shown in Fig. 3-10. Better crystal could be grown even at temperatures below 650°C by precisely matching the lattice parameter. About 1×10^5 cm^{-2} may be the lower limit of the EPD, because the Cr-doped InP substrate has approximately the same density of etch pits as revealed by etching with the R-C solution. An example of etch pits in InGaAs is shown in Fig. 3-9.

GROWTH TEMPERATURE (°C)	AVERAGE EPD (cm^{-2})
550	$>> 1x10^6$
600	$> 1x10^6$
650	$> 5x10^5$
700	$\sim 5x10^5$
750	$\sim 1x10^5$

Table 3-1 Average EPD of alloys at each growth temperature.

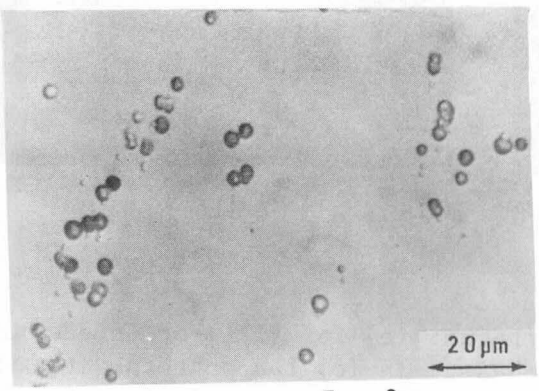

176 EPD (5.2×10^5 cm^{-2})

Fig. 3-9 An example of the etch pits in InGaAs (# 176).

3-3-6. Composition and Composition Homogeneity

The composition *vs.* growth temperature is shown in Fig. 3-10. Although the In-Ga-As solution with the solidus composition of $In_{0.50}Ga_{0.50}As$ at each growth temperature is used, the composition of the alloys grown at temperatures between 650°C and 750°C is $In_{0.53}Ga_{0.47}As$ at which the lattice constant of the grown layer matches with that of InP. Below 650°C, the mismatch becomes greater with decreasing growth temperature.

As pointed out by Wu and Pearson[1] the accuracy of the solidus data in their experiment is $\pm$ 3 mole percent. In our experiments at 600°C and 550°C the deviation is over this range. It is possible that the lower Ga composition obtained at these temperatures is due to inaccuracy of the Wu and Pearson phase diagram. Only a few experimental data were examined in their phase diagram calculation at these lower temperatures, as pointed out in Chapter II, §2-5. Correction to the phase diagram is discussed in §3-3-8.

Influence of the weighing accuracy of the melt materials to the composition is briefly discussed here. Since Ga is the

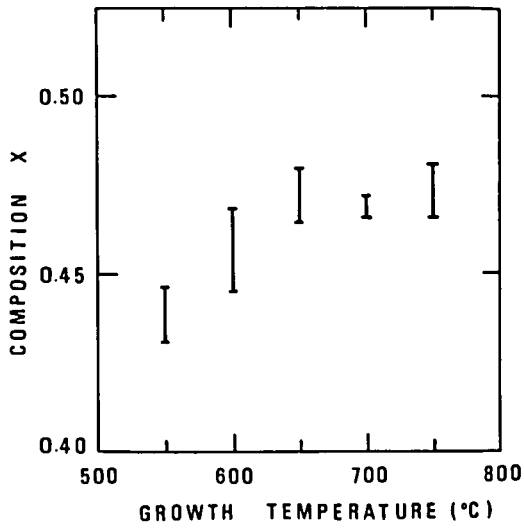

Fig. 3-10 Composition *vs.* growth temperature. The In-Ga-As solution of solidus composition 0.5 which is calculated from the phase diagram is used at each growth temperature.

smallest in its weight, this is weighed at first and the weights of In and InAs are corrected using the Ga weight as a standard. Between In and InAs, the weighing inaccuracy of In affects the solidus composition deviation more than that of InAs. This is calculated from the phase diagram. If In is weighed within $\pm$ 1.0$\times 10^{-3}$, the solidus composition is within $\pm$ 0.0005 at around 0.47. This gives the mismatch as small as $\pm$ 3.4$\times 10^{-5}$.

Examples of (444) reflections are shown in Figs. 3-11-a, b, and c. The reflections from the epitaxial layer and the substrate are detected at this high angle. In Fig. 3-11-a the lattice is very closely matched, and in Fig. 3-11-b a mismatch of 0.066% is calculated. The $K\alpha_1$ and $K\alpha_2$ peaks are clearly resolved, indicating good composition homogeneity of these alloys. A mismatch of 0.03% is well resolved in this alloy system, using a conventional x-ray diffractometer. The half-width of the spectrum from the epitaxial layer increases with decreasing growth temperature as shown in Fig. 3-11-c.

A result of the EPMA along the grown layer and the surface is shown in Fig. 3-12. The sample is angle-lapped by 3° as shown in Fig. 3-2. The result shows very good composition homogeneity and constant composition along the grown layer and the surface. A slight decrease in intensity both of Ga and In along the surface is due to the off-angle of the sample surface as shown in Fig. 3-2. Electron beam and x-ray detection system are mis-aligned due to the off-angle of the sample surface. The intensity decrease at the left end is due to the attenuation of signals by epoxy resin over the surface.

Fig. 3-13 shows an example in which the Ga inclusions are detected in the grown layer. The inclusions are seen in the angle-lapped layer also through the optical microscope. The wafer might be grown with a much higher cooling rate (> 5°C/min) than the Ga-diffusion limited growth-velocity. Moreover, the quasi-grown layer

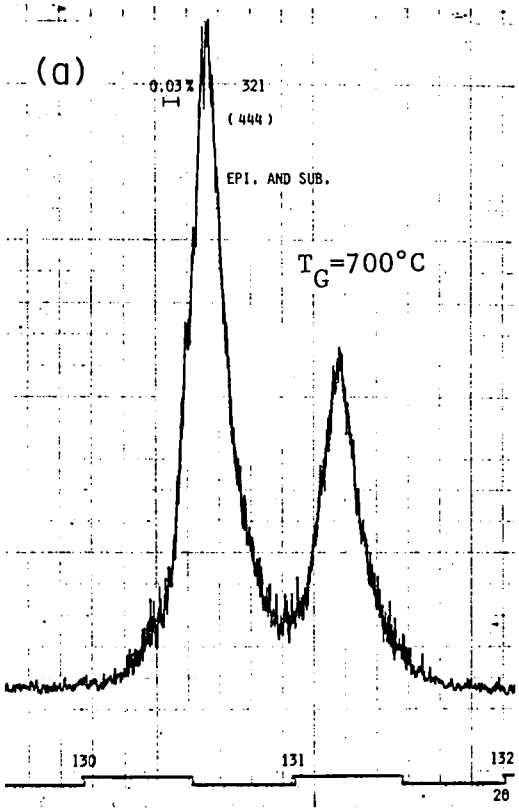

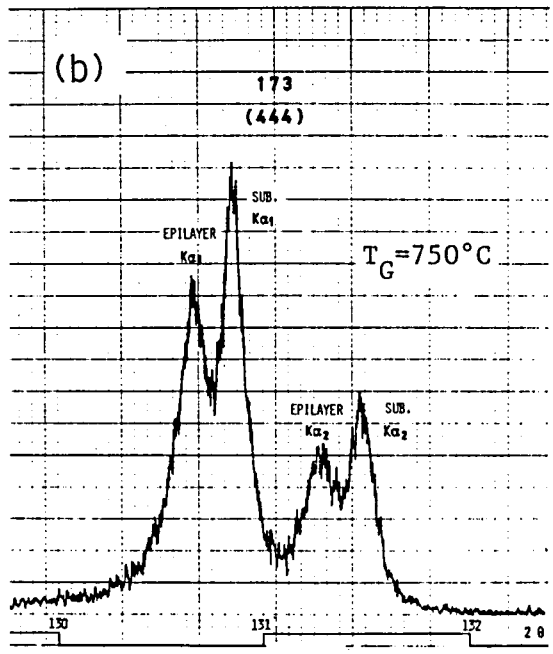

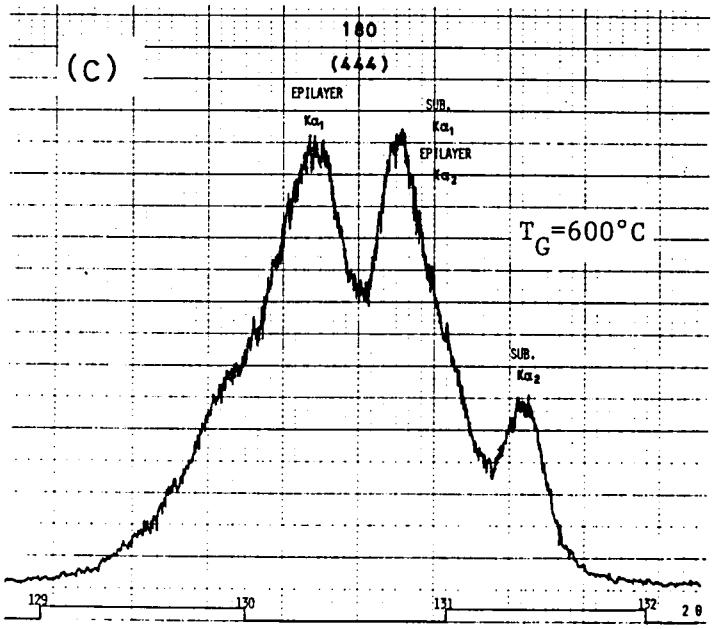

Fig. 3-11 Examples of (444) reflections from InGaAs on InP. In (a) the lattice is closely matched, and in (b) a mismatch of 0.066% is calculated. In (c) the half-width of the spectrum is wider.

(see Chapter IV) is contained in the layer.

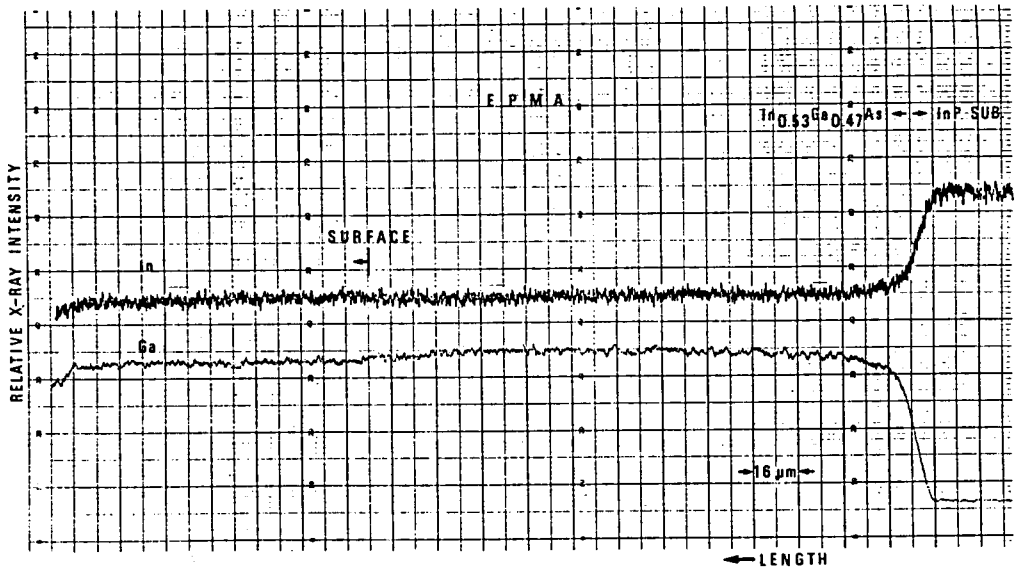

Fig. 3-12 Electron probe microanalysis along the angle-lapped grown layer and the surface. The intensity is quite constant along the grown layer.

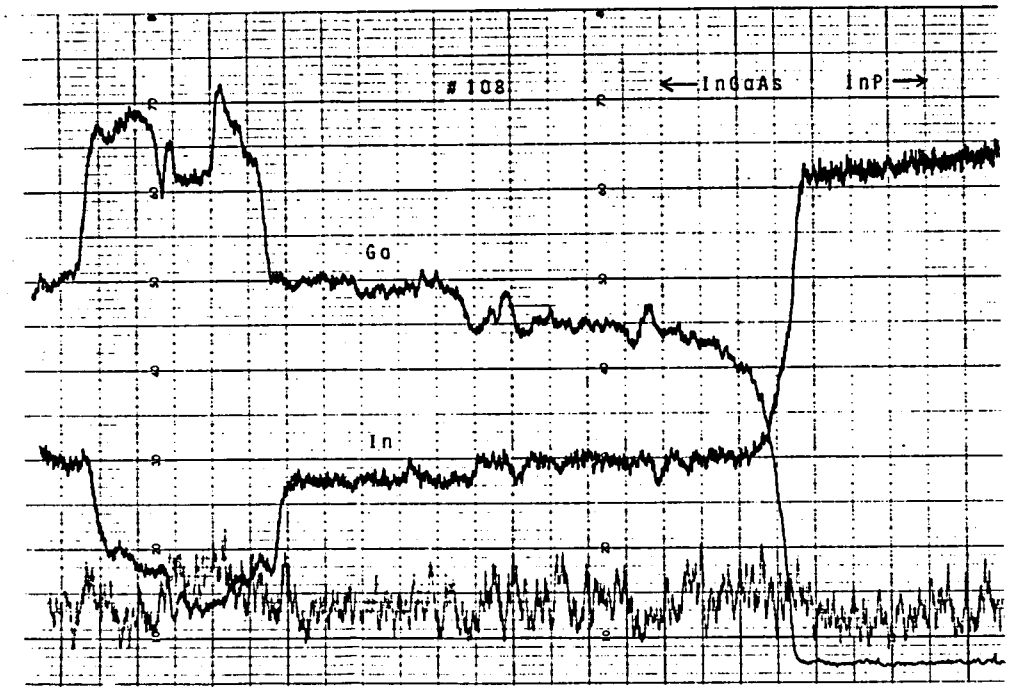

Fig. 3-13 Electron probe microanalysis along a poor quality layer.

3-3-7. Photoluminescnece

Emission spectra of two epitaxial layers grown at different temperatures are compared in Fig. 3-14. There are three distinctions in the spectra: the photon energy at peak intensity, the half spectral width, and the relative intensity of the peak at lower photon energy. The composition determined by the photon energies at peak intensities are close to those in Fig. 3-10 obtained by x-ray diffraction. A good fit to the photon energy ($h\nu$) *vs.* composition (x) in the region $0.43 < x < 0.48$ and at $x = 0$ (InAs) and $x = 1$ (GaAs) at 77 K is given by

$$h\nu(eV) = 0.404 + 0.649\,x + 0.457\,x^2$$

The curve gives quite the same values as those by Wu and Pearson at 77 K[1].

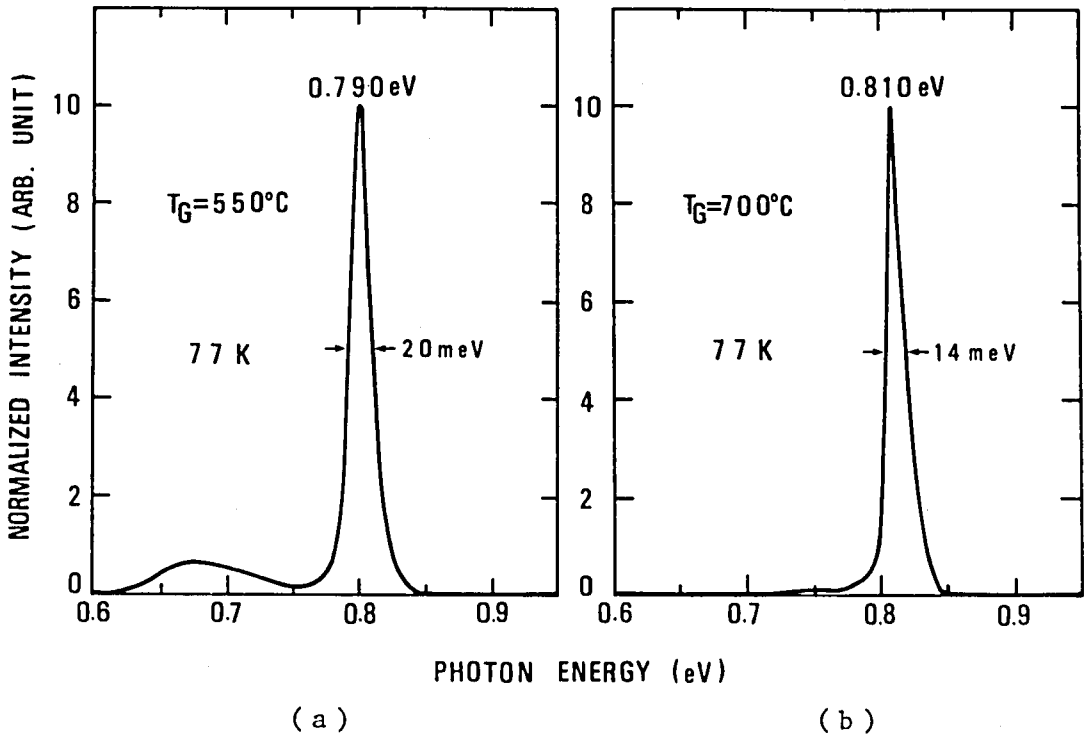

Fig. 3-14 Photoluminescence spectra at 77 K of two epitaxial layers grown at 550°C (a) and 700°C (b).

The full width at half-maximum(FWHM) of the spectra decreases linearly with the increase of the growth temperature, *i.e.*, from ∿20 meV at 550°C to ∿13 meV at 750°C as shown in Fig. 3-15. This depend-

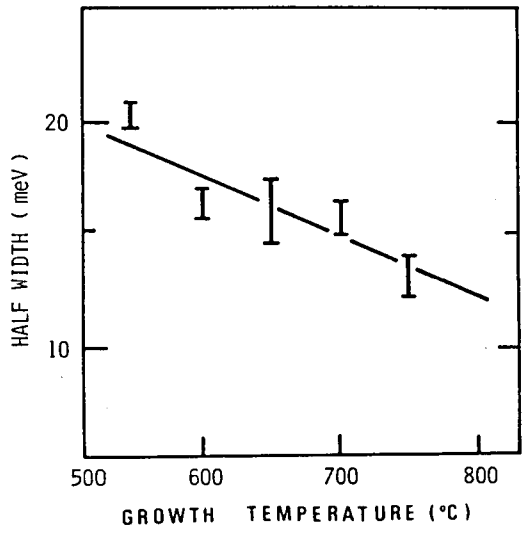

Fig. 3-15 Growth temperature dependence of half-width of PL spectra at 77 K.

ence is not based on the composition variation across the grown layer within the penetration depth of the He-Ne laser beam. Such a composition variation can be expected from the phase diagram[1]. However, the lower the growth temperature is, the smaller the composition variation for a cooling interval of 10°C at $x \triangleq 0.5$. Furthermore, in the experiments, the composition variation from near the interface to the surface is measured to be within $\pm$ 1% by the EPMA and the photoluminescence. Moreover, the penetration depth of the laser beam is less than 1 μm. Along with the growth temperature dependence of the half width of x-ray reflection peak, which has been described in §3-3-6, it is understood that alloys of better composition homogeneity are grown at higher temperature.

As for the origin of the sub-peak at lower photon energy, no extensive investigation has been done. Since the material preparation and the growth conditions except for the growth temperature are

the same for all the growth, the sub-peak does not seem to be due to an impurity atom, but it might be related to the lattice-mismatch induced defects. In the samples grown at lower temperature both the lattice-mismatch and the electron concentration increase, suggesting the above speculation.

The variations of the photon energy at peak intensity, the intensity, and the FWHM along the angle-lapped grown layer are shown in Fig. 3-16 for sample # 153 as an example. Constant photon energy indicates the uniformity in the composition, and very small variations of the intensity and the FWHM show a homogeneous crystal quality across the grown layer. Similar results

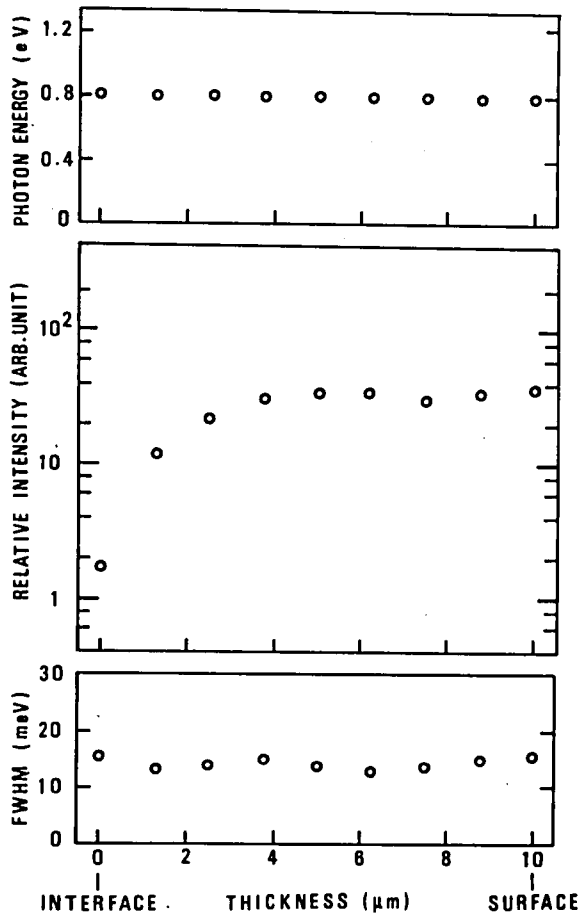

Fig. 3-16 Variations of the photon energy at peak intensity, the intensity, and the FWHM at 77 K along the angle-lapped surface in sample #153, showing good composition homogeneity and uniform crystal quality.

are obtained in every sample at different growth temperature. A relatively low intensity near the interface is due to the finite diameter of the laser beam (∿50 μm), *i.e.*, at distance 0 μm, most of the laser spot irradiates the substrate and at about 3 μm (corresponding to about 50 μm in a layer angle-lapped by 3°) the whole spot is on the grown layer.

3-3-8. Effects of Lattice Mismatch

In the crystal growth the ternary melt having a solidus composition of $In_{0.50}Ga_{0.50}As$ was used at each growth temperature. The result is that the melt did not give the solidus composition $x = 0.5$ due to the inaccuracy of the phase diagram. There are two main problems left to be solved. The first is to find the liquidus composition which gives the solidus composition at the lattice-matching condition at each growth temperature, and the second is to distinguish the characteristics of the alloy layer caused by the lattice mismatch from those due to the growth temperature. The second one will be solved easily if the first one is found.

The weights of melt constituents which give the lattice-matching solidus composition (within the accuracy of 0.03%) at some growth temperatures are listed in Table 3-2. Since the phase diagram is calculated by the author at the interval of 0.01 solidus

T_G(°C)	In(g)	Ga(mg)	InAs(mg)
620	1.000	18.1	77.9
625	1.000	18.55	82.6
650	1.000	21.2	108.6
700	1.000	27.2	179.5

Table 3-2 The weights of melt constituents which give the lattice-matching solidus composition.

composition at each growth temperature, it is a simple process to approach the lattice-matching composition using the phase diagram as a guidance. Several times of growth, at most, were necessary. The substrate surface was etched by pure In just prior to the growth. The influence of the thermal etching of the substrate surface is expected to be eliminated by this etching process.

Most remarkable changes in the characteristics, which have been expected and discussed in §3-3-2 and 5, are the surface morphology and the etch pit density of the grown layer.

At any growth temperature between 620°C and 700°C, the surface is the same and smooth. In the growth from the melts with $x = 0.5$, the lattice-mismatch would be thought to have affected the surface morphology through non-uniform nucreation at the early stage of the growth and the distortion of the lattice. No noticeable variation of the EPD with growth temperature is found. The results indicate that the discussion in §3-3-5 is correct.

There seems to be no large difference in the characteristics of the layers grown at temperatures between 620°C and 700°C, except for the layer thickness. The best suited growth temperature will be selected considering other characteristics such as electrical properties, the diffusion behavior of the dopant at the growth temperature, and film thickness controllability.

Finally, a tetragonal distortion of the lattice in the lattice-mismatched heteroepitaxial layer must be discussed here. It has been reported and very often used that Vegard's law, *i.e.*, the lattice constant is a linear function of the composition in a pseudo-binary alloys, is applied to $In_{1-x}Ga_xAs$[5]. This law will be true in the case of somewhat rough (*e.g.*, $>10^{-2}$) determination of the relation and in the case of the bulk materials which is free from the lattice mismatch with a substrate. In VPE-grown $In_{1-x}Ga_xAs$ on GaAs[12], $Ga_xIn_{1-x}P$ on GaAs[13], LPE-grown $In_{1-x}Ga_xAs_{1-y}P_y$ on InP[14], and

MBE-grown $In_{1-x}Ga_xAs$ on InP[15], the lattice distrotion has been observed by a x-ray diffraction technique. It is evident that Vegard's law is inapplicable to the lattice-mismatched and lattice-distorted heteroepitaxial layer.

If the distortion is a simple tetragonal one, *i.e.*, the lattice parameter parallel to the interface (a_ℓ) is equal to the parameter of InP (a_o) and the parameter perpendicular to the interface (a_p) is equal to that of the strain-free alloy as shown in Fig. 3-17, the lattice parameter determined from the conventional x-ray diffraction is the same as a_p, since the plane separation for the reflection is not changed by the distortion. Therefore, the estimation of the lattice-mismatch by the x-ray diffraction can be used as a good guidance. However, the composition is different from the strain-free alloy because the unit cell is smaller (in the case of $x < 0.47$) by a factor of $a_\ell^2 a_p / a_p^3$.

Y. Kawamura and H. Okamoto have shown that 80% of the mismatch is accomodated by the elastic strain of the lattice, *i.e.*, the elastic distortion of lattice, between $x = 0.45$ and 0.49[15]. In a system with a larger mismatch, *e.g.*, $>10^{-3}$, the accomodation will break down and Vegard's law can be applied. However, the crystal quality must be much degraded due to a large number of misfit dislocations and microcracks in the layer with the larger mismatch.

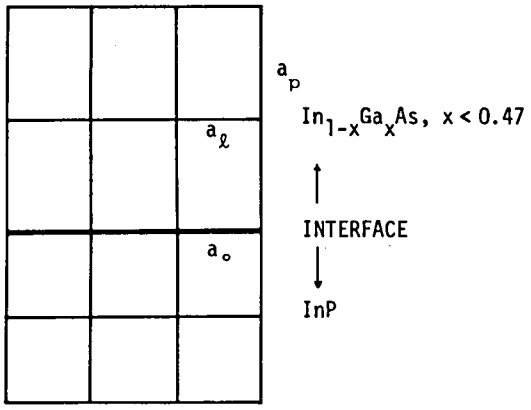

Fig. 3-17 Schematic drawing of tetragonal lattice-distortion in $In_{1-x}Ga_xAs$ ($x < 0.47$) on InP.

3-4. SUMMARY

In this chapter, many characterizations on the $In_{1-x}Ga_xAs$ layers have been carried out. The results obtained from the characterizations are listed below.

1) The InP substrate surface is thermally etched during the saturation period by the evaporation of the phosphorus.

2) The surface morphology of the grown layer is affected both by the lattice mismatch and by the roughness of the thermally etched substrate surface.

3) The thickness of the grown layer decreases with decreasing growth temperature except at 750°C, following qualitatively the temperature dependence of the As fraction in the melt.

4) The x-ray transmission Laue pattern gives clear evidence of the epitaxy of the grown layer and shows lattice distortion in a mismatched layer.

5) The EPD increases with lattice mismatch ($x<0.47$) and the lower limit is about 1×10^5 cm^{-2}.

6) The composition is estimated by x-ray diffraction at high reflection angles using the InP reflection as an internal standard.

7) The composition and crystal quality have been shown to be very homogeneous and uniform along the growth direction and over the surface by the EPMA and the photoluminescence.

8) The same quality of layers are obtained at temperatures between 620°C and 700°C by etching back the substrate surface with pure In just prior to growth.

References

[1] T. Y. Wu and G. L. Pearson, J. Phys. Chem. Solids, 33, 409 (1972)

[2] M. S. Abrahams and C. J. Buiocchi, J. Appl. Phys., 36, 2855 (1965)

[3] G. H. Olsen and M. Ettenberg, J. Appl. Phys., 45, 5112 (1974)

[4] J. L. Richards and A. J. Crocker, J. Appl. Phys., 31, 611 (1960)

[5] J. C. Woolley and B. A. Smith, Proc. Phys. Soc. (London) 72, 214 (1958)
E. F. Hockings, I. Kudman, T. E. Seidel, C. M. Schmeltz, and E. F. Steigmeier, J. Appl. Phys., 37, 2879 (1966)

[6] G. A. Hutchins, " Electron Probe Microanalysis," in *Characterization of Solid Surfaces* edited by P. F. Kane and G. B. Larrabee (Plenum, New York, 1974)

[7] K. Pak, T. Nishinaga, and S. Uchiyama, Japan. J. Appl. Phys., 14, 1613 (1975)

[8] D. L. Rode and R. G. Sobers, J. Cryst. Growth, 29, 61 (1975)

[9] S. Isozumi, Ph.D. Thesis, Kyoto Univeristy (1979)

[10] S. Isozumi, Y. Komatsu, N. Okazaki, S. Koyama, and T. Kotani, J. Cryst. Growth, 41, 166 (1977)

[11] B. D. Cullity, *Elements of X-Ray Diffraction* (Addison-Wesley, Reading, 1956)

[12] H. Nagai, J. Appl. Phys., 45, 3789 (1974)

[13] G. H. Olsen and M. Ettenberg, " Growth Effects in Heteroepitaxy of III-V Compounds," in *Crystal Growth - Theory and Techniques* edited by C. H. L. Goodman (Plenum Press, New York, 1978) Vol. 2

[14] K. Oe, Y. Shinoda, and K. Sugiyama, Appl. Phys. Lett., 33, 962, (1978)

[15] Y. Kawamura and H. Okamoto, Spring Meeting of Japan. Soc. Appl. Phys. and Related Socs., Tokyo, March 1979, 29a-H-7 (in Japanese)

IV. QUASI-GROWN LAYERS*

4-1. INTRODUCTION

In a liquid phase epitaxial growth, an additional layer is often obtained with a residue of melt materials over a grown layer, when the melt has not been completely wiped away at the end of a pre-determined growth process, even with a small tolerance between the substrate surface and the slider. The characterization of the grown layer is usually conducted after taking off the remaining melt by dipping into H_g, selectively etching, and/or evaporating the melt materials, depending on its chemical properties. Surface morphology, crystal quality, electrical and optical properties of the layer deposited from the remaining melt would be much different from those of an actual layer. The additional layer is called "quasi-grown layer" in this thesis.

There seem to be few published papers which notice the effects of the incomplete removal of melt on these characteristics of the grown layer, except for those of Hakki[1] and Coleman *et al.* [2]. The former reported that in the experiments of the growth of $In_{1-x}Ga_xP$ on GaAs, the composition of the layer deposited out of a residue of melt materials varied more rapidly along the growth direction than that of the layer deposited during the actual growth process. The latter showed the importance of complete melt removal in ensuring a planar surface or boundary on an $In_{1-x}Ga_xP_{1-z}As_z$ LPE-layer and the effect of incomplete removal on the quaternary heterojunction devices.

In this chapter, taking the growth of $In_{1-x}Ga_xAs$ on InP as an example, the author reveals through experiments that characterization of the grown layer is in error when the melt remains at the end of

---

* Y. Takeda, Y. Imamura, and A. Sasaki, J. Cryst. Growth, 46, 75 (1979)

a pre-determined growth process and that it is very important to conduct the characterization of the grown layer with complete removal of the melt at the end of the LPE-growth or after taking away the quasi-grown layer completely.

4-2. INCOMPLETE REMOVAL OF MELT IN LPE-GROWTH

When the growth is not under proper conditions, the surface of a grown layer would not be smooth or the periphery would be stepped up due to the excess edge growth which is often observed in the LPE-growth. Even with a small tolerance between the substrate surface and the slider, the grown layer is covered, wholly or partly, with the melt materials when taken out of the furnace. After taking off the remaining melt on the grown layer by means of, for example, dipping into H_g, the surface can be observed. An example of the grown surface after removing the melt is shown in Fig. 4-1-a. The melt remained due to the excess edge growth which worked as a surrounding barrier to the melt. The periphery is stepped up as shown in Fig. 4-1-a, and Fig. 4-1-b is the microscopic observation of Fig. 4-1-a.

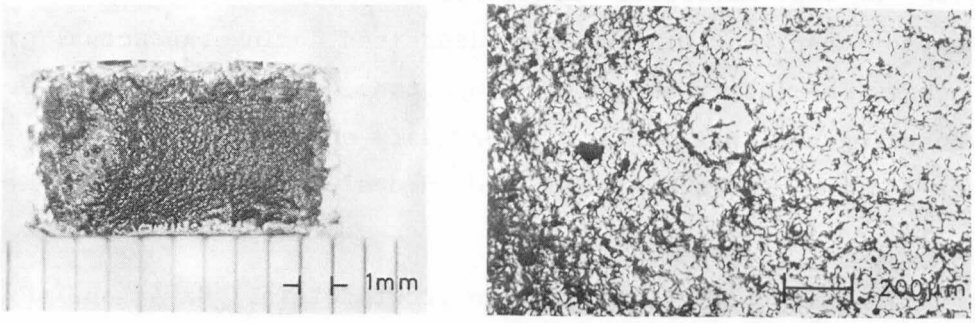

(a) (b)

Fig. 4-1 As-grown surfaces of an alloy observed after removing the melt: (a) whole surface and (b) microscopic observation.

4-3. PL MEASUREMENTS ALONG GROWN LAYERS

For the characterization the sample is angle-lapped, polished, and etched with the 1% Br:methanol solution for several sec at RT. Photoluminescence(PL) measurements are carried out at 77 K across the angle-lapped surface. PL is excited by a He-Ne laser (6328 Å) beam focused on the surface with a spot size about 50 μm. The results indicate that the sample is composed of two distinct layers besides the InP substrate, as shown in Fig. 4-2. Those are $In_{1-x}Ga_xAs$ ($x \cong 0.5$) with the PL peak around 0.80 eV and $In_{1-x}Ga_xAs$ ($x < 0.5$) with the peak around 0.57 eV. The variations of the PL intensity and the half width across the angle-lapped surface are shown in Fig. 4-3. There are abrupt changes in the characteristics observed from the PL measurements. The PL characteristics should be compared with those in Fig. 3-16.

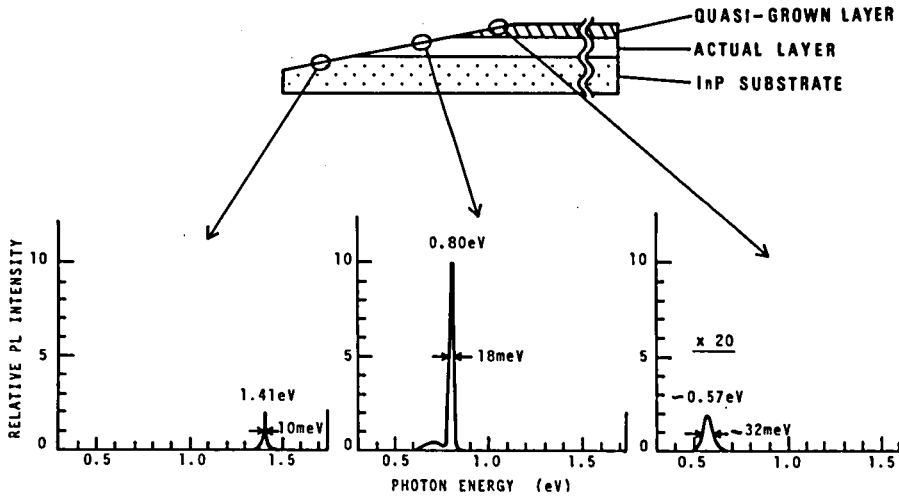

Fig. 4-2 PL measurements across the angle-lapped surface. The grown layer is composed of two distinct layers besides InP substrate. The PL intensities are not corrected with the spectral response of the measurement system.

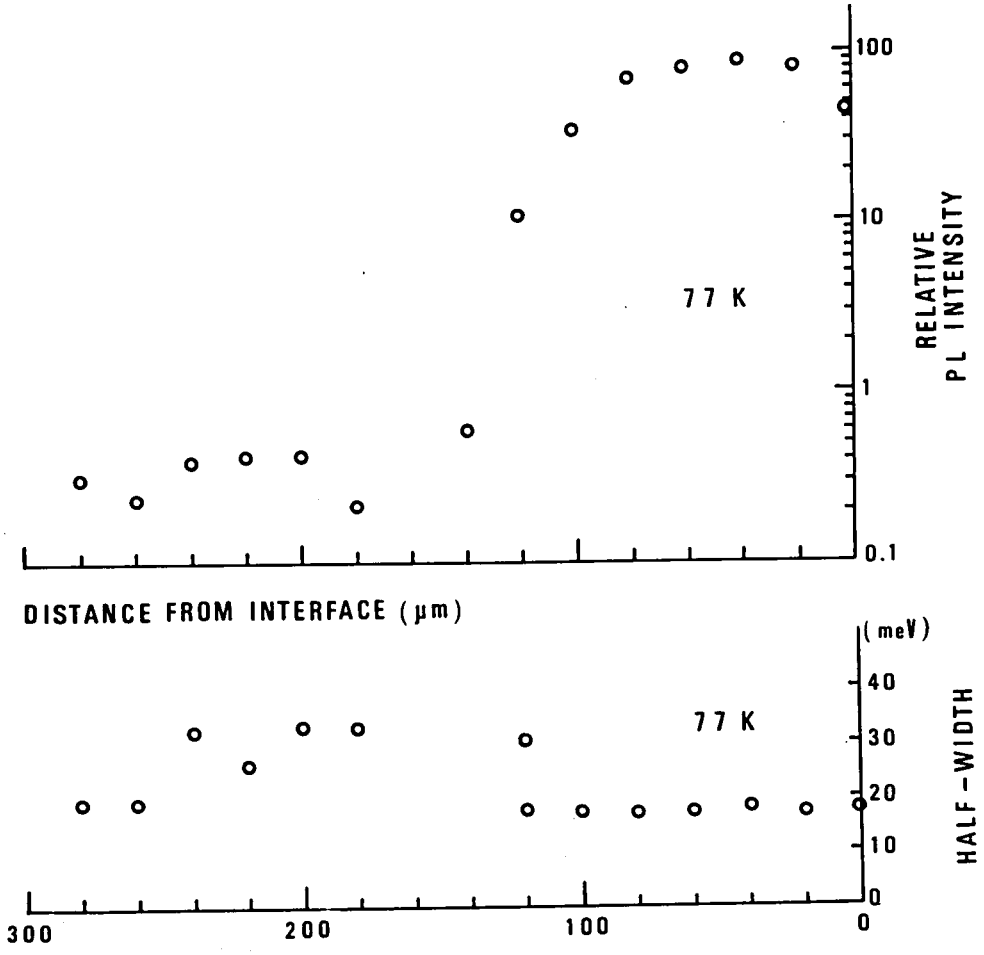

Fig. 4-3 Variations of PL intensity and half width of spectra across the angle-lapped surface.

4-4. CHEMICAL ETCHING AND EPMA ALONG GROWN LAYERS

The angle-lapped surface is etched with the A-B solution[3,4] for 10 to 30 sec at RT. The etched surface is shown in Fig. 4-4 along with the composition variation measured with the electron probe microanalysis(EPMA). There are in the grown layer the constant composition layer of $x \triangleq 0.5$ and the varying composition layer around $x = 0.3$. Between them there is the layer with a high etch pit density

(EPD). The trace of the EPMA signals from all the constituent elements is shown in Fig. 4-5. Compare it with Fig. 3-12.

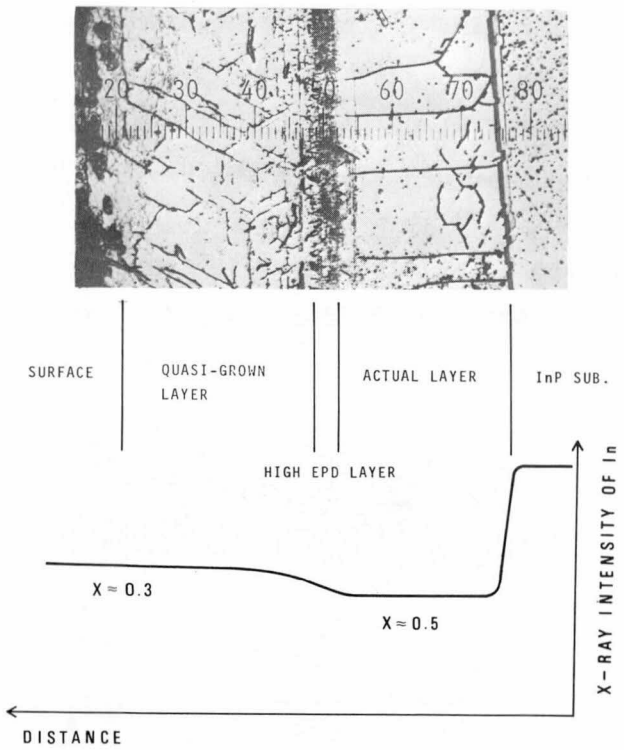

Fig. 4-4 Etched surface and composition variation observed by EPMA across the angle-lapped surface: 6.6 μm per division.

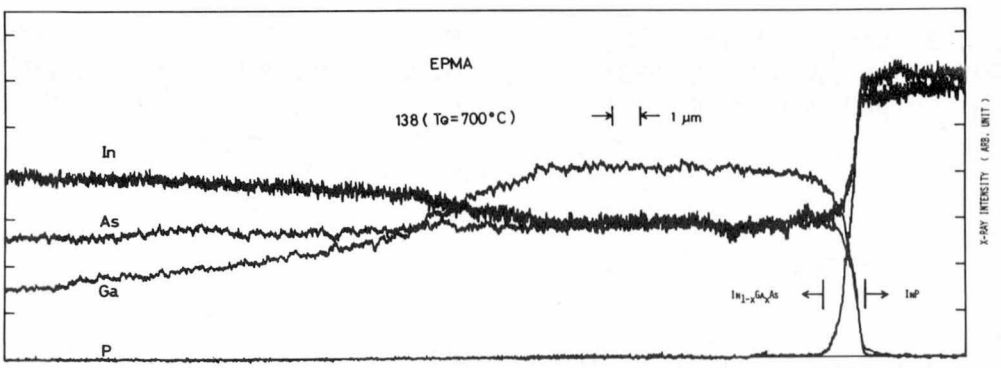

Fig. 4-5 The trace of the EPMA signals. The x-ray intensity variations of the four constituent elements are shown.

4-5. QUASI-GROWN LAYERS

Fig. 4-6 shows the grown layer of $In_{1-x}Ga_xAs$ ($x \cong 0.5$) where the melt materials are completely wiped away from a portion of the grown surface. This portion is mirror-like smooth, but the grown surface covered with the melt material has the same morphology as shown in Fig. 4-1. The grown layer of the mirror portion is composed of single constant composition $x = 0.47$ which has been intended, but the grown layer covered with the melt material is composed of the same two layers as shown in Figs. 4-2 ∿ 4-5. The cleaved cross section is shown in Fig. 4-7. It shows clearly that the quasi-grown layer is deposited on the actual layer.

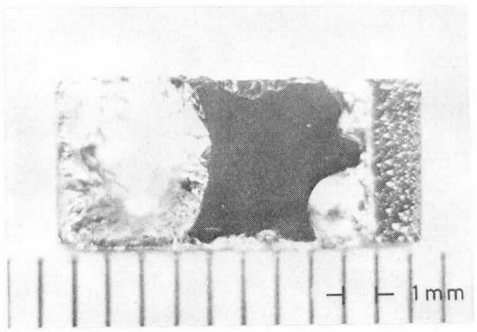

Fig. 4-6 Sample of $In_{1-x}Ga_xAs$ ($x \cong 0.5$) where melt is completely wiped away on the black portion.

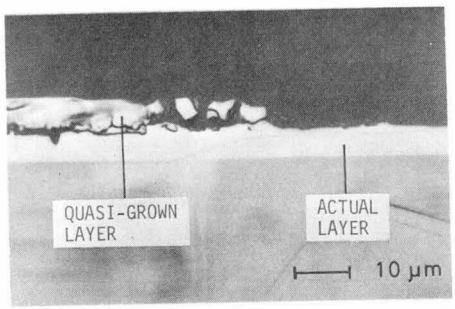

Fig. 4-7 Cleaved cross section of the sample in Fig. 4-6 after removing the melt. Quasi-grown layer is deposited on the actual layer.

4-6. DISCUSSION

The grown layer of a low crystal quality, *i.e.*, a low PL intensity, large spectral half-width, and a varying composition, is grown by the deposition from the remaining melt materials during the temperature cooling from the end of the pre-determined growth temperature to room temperature. This low-quality layer is not

the layer grown during the actual growth process, but the layer grown unintentionally after that process. Thus, it may be called a quasi-grown layer.

4-6-1. Effects of Quasi-Grown Layers

One example of the mis-evaluation of the grown layer observed in the experiments is the electron mobility in it. The highest mobility in the grown layer with the quasi-grown layer is 9 440 cm^2/Vsec, but that in the actual layer is 7 600 cm^2/Vsec at 300 K. Although the crystal quality of the quasi-grown layer is much worse than that of the actual layer, the mobility in the total layer is higher because the composition of the quasi-grown layer is near to InAs which has a very high mobility ($\sim$ 30 000 cm^2/Vsec)[5].

B. W. Hakki[1] observed in the LPE-growth of $In_{1-x}Ga_xP$ on GaAs that if during the tipping-off process a residue of the melt remained on the substrate surface, this residue continued to deposit material down to RT and that the composition of the ternary alloy that deposited out of the residue varied more rapidly as a function of distance than that of the layer deposited during the actual growth process.

J. J. Coleman *et.al.*[2] fabricated by LPE yellow DH lasers consisted of lattice-matching $In_{1-x}Ga_xP_{1-z}As_z$ quaternary and $GaAs_{1-y}P_y$ ternary layers at constant temperature ($\sim$ 800°C) from supersaturated melts. They found in the lasers small red shunts penetrating the DH structure, or irregular or shorted junctions. They provided evidence that these problems are associated with incomplete melt removal or wipe-off between the growth of one LPE-layer and the growth of the next. They noted that only a small amount of drag-over of one quaternary melt under a different composition melt is sufficient to cause attack of the underlying substrate or LPE-layer and to destroy locally the lettice-matching

ability of the second melt.

I. Hayashi[6] described the effects of the remaining melt on the LPE-grown GaAlAs/GaAs DH structure. He pointed out that the complete melt removal was achieved both by a small tolerance between the substrate surface and the boat and by the improved quality of the grown layer. Even with a small tolerance, the melt remained spotty on defect parts of an epitaxial layer. The Ga melt which was contaminated by the drag-over of the Al-contained melt affected the thickness and uniformity of the GaAs layer, and caused the fluctuation of the lasing wavelength. Further, the remaining melt on the last layer deposited excess GaAs islands, and it affected the heat dissipation in the laser mounted up-side down.

4-6-2. Complete Removal of Melt

It has been shown above that the complete removal of melt is very important to avoid errors in the characterization of the grown layer and to fabricate multi-layered structures.

The melts are completely removed except at the edge portion of the substrate by the improved boat and slider structure with a larger size of the melt wells as compared with the substrate size, and a close lattice-matching of the alloy with the substrate.

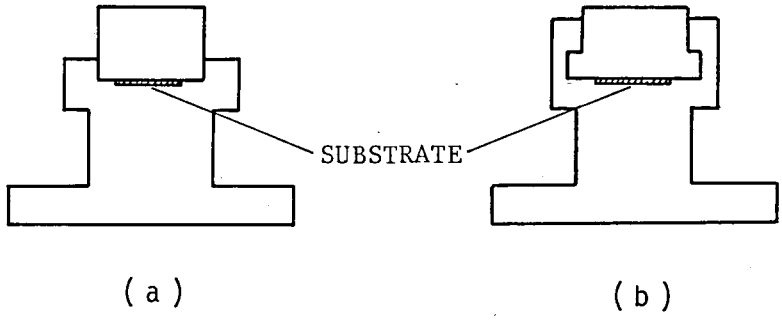

Fig. 4-8 Cross sectional view of the boat and slider. (a) The original structure. The slider is put on the boat. (b) The improved structure.

A cross sectional view of the original boat and slider structure is shown in Fig. 4-8-a, which has been illustrated in § 2-2. The slider is put on the boat and will easily be pushed up by an excess growth of the layer and/or adhesive melt materials on the grown layer. The structure has been improved to keep the tolerance unchanged during the slide by extending the bottom corner of the slider as shown in Fig. 4-8-b. Even when the edge grows high, the melts are removed from the most part of the grown-layer surface with this improved boat.

In our experiments of the LPE-growth of InGaAs on the InP (111)B surface, the edge tends to grow higher than the other flat portion when the size of the melt well is smaller than that of the substrate. From a carefull observation of the excess edge growth, it has been found that the edge grows along the circumference of the melt contacted to the substrate surface as shown in Fig. 4-9-a. The width of the melt well has been widened so that the substrate edge contacts to the flat bottom of the melt as shown in Fig. 4-9-b. The width perpendicular to the sliding direction is kept smaller by 0.5 mm than that of the substrate. The excess edge growth along the sliding direction does not much affect the melt removal.

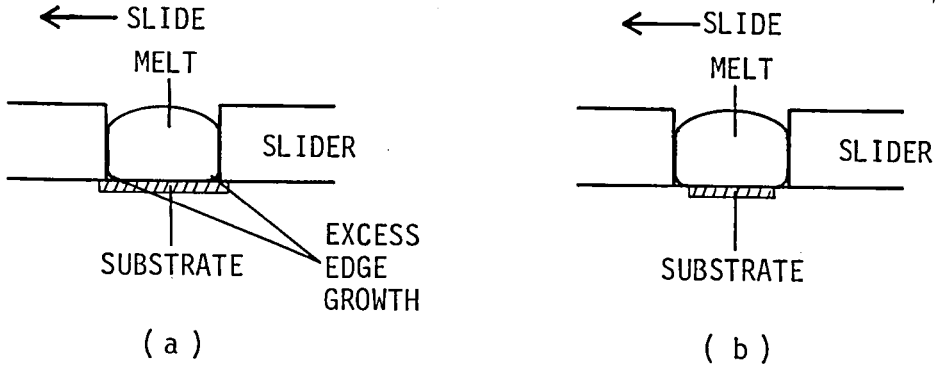

Fig. 4-9 In (a) the excess edge growth is observed along the circumference of the melt. In (b) the edge growth is much suppressed.

4-7. SUMMARY

The author has shown through experiments the effects of the incomplete melt removal in LPE on the characteristics of the grown layer, taking the growth of $In_{1-x}Ga_xAs$ on InP as an example.

1) The grown layer with a residual melt remaining unintentionally may involve the quasi-grown layer whose characteristics are much different from those of the actual layer which was intended.
2) The surface of the quasi-grown layer is rough as compared with that of the actual layer.
3) The PL intensity is low and the spectral half-width is larger in the quasi-grown layer. The actual layer has a constant PL intensity, half-width, and energy at peak along the growth direction.
4) The composition varies along the growth direction in the quasi-grown layer, but quite constant in the actual layer.
5) The EPD is high in the quasi-grown layer.
6) The quasi-grown layer deposits on the actual layer.
7) Growth of the quasi-grown layer is avoided by the complete removal of melt with a well-designed boat structure.

Such a grown layer has to be characterized by distinguishing carefully the actual layer from the quasi-grown layer. Otherwise, the characterization may be in error and lead to mis-evaluation of the actual layer.

References

[1] B. W. Hakki, J. Electrochem. Soc., 118, 1469 (1971)
[2] J. J. Colemann, N. Holonyak, Jr., and M. J. Ludowise, Appl.

Phys. Lett., 28, 363 (1976)

[3] M. S. Abrahams and C. J. Buiocchi, J. Appl. Phys., 36, 2855 (1965)

[4] G. H. Olsen and M. Ettenberg, J. Appl. Phys., 45, 5112 (1974)

[5] M. Neuberger, *III-V Semiconducting Compounds, Handbook of Electronic Materials* (IFI/Plenum, New York, 1971) Vol. 2

[6] I. Hayashi, BUSSEI, 11, 686 (1973) (in Japanese)

V. EFFECTS OF LATTICE MISMATCH ON GROWN LAYERS*

5-1. INTRODUCTION

In the epitaxial growth of ternary alloys, there is usually a lattice mismatch between the epilayer and the substrate. By liquid phase epitaxy, it is impossible so far to grow epilayers over the whole composition range on one substrate except for the Al-Ga-V system, such as Al-Ga-As[1], Al-Ga-Sb[2], and Al-Ga-P[3], in which the mismatch is very small.

The lattice mismatch between InAs and GaAs is 6.9% and good crystalline epilayers over the whole composition range cannot be grown on either InAs or GaAs substrate. It is reported by Wu and Pearson[4] that satisfactory $In_{1-x}Ga_xAs$ of $1 \geq x \geq 0.8$ can be grown directly on GaAs and that of $0.3 \geq x \geq 0$ on InAs by LPE. Between $x = 0.3$ and 0.8 InP is thought to be advantageous as a substrate; the lattice matches at $x = 0.47$ and good epilayers can be grown on an InP substrate[5-7].

In this chapter, the author describes (1) the possible composition range of $In_{1-x}Ga_xAs$ grown directly on InP substrate by LPE, (2) the expansion of the composition range using $In_{0.53}Ga_{0.47}As$ as a buffer layer, (3) the composition latching phenomenon in a certain range of composition, and (4) the effects of the lattice mismatch on crystal perfection and surface morphology of the epilayer.

5-2. GROWTH PROCEDURES

Growth apparatus and material preparation are the same as described in Chapter II. The substrate is (111)B-oriented InP. The growth temperature (T_G) is 650°C, the cooling rate (T_R) is 0.15 - 0.20°C/min, and the step-cooling interval (T_S) is 0°C, unless

---

* Y. Takeda and A. Sasaki, J. Cryst. Growth, 45, 257 (1978)

otherwise specified. Some of the melt compositions used in the experiments are listed in Table 5-1. These compositions and weight ratios are calculated using Wu and Pearson's model as described in Chapter II. The composition of the grown layer is determined by x-ray diffraction using Cu $K\alpha_1$ and $K\alpha_2$ radiation and assuming Vegard's law[8].

x	N_{In}	N_{Ga}	N_{As}	W_{Ga}/W_{In}	W_{InAs}/W_{In}
0.40	0.915	0.0261	0.0592	0.0185	0.114
0.45	0.914	0.0293	0.0568	0.0208	0.110
0.47	0.914	0.0306	0.0559	0.0217	0.108
0.50	0.913	0.0327	0.0544	0.0231	0.105
0.55	0.912	0.0365	0.0518	0.0258	0.0995

Table 5-1 Some of the melt compositions at 650°C used in the experiments. N_X: atomic fraction of atom X, W_Y: weight of Y.

5-3. DIRECT GROWTH ON InP

The growth of alloy epilayers directly on InP(111)B surface is attempted from an equilibrated solution (T_S=0°C) at 650°C with a cooling interval of 5∿7°C. The solidus compositions calculated from the phase diagram (x^c) are changed between x^c =0.3 and 0.65, and a finer change is made at around x^c =0.45.

The composition of the grown layer (x) *vs.* x^c is shown in Fig. 5-1. Microphotographs of the as-grown surfaces at each composition indicated in Fig. 5-1 are shown in Figs. 5-2-a∿h.

Composition latching phenomenon is observed, *i.e.*, only x= 0.445±0.005 layers are grown from the melts of any x^c between 0.40 and 0.45. The lattice mismatch between the layer of x=0.445±0.005 and the substrate is $(1.7\pm0.3)\times10^{-3}$. The surface of the composi-

tion-latched layer is not smooth, but the thermal etch pattern of the substrate surface appears on the 10 μm thick epilayer surface as shown in Fig. 5-3-a. The surface of the substrate, shown in Fig. 5-3-b, is revealed after removal of the epilayer by ething with the A-B solution[9] at room temperature. InGaAs is selectively etched by this solution. At $x = 0.47$, where the lattice matches, these patterns do not appear even on a thin (∿1.5 μm) epilayer surface.

The layer deposited from the melt of $x^c = 0.39$ is composed of two compositions, x=0.37 and 0.44.

From the melts of $0.45 \leqq x^c \leqq 0.50$ uniform layers of the calculated composition grow, but only island growth is obtained when x^c = 0.35, 0.375 and 0.55, and no growth from $x^c = 0.30$ and 0.60.

Although the as-grown surface is smooth in the case of a small mismatch ($\sim 6.6 \times 10^{-4}$) (Fig. 5-4-a), a very large number of etch pits appear along (110) direction appear on the substrate surface under the epilayer in a sample with $x<0.47$ when it is etched with the R-C solution[10] for 10 min at 60°C (Fig. 5-4-b). In a sample $x>0.48$, no such pits appear on the substrate surface, but line imperfections in the epilayer along the cleavage direction (110) are observed after a slight etching with the A-B solution (Fig.5-4-c). In the sample of a larger x, cracks are seen in the epilayer and they penetrate into the substrate (Fig. 5-5).

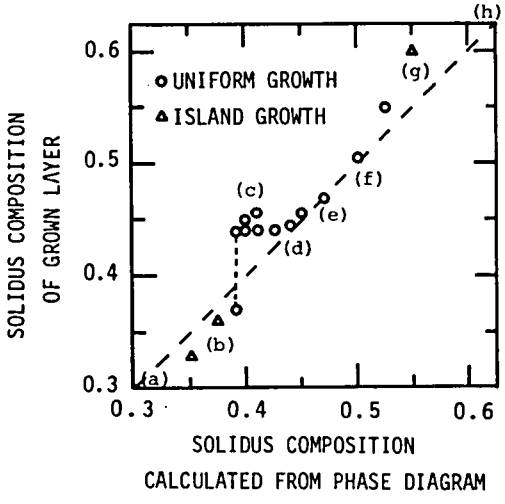

Fig. 5-1 Composition of the grown layer *vs.* solidus composition calculated from the phase diagram. (o) Uniform growth and (Δ) island growth.

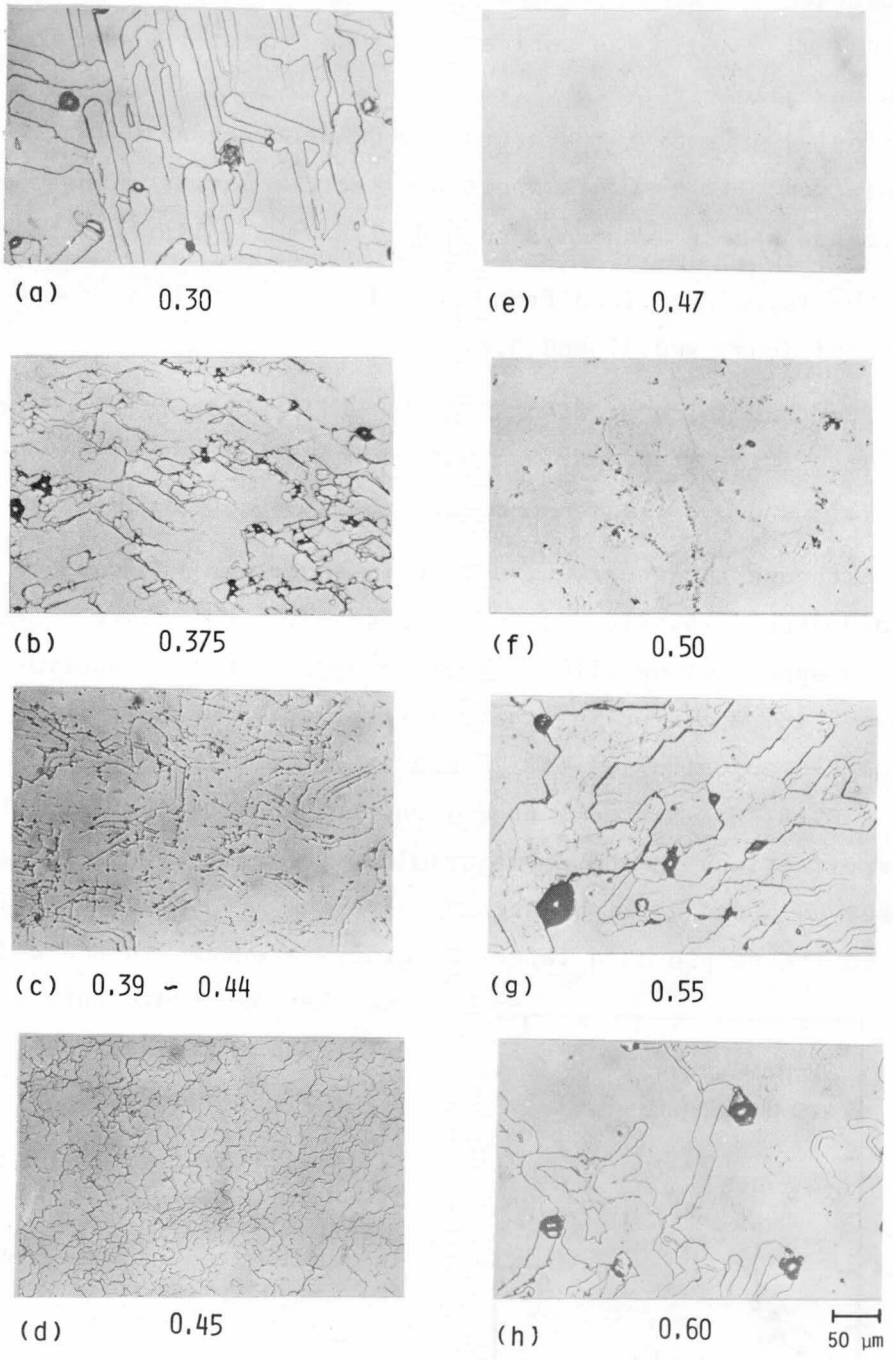

Fig. 5-2 As-grown surfaces of the epilayers at the compositions indicated in Fig. 5-1 as (a) ∿ (h). Scale is the same as (h).

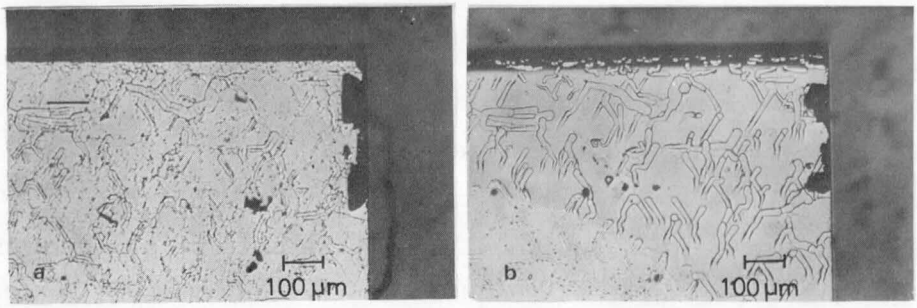

Fig. 5-3 (a) As-grown surface of a composition-latched layer. (b) The InP substrate under the layer (a).

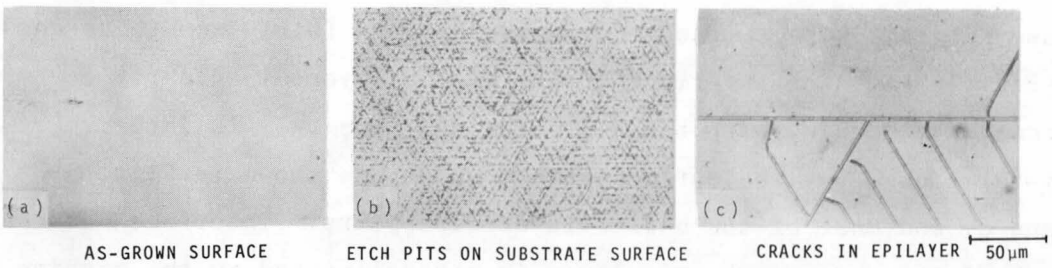

Fig. 5-4 As-grown surface is smooth as (a) when the mismatch is small, but (b) etch pits appear on the substrate surface under the epilayer with $x<0.47$ and (c) line imperfections are seen in the epilayer with $x>0.48$.

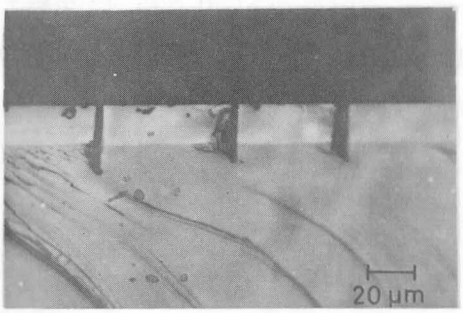

Fig. 5-5 Cracks in the epilayer which has a larger composition ($x\simeq0.5$). They penetrate into the substrate.

5-4. GROWTH ON $In_{0.53}Ga_{0.47}As$ BUFFER LAYER

$In_{1-x}Ga_xAs$($0.40 \leqq x \leqq 0.70$) epilayers are grown on $In_{0.53}Ga_{0.47}As$ ($\sim$10 μm thick) which are in turn grown on InP substrates. The temperature cycle for the growth is shown in Fig. 5-6. The growth temperature for $In_{1-x}Ga_xAs$($x \neq 0.47$) is 650°C, the same as that for the buffer layer, to avoid a supercooling of the melt of the second layer. Thus, the growth of the second layer is thought to be grown from the equilibrium liquid.

As shown in Fig. 5-7, at x^c =0.40, 0.425 and 0.50, the composition of the grown layer is almost the same as x^c and composition latching is not observed. This means that the latching in the direct growth on InP substrate is not due to the inaccuracy of the phase diagram. The surface of x=0.50 layer is fairly smooth as shown in Fig. 5-8-a. The interface of the two epilayers is clearly delineated by etching with the A-B solution. When x^c is larger, crystal grows, but the surface is not smooth as shown in Figs. 5-8-b and c, and most of the buffer layer disappears. Interface between the buffer layer and the top layer is not delineated by the etching and x=0.47 layer is not detected by the EPMA. The 0.47 layers are dissolved into the melts with larger x^c 's. The results suggest that a smaller step of composition grading is necessary to grow step-wise grading layers to keep each layer unaffected by the melt over it. An example of the step-wise composition grading, 0.525/0.50/0.47 on InP is shown in Fig. 5-9-a. The surface of 0.525 layer is much smoother than that grown directly on InP (Fig. 5-9-b). Three grown layers are seen after etching the cleaved surface with the A-B solution.

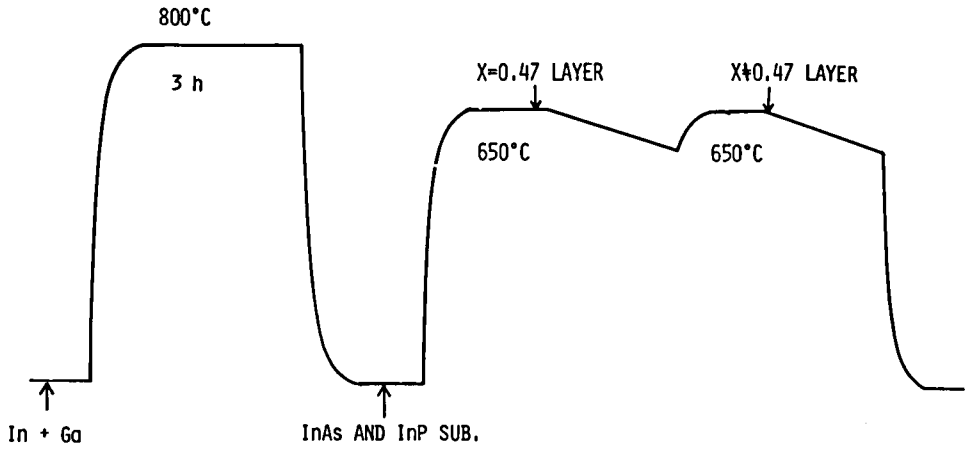

Fig. 5-6 Temperature cycle for the growth of double layers.

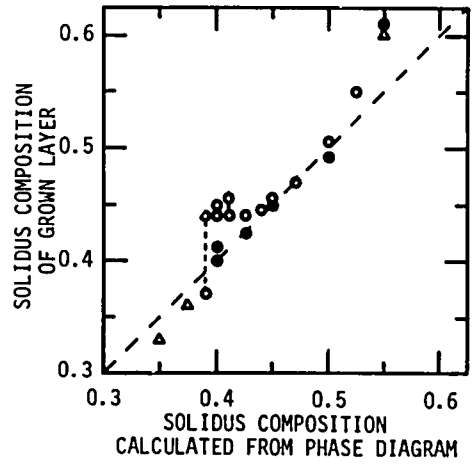

Fig. 5-7 (●) Growth on the buffer layer. Composition latching is not observed. Open circles and triangles denote the same as in Fig. 5-1.

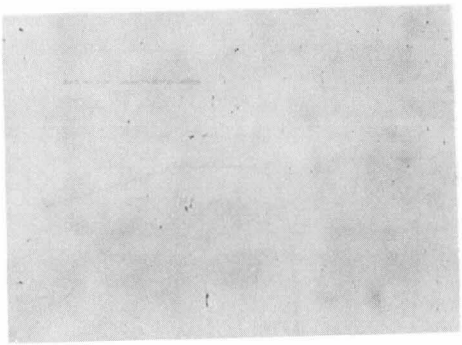

(a) 0.50 on 0.47

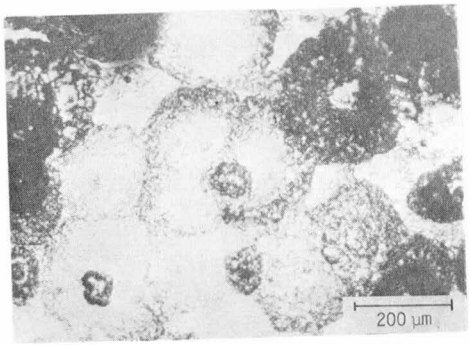

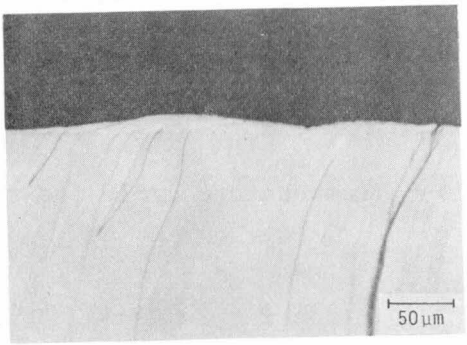

(b) 0.60 on 0.47

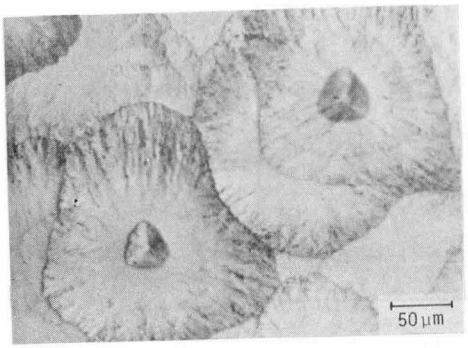

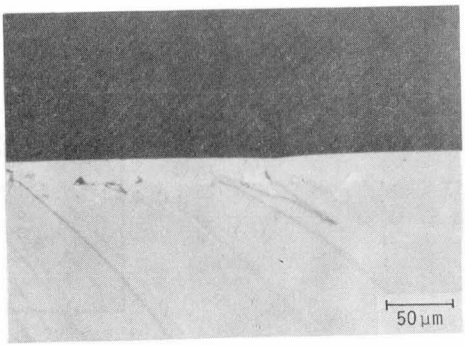

(c) 0.65 on 0.47

Fig. 5-8 (a) is the as-grown surface of x=0.50 layer on the buffer layer, and (b) and (c) are the as-grown surfaces of x=0.60 and 0.65 layers on the buffer layer, respectively.

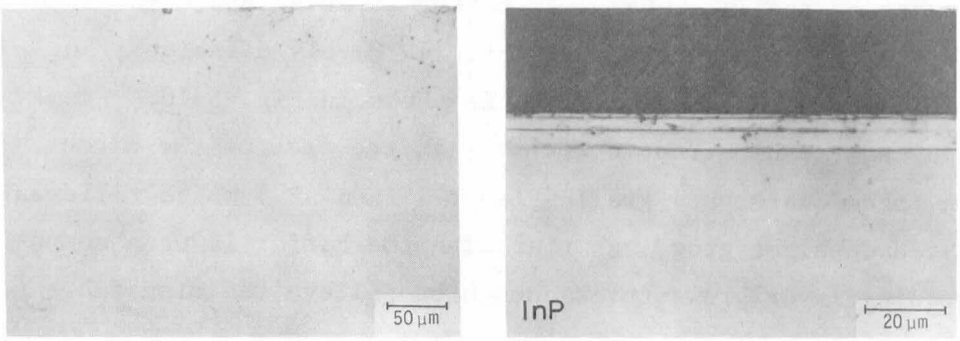

(a) 0.525 - 0.50 - 0.47

(b) 0.525 direct

Fig. 5-9 (a) The as-grown surface (left) and etched cross section (right) of 0.525 layer grown by the step-wise composition grading, and (b) the as-grown surface of 0.525 layer grown directly on InP.

5-5. COMPOSITION LATCHING PHENOMENON

Only $x=0.445\pm0.005$ layers are grown from the melt of any x^c between 0.40 and 0.45. This phenomenon is called as "composition latching phenomenon". It is not observed in the growth of $In_{1-x}Ga_xAs$ ($x\neq0.47$) on $In_{0.53}Ga_{0.47}As$ buffer layer. Additional experiments are carried out to find the difference between the two growth procedures.

When the melts of x^c =0.40 and 0.60 are contacted with the InP substrate or the $In_{0.53}Ga_{0.47}As$ buffer layer at 650°C for 30 min while keeping the temperature constant, InP hardly dissolves, but most of $In_{0.53}Ga_{0.47}As$ does dissolve as shown in Fig. 5-10. From these results it can be considered that in the case of the direct growth on InP a quaternary grading layer (InGaAsP) which relieves the mismatch does not grow, but that with the buffer layer a composition grading layer grows thick enough to relieve the mismatch.

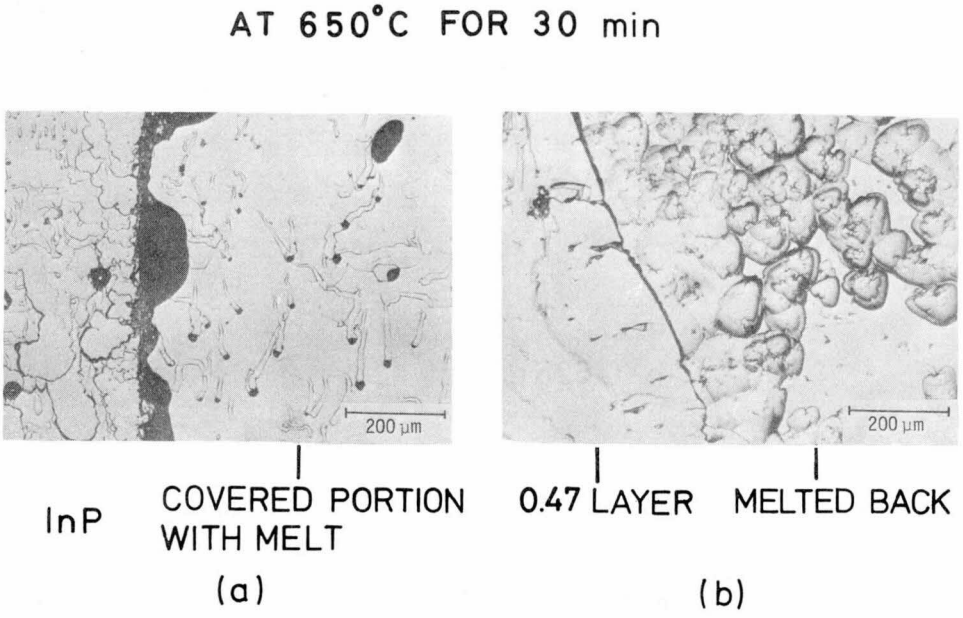

Fig. 5-10 The melts of x^c =0.40 and 0.60 does not appear to dissolve InP (a), but dissolves the $In_{0.53}Ga_{0.47}As$ layer (b).

5-5-1. Variation of Cooling Rate and Step Cooling

Keeping the melt composition and other growth conditions the same, *i.e.*, x^c =0.425, T_G=650°C, and T_S=0°C, the cooling rate (T_R) is varied between 0.20 and 1.25°C/min. The results are that when T_R<

0.25, T_R=0.40, 0.50 and T_R>0.50°C/min, the compositions x=0.44, 0.435, 0.43, and a broad composition (x=0.42∿0.47) are obtained, respectively. With T_R=0.2°C/min and other conditions unchanged, the growth with T_S=2, 3, and 5°C give x=0.43, 0.42, and two x=0.42 and 0.435, respectively.

The results indicate that the composition latching phenomenon is quite sensitive to the cooling rate and the step-cooling interval. $Ga_xIn_{1-x}P$ in which this latching was observed was grown on GaAs by the steady state LPE[11]. The conditions of a small cooling rate and a small step-cooling interval can be thought to approximate the steady state. Investigations on the latching phenomenon on other alloys and a theoretical study should be made with care for these growth conditions.

5-5-2. Variation of Growth Temperature

Growth at 700°C between x^c =0.38 and 0.48 shows a similar phenomenon, *i.e.*, only x=0.45±0.01 is obtained from the melts between x^c =0.40 and 0.45. The results are shown in Fig. 5-11. The latching phenomenon does not seem to be sensitive to the growth

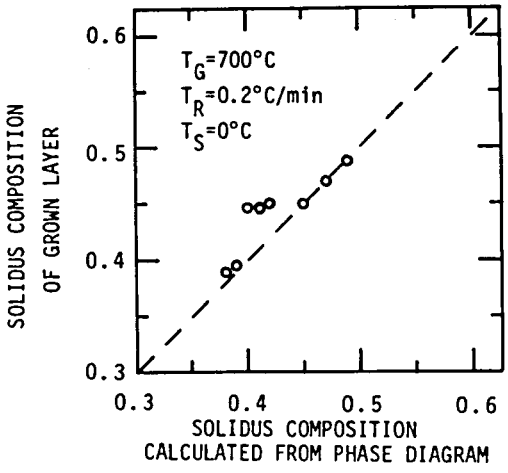

Fig. 5-11 Composition latching is observed also in the growth at 700°C.

temperature. Our results deviate from the calculated phase diagram. The phase diagram is modified to fit the experimental data. The x^c indicated above and in the figure is the corrected composition.

5-6. DISCUSSION

In a study of steady state LPE-growth of $Ga_xIn_{1-x}P$ on (111)B-oriented GaAs substrate, Stringfellow observed that growth from liquidus with a certain range of compositions produced the same solid composition x=0.51, that is the composition latching, as shown in Fig. 5-12[11]. Other people have reported similar phenomenon in the LPE-growth of $Ga_xIn_{1-x}P$ on (100)-oriented GaAs[12] and on (111)B-oriented $Ga_yAl_{1-y}As$ substrate[13].

On the other hand, in the case of LPE-growth of $In_{1-x}Ga_xAs$, the composition latching phenomenon is observed only on the smaller composition side, where the strain in the epilayer is compressive. The tensile strain in the epilayer on the larger composition side may be relieved by microcrack formation along the cleavage direction, (110), and composition latching does not occur. No cracks are observed in the islands which are grown from the melt of x^c =0.55 and

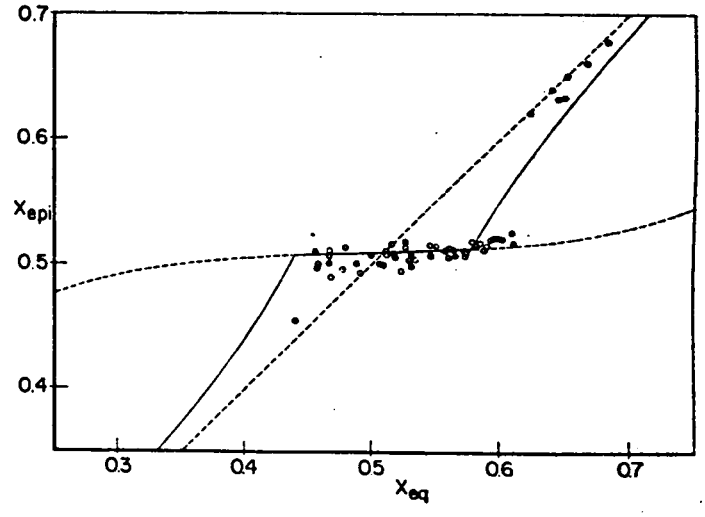

Fig. 5-12 Composition latching was observed in LPE-growth of GaInP on GaAs substrate.

have a solidus composition x=0.61∿0.62. The strain energy due to the mismatch as large as 9.7×10^{-3} seems to have not allowed formation of a continuous layer. Growth and stress characteristics in the $In_{1-x}Ga_xAs$ layer on InP is schematically drawn in Fig. 5-13.

In the layers with x between 0.45 and 0.49, a tetragonal distortion[14] of the lattice parameter may occur as discussed in §3-3-6. The distortion comes about from the strain caused by the lattice mismatch in the interfacial plane. Y. Kawamura and H. Okamoto have very recently reported that more than 80% of the total mismatch is accomodated by the elastic strain and 20% of it by the misfit dislocations in the MBE(molecular-beam epitaxy)-grown $In_{1-x}Ga_xAs$ on InP[14]. The same distortion would be expected in LPE-grown $In_{1-x}Ga_xAs$ on InP and the mismatch would be accomodated by it in the layers of x between 0.45 and 0.49. Smooth surface of the

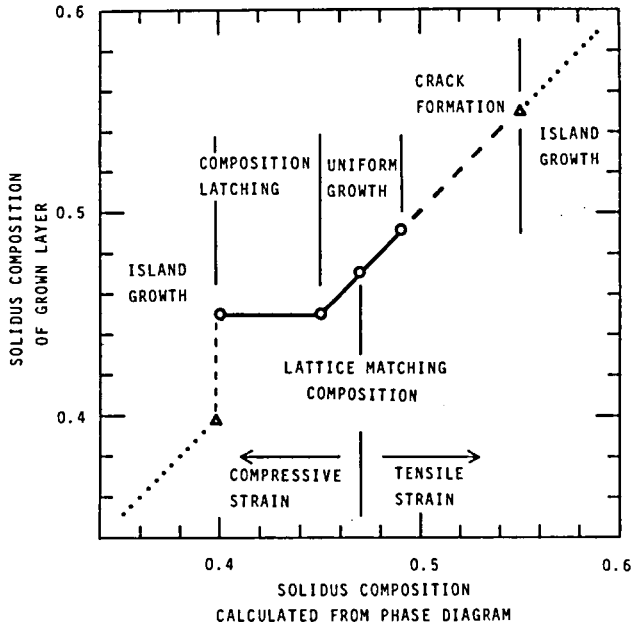

Fig. 5-13 Schematic diagram of the growth and strain characteristics in the LPE-growth of $In_{1-x}Ga_xAs$ layers on InP. Strains indicated are in the epilayer.

layers may be an evidence that misfit dislocations (a large number of them degrade the surface morphology) play a minor roll in the strain accomodation.

Continuous layers of x between 0.49 and 0.55 are obtained, but many cracks are observed as shown in Fig. 5-4 and 5-5. The critical value of misfit strain necessary for the onset of cracking in deposits of $Ga_xIn_{1-x}P$ on GaAs was found to be $\sim 3\times10^{-3}$ [15]. The misfit strain at x=0.49 in $In_{1-x}Ga_xAs$ is $\sim 1.3\times10^{-3}$. The value might depend on the mechanical strength of the materials.

In the smaller composition side than x^c =0.45, where the strain is compressive, there is no such a mechanism as crack formation to accomodate a large misfit strain. The strain will be relieved by introducing a large number of dislocations or shifting the equilibrium solidus composition. In the growth of $In_{1-x}Ga_xAs$ on InP both phenomena are observed. Thermal etch pattern which appeared on the surface of composition latched layers is due to the misfit dislocations originated from the interface between the layer and the substrate. A part of the strain is accomodated by the dislocations and the rest of it by shifting the equilibrium solidus composition, and it resulted in the composition latching around 0.45. That would be an explanation of the observed phenomena.

5-7. SUMMARY

1) The composition is latched in the LPE-growth of $In_{1-x}Ga_xAs$ on the InP substrate at T_G=650°C and 700°C with a small cooling rate and a small step-cooling interval.

2) The latching does not occur on the larger composition side relative to the lattice matching composition of x=0.47, but on the smaller side.

3) The layer with the composition in the range from x=0.45 and 0.50 deposits uniformly.

4) Island growth is obtained at $x^c \leqq 0.375$ and $x^c \geqq 0.55$.

5) An $In_{0.53}Ga_{0.47}As$ buffer layer between $In_{1-x}Ga_xAs$ ($x \neq 0.47$) and InP seems to relieve the mismatch energy forming a composition grading layer to allow the growth of a wider range of composition from x=0.40 to 0.70.

6) Fairly good layer of x=0.525 is obtained by a step-wise composition grading.

References

[1] M. B. Panish and S. Sumski, J. Phys. Chem. Solids, 30, 129 (1969)

[2] S. J. Anderson, F. Scholl, and J. S. Harris, in *Gallium Arsenide and Related Compounds*, 1976 Conference, Series 33b (Institue of Physics, London, 1977) p. 346

[3] H. P. Kleinknecht and A. E. Widmer, J. Appl. Phys., 45, 3453 (1974)

[4] T. Y. Wu and G. L. Pearson, J. Phys. Chem. Solids, 33, 409 (1972)

[5] Y. Takeda, A. Sasaki, Y. Imamura, and T. Takagi, J. Appl. Phys., 47, 5405 (1976)

[6] Y. Takeda, A. Sasaki, Y. Imamura, and T. Takagi, J. Electrochem. Soc., 125, 130 (1978)

[7] R. Sankaran, R. L. Moon, and G. A. Antypas, J. Cryst. Growth, 33, 271 (1976)

[8] J. C. Woolley and B. A. Smith, Proc. Phys. Soc., (London) 72, 214 (1958)

[9] M. S. Abrahams and C. J. Buiocchi, J. Appl. Phys., 36, 2855 (1965)

[10] J. L. Richards and A. J. Crocker, J. Appl. Phys., 31, 611 (1960)

[11] G. B. Stringfellow, J. Appl. Phys., 43, 3455 (1972)

[12] W. R. Hitchens, N. Holonyak, Jr., M. H. Lee, and J. C. Campbell, J. Cryst. Growth, 27, 154 (1974)

[13] H. Beneking, N. Grote, P. Mischel, and G. Schul, in *Gallium Arseinde and Related Compounds*, 1974 Conference, Series 24

(Institute of Physics, London, 1975) p. 113

[14] Y. Kawamura and H. Okamoto, Spring Meet. of Japan. Soc. Appl. Phys. and Related Socs., Tokyo, March 1979, 29a-H-7 (in Japanese)

[15] G. H. Olsen and M. Ettenberg, "Growth Effects in the Heteroepitaxy of III-V Compounds," in *Crystal Growth - Theory and Techniques* edited by C. H. L. Goodman (Plenum, New York, 1978) Vol. 2

VI. ENERGY GAP OF $In_{0.53}Ga_{0.47}As$*

6-1. INTRODUCTION

Although the energy gap E_g is one of the most important fundamental parameters of a semiconductor, there has been a large scatter in the reported values of the E_g of $In_{1-x}Ga_xAs$[1-7]. The highest is 0.91 eV and the lowest is about 0.60 eV at around x=0.5 as can be seen in Fig. 6-1. In one paper the energy gap was taken as the energy at half maximum transmission. In other samples the composition was not homogeneous enough to evaluate the energy gap or the lattice matching was not good enough to be free from the lattice strain

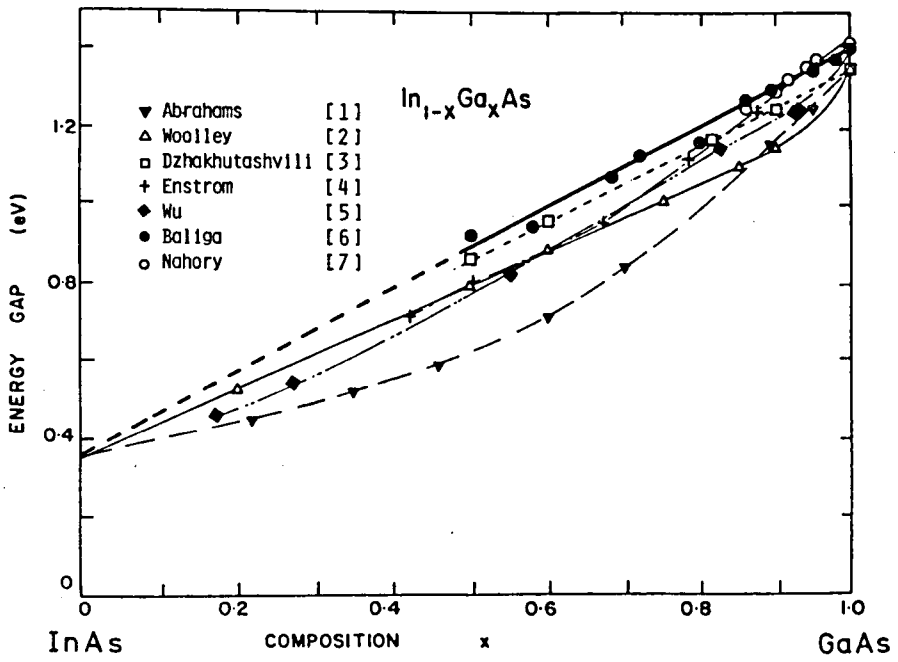

Fig. 6-1 Reported values of energy gap of $In_{1-x}Ga_xAs$. There is a large scatter.

* Y. Takeda, A. Sasaki, Y. Imamura, and T. Takagi, J. Appl. Phys., 47, 5405 (1976)

which varies the energy gap. Therefore, it must be carefully carried out to determine the true value of the energy gap of $In_{1-x}Ga_xAs$ which is free from the composition inhomogeneity and lattice strain.

In this chapter, the energy gap of $In_{0.53}Ga_{0.47}As$ is determined accurately. The composition is confirmed to be very homogeneous along and over the layer by the EPMA and the PL measurements, as shown in Chapter III, §3-3. The electron Hall mobility of $In_{0.53}Ga_{0.47}As$ is as high as 8 500 cm^2/Vsec at RT which is one of the highest ever reported[8-9]. The steep change of the absorption spectrum is shown. The calculation of the intrinsic carrier concentration in this alloy is described. Discussion on the energy gap determination and bowing parameters are also given here.

6-2. INFRARED TRANSMISSION

The infrared transmission, t, and reflectivity, r, spectrum of the grown layer with the InP substrate are measured between 0.70 and 1.45 μm by a double beam spectrometer[i] at 294 K. The transmission spectrum changes steeply near the absorption edge of the alloy as shown in Fig. 6-2. The absorption coefficient, α, is calculated with the measured values of transmission and reflectivity, using the equations[10]:

$$t = \frac{(1-R)^2 \exp(-\alpha d)}{1-R^2\exp(-2\alpha d)} \quad , \qquad r = R\,[\,1 + t\exp(-\alpha d)\,]$$

where R is the reflectivity of a semi-infinitely thick sample and d is the sample thickness. It can be used in the calculation that the reflectivity of the grown layer and the substrate are the same, and that InP is transparent in the vicinity of the absorption edge of the alloy.

---

i) MPS-50L, Shimadzu Corp.

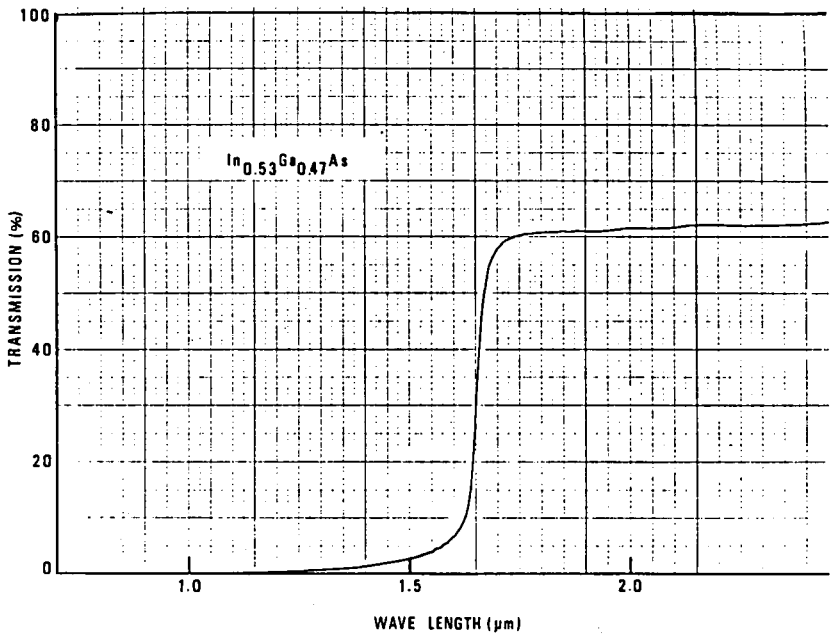

Fig. 6-2 Infrared transmission spectrum of $In_{0.53}Ga_{0.47}As$. It changes steeply near the absorption edge.

6-3. ENERGY GAP

The energy gap E_g of this high quality material is determined from the photon-energy dependence of the absorption coefficient. The result is shown in Fig. 6-3 with the PL spectrum measured in the same sample at 294 K. The calculated absorption coefficient agrees well along the curve of

$$\alpha \propto (h\nu)^{-1}(h\nu - 0.750)^{\frac{1}{2}}$$

in the range of $0.750 \sim 0.82$ eV. It is evident from the photon-energy dependence of the absorption coefficient that the alloy is the direct gap semiconductor as expected.

The PL spectrum peaks at 0.749 eV, a little lower than the

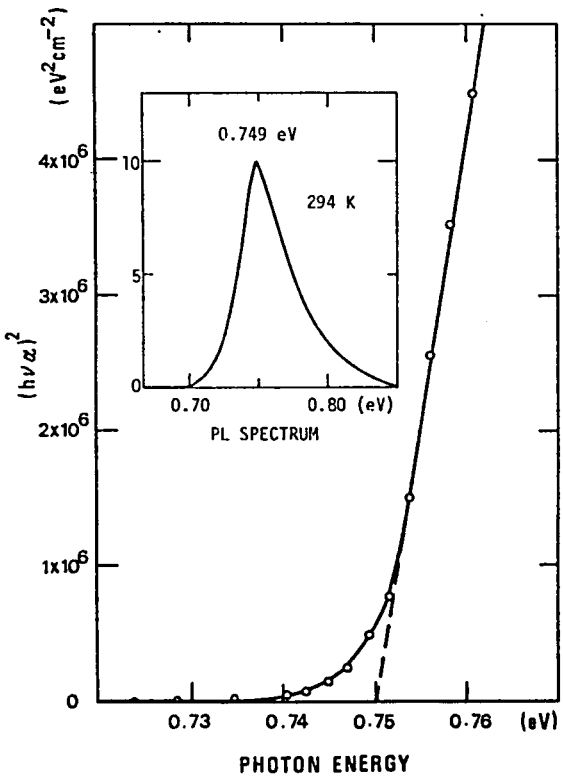

Fig. 6-3 Determination of the energy gap from the absorption coefficient. Intersection of the broken line with the abscissa corresponds to the optical energy gap E_g. The PL spectrum is given in the inset where the intensity is shown in arbitrary unit.

energy gap. When the radiative recombination is a band-impurity transition, the intensity has been given by

$$I \propto (h\nu - E_g + E_i)^{\frac{1}{2}} \exp[-(h\nu - E_g + E_i)/k_B T],$$

and the photon energy at peak by

$$h\nu = E_g - E_i + \frac{1}{2}k_B T,$$

where E_i is the impurity level, k_B is the Boltzmann constant, and T is the temperature[11]. At 294 K, using E_g=0.750 eV and $h\nu$=0.749 eV, E_i is calculated to be 14 meV. The energy diagram and the PL spectrum are shown in Fig. 6-4. On the other hand, from the temperature dependence of the PL intensity measured in this material between 4.2

and 77 K, the estimation of the activation energy[12] gives ∿13 meV. as shown in Fig. 6-5.

Thus, the energy gap of this high-quality material is determined to be 0.750 eV at RT.

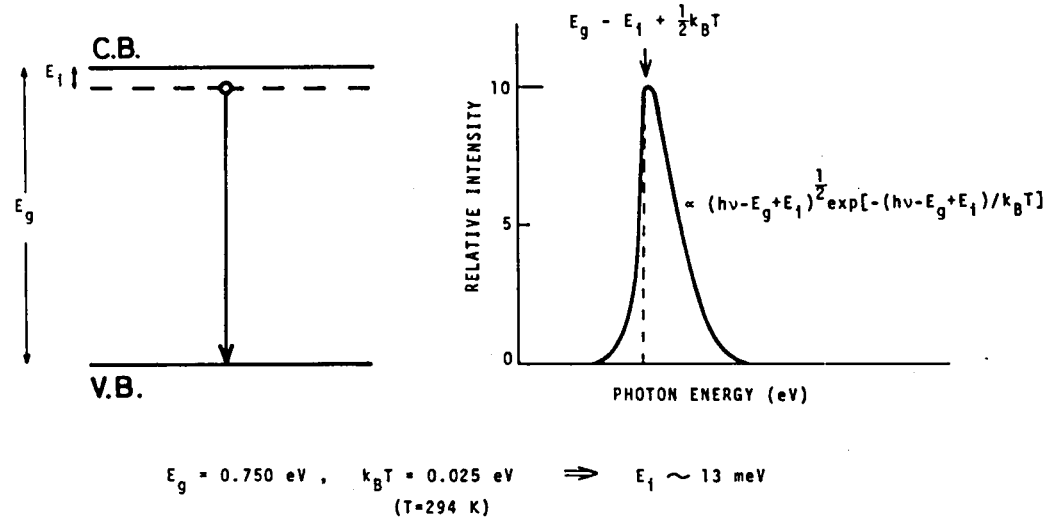

Fig. 6-4 The energy diagram and the PL spectrum.

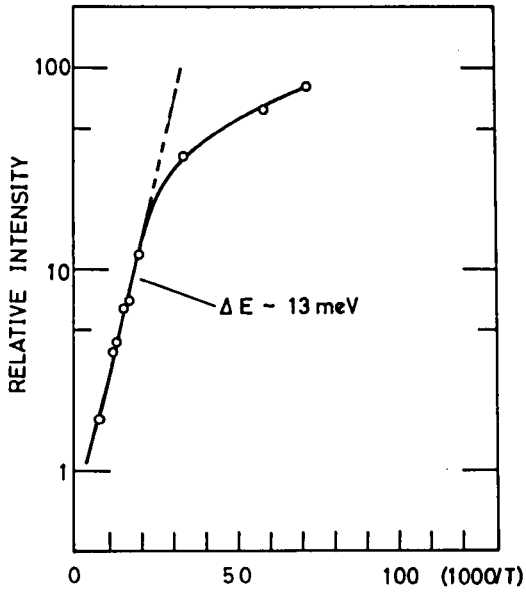

Fig. 6-5 Temperature dependence of the PL intensity. The activation energy is estimated to be ∿13 meV.

6-4. INTRINSIC CARRIER CONCENTRATION

A semiconductor is generally used in the extrinsic state. A semiconductor is extrinsic when the excess carrier concentration is greater than the intrinsic carrier concentration n_i. The n_i can be calculated with an energy gap E_g, density-of-state effective masses for electron m_{de} and hole m_{dh}, and a temperature T:

$$n_i = 4.83\times10^{15}\left(\frac{m_{de}m_{dh}}{m_o^2}\right)^{\frac{3}{4}} T^{\frac{3}{2}} \exp\left(-\frac{E_g}{2k_BT}\right)$$

where m_o is the free-electron mass. In the calculation the reported value of $m_{de} = 0.043\, m_o$ [13] and the measured value of $E_g = 0.75$ eV are used. Here, m_{dh} is equal to $\left(m_{lh}^{\frac{3}{2}} + m_{hh}^{\frac{3}{2}}\right)^{\frac{2}{3}}$, where m_{lh} is the light-hole effective mass and m_{hh} the heavy-hole effective mass[14]. The values of m_{lh} and m_{hh} of $In_{0.53}Ga_{0.47}As$ are calculated from the assumed linear dependence of them on composition. Thus, the m_{dh} of $In_{0.53}Ga_{0.47}As$ is obtained to be $0.44\, m_o$.

The n_i's for $In_{0.53}Ga_{0.47}As$, Ge, Si, and GaAs at 300 and 400 K are listed in Table 6-1. The n_i of $In_{0.53}Ga_{0.47}As$ comes between those of Ge and Si. The value can be thought low enough for use at RT as a device which has extrinsic carrier concentration of $1\times10^{16} \sim 1\times10^{17}$ cm^{-3}. Therefore, this semiconductor has a large energy gap sufficient to be used at RT.

	$In_{0.53}Ga_{0.47}As$	Ge	Si	GaAs
300 K	6.4×10^{11}	1.9×10^{13}	1.6×10^{10}	1.1×10^{7}
400 K	3.7×10^{13}	7.5×10^{14}	5.5×10^{12}	1.7×10^{10}

INTRINSIC CARRIER CONCENTRATION (cm^{-3})

Table 6-1 Intrinsic carrier concentration in $In_{0.53}Ga_{0.47}As$, Ge, Si, and GaAs.

6-5. DISCUSSION

The energy gap of $In_{0.53}Ga_{0.47}As$ determined here is the most accurate value ever reported and has settled the scattered values in the energy gap. The composition of the alloy is examined to be very homogeneous. The lattice is closely matched to that of InP and free from strain (except for a slight strain due to the difference of the thermal expansion coefficient between the alloy and the substrate InP). The energy gap is determined from the photon energy dependence of the absorption coefficient. Moreover, the electron mobility of the alloy is as high as 8 500 cm^2/Vsec, indicating the high quality of the material. The energy gap of $In_{0.53}Ga_{0.47}As$ reported[15,16] after us agrees with the value determined here.

An example of mis-evaluation of the energy gap is illustrated here. Since the alloy is the direct-gap semiconductor, the absorption coefficient is very large in the photon energy region higher than the band gap energy, *e.g.*, the alloy is highly absorptive. If the alloy is composed of two layers, for example, one layer has E_g= 0.75 eV and another has E_g=0. 50 eV, the transmission spectrum of the alloy would represent that of the layer with E_g=0.50 eV. Fig. 6-6 is the transmission spectrum of InGaAs with the quasi-grown layer(see Chapter IV). With successive etching the steep portion in the spectrum shifts toward shorter wavelength, and finally reaches to that of $In_{0.53}Ga_{0.47}As$. The quasi-grown layer concealed the energy gap of the actual layer. In the determination of the energy gap, the homogeneity of the composition must be examined carefully.

The "bowing" of the energy gap as a function of the alloy composition is commonly observed in III-V ternary alloys[17], and often approximated with the quadratic composition dependence, $E_g(x)= a+bx+cx^2$ or alternatively $E_g(x)= E_1+(E_2-E_1)x+c(x^2-x)$, where E_1 and E_2 are the energy gaps of two binary semiconductors and c is the "bowing parameter ". A. G. Thompson and J. C. Woolley[18] proposed

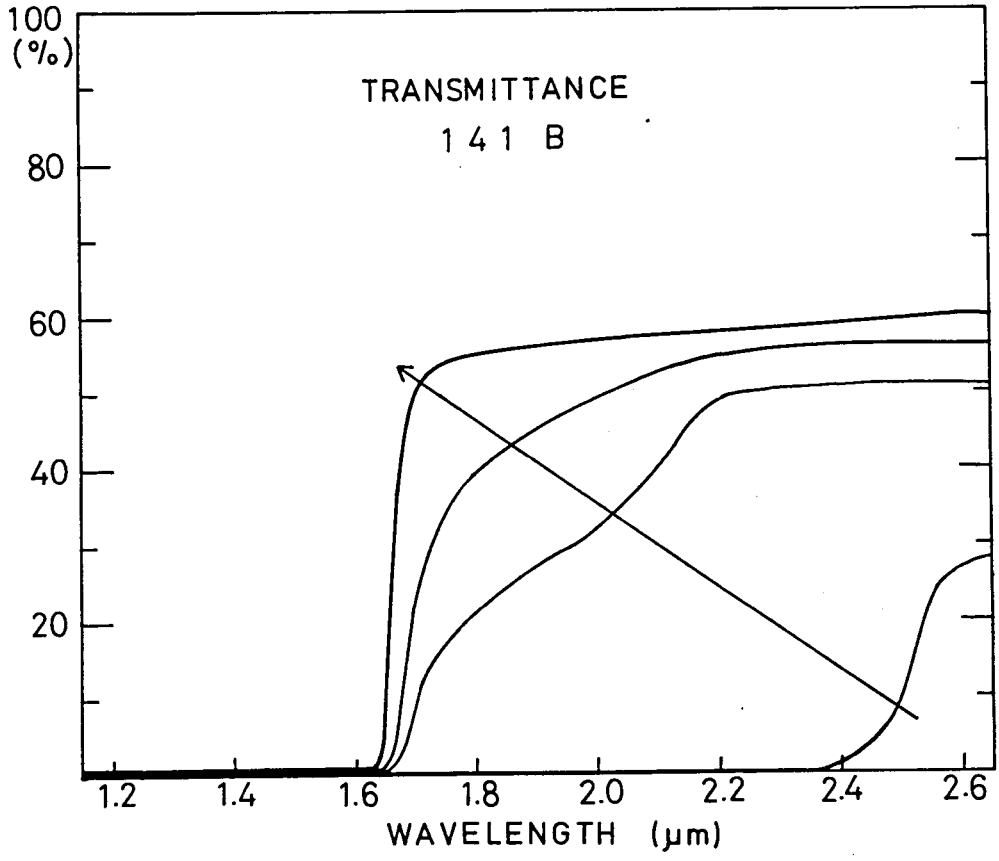

Fig. 6-6 Transmission spectrum of the alloy with a quasi-grown layer changes after successive etching.

empirical rules for the composition dependence of the energy gap of ternary alloys, after investigating the experimental data ever reported at that time. For the III-V ternary alloys they proposed that the bowing parameter, c, is given by $0.3/\sqrt{(E_1+E_2)/2}$.

On the other hand, J. A. Van Vechten and T. K. Bergstresser calculated the bowing parameter using the dielectric model[19]. They proposed that the total bowing parameter, c, should be the sum of the intrinsic bowing c_i which is found in the virtual-crystal approximation[20] and the extrinsic bowing c_e due to the effect of

disorder:

$$c = c_i + c_e$$

For $In_{1-x}Ga_xAs$ c_i=0.28 and c_e=0.29 were calculated.

The two equations at RT are summarized below along with the empirical equation determined from the value obtained in this chapter. The energy gaps of InAs and GaAs are found in Ref. 21 to be 0.356 eV and 1.428 eV, respectively.

Thompson and Woolley

$$E_g(x) = 0.356 + 1.072x + 0.318(x^2 - x)$$

Van Vechten and Bergstresser

$$E_g(x) = 0.356 + 1.072x + 0.57(x^2 - x)$$

$$c = 0.28 + 0.29$$
$$c_i \quad c_e$$

This study

$$E_g(x) = 0.356 + 1.072x + 0.437(x^2 - x)$$

There is an arbitrariness in the determination of c_e in Van Vechten's calculation, which was based on the largest value of $ZnS_{1-x}Te_x$ alloy. In comparison of the author's curve with the theoretical one, it would be said that $In_{0.53}Ga_{0.47}As$ on InP is somewhat nearer to the virtual-crystal approximation, *i.e.*, the effect of aperiodicity or disorder on the energy gap is smaller than that expected for the $ZnS_{1-x}Te_x$ alloy. Some of the theoretical analyses based on or compared with the experimental data obtained from low quality alloys would be modified by the new data of high quality alloys.

The strain due to the lattice mismatch shifts the energy gap, since the uniaxial or hydrostatic pressure is known to shift the band edge through the deformation of the lattice[22]. There has

been no experiments of the effects of the strain due to the lattice mismatch, uniaxial, or hydrostatic pressure on the band edge shift in $In_{1-x}Ga_xAs$. In other alloys such as AlGaAs[23], the hydrostatic pressure effects have been investigated. Very recently, G. H. Olsen *et. al.* measured the variation of energy gap shift with the elastic strain due to lattice mismatch in VPE-grown InGaP/GaAs system[24]. They found as large as ∿15 meV of the shift in the compressed InGaP layer which has a lattice mismatch greater than 0.4%. Since $In_{1-x}Ga_xAs$ ($x \simeq 0.5$) grown on GaAs has as large as ∿3.5% of lattice mismatch, the shift of the band gap would be greater, unless the strain is relieved. The author suspects that the high energy gap in VPE-grown $In_{1-x}Ga_xAs$ on GaAs[6] would be resulted from the energy gap shift due to the large strain in the $In_{1-x}Ga_xAs$ layer.

6-6. SUMMARY

1) The infrared transmission spectrum of $In_{0.53}Ga_{0.47}As$ changes steeply near the absorption edge, indicating good composition homogeneity and crystal quality of the alloy.

2) The energy gap of $In_{0.53}Ga_{0.47}As$ has been determined to be 0.75 eV at RT from the photon-energy dependence of the absorption coefficient.

3) The value of E_g is consistent with the PL measurement.

4) The intrinsic carrier concentration has been calculated to be 6.4×10^{11} cm^{-3} at RT.

5) Composition inhomogeneity and lattice strain in the layer should be eliminated in the determination of the energy gap, especially of alloys.

References

[1] M. S. Abrahams, R. Braunstein, and F. D. Rosi, J. Phys. Chem. Solids, 10, 204 (1959)

[2] J. C. Woolley, C. M. Gillett, and J. A. Evans, Proc. Phys. Soc. (London) 77, 700 (1961)

[3] T. V. Dzhakhutashvili, A. A. Mirtskhulava, L. G. Sakvarededidze, A. L. Shkol'nik, and M. S. Matinova, Sov. Phys.-Semicond., 5, 190 (1971)

[4] R. E. Enstrom, D. Richman, M. S. Abrahams, J. R. Appert, D. G. Fisher, A. H. Sommer, and B. F. Williams, in *Gallium Arsenide and Related Compounds,* 1970 Conference, Series 9 (Institute of Physics, London, 1971) p. 30

[5] T. Y. Wu and G. L. Pearson, J. Phys. Chem. Solids, 33, 409 (1972)

[6] B. J. Baliga and S. K. Ghandhi, J. Electrochem. Soc., 122, 683 (1975)

[7] R. E. Nahory, M. A. Pollack, and J. C. DeWinter, J. Appl. Phys., 46, 775 (1975)

[8] Y. Takeda, A. Sasaki, Y. Imamura, and T. Takagi, J. Appl. Phys., 47, 5405 (1976)

[9] R. Sankaran, R. L. Moon, and G. A. Antypas, J. Cryst. Growth, 33, 271 (1976)

[10] P. A. Scumann, Jr., W. A. Keenan, A. H. Tong, H. H. Gegenworth, and C. P. Schneider, J. Electrochem. Soc., 118, 145 (1971)

[11] E. W. Williams and H. B. Bebb, in *Semiconductors and Semimetals* edited by R. K. Willardson and A. C. Beer (Academic Press, New York, 1972) Vol. 8, p. 331

[12] E. H. Bogardus and H. B. Bebb, Phys. Rev., 176, 993 (1968)

[13] M. B. Thomas and J. C. Woolley, Canad. J. Phys., 49, 2052 (1971)
E. H. Perea, E. Mendez, and C. G. Fonstad, 21st Electron. Mater. Conf., Boulder, 1979, L-4

[14] R. A. Smith, *Semiconductors* Cambridge at the University Press, (1959)
S. M. Sze, *Physics of Semiconductor Devices* (John-Wiley & Sons, New York, 1969) p. 27

[15] K. Nakajima, A. Yamaguchi, K. Akita, and T. Kotani, J. Appl. Phys., 49, 5944 (1978) and references therein.

[16] R. E. Nahory, M. A. Pollack, and W. D. Johnston, Jr., Appl. Phys. Lett., 33, 659 (1978)

[17] See for example, O. Madelung, *Physics of III-V Compounds* (John-Wiley & Sons, New York, 1964), and for recent reviews, H. Kressel and J. K. Butler, *Semiconductor Lasers and Heterojunction LEDs* (Academic Press, New York, 1977), and H. C. Casey, Jr. and M. B. Panish, *Heterostructure Lasers* (Academic Press, New York, 1978) Part B.

[18] A. G. Thompson and J. C. Woolley, Canad. J. Phys., 45, 255 (1967)

[19] J. A. Van Vechten and T. K. Bergstresser, Phys. Rev., B8, 3351 (1970)

[20] In the virtual-crystal approximation there is no aperiodicity and the parameters are the average of two end materials, see L. Nordheim, Ann. Physik, 9, 607 and 641 (1931)

[21] M. Neuberger, *III-V Semiconducting Compounds, Handbook of Electronic Materials* (IFI/Plenum, New York, 1971) Vol. 2

[22] See for example, J. I. Pankove, *Optical Processes in Semiconductors* (Prentice-Hall, New Jersey, 1971) chapter 2

[23] T. Sugeta, A. Majerfeld, A. K. Saxena, and P. N. Robson, Appl. Phys. Lett., 31, 842 (1977)

[24] G. H. Olsen, C. J. Nuese, and R. T. Smith, J. Appl. Phys., 49, 5523 (1978)

VII. HALL MOBILITY AND HALL FACTOR OF TERNARY ALLOYS*

7-1. INTRODUCTION

The scattering mechanisms in semiconductors have been very often analysed by comparing the measured mobility with the theoretically calculated mobility, taking several possible scattering mechanisms into account. The mobility obtained through experiments are in most cases the Hall mobility (μ_H) measured under the applied magnetic field. On the other hand, most of the calculated mobility are, because of simplicity of the calculation, the drift mobility (μ_D), and in the comparison it has been often assumed that the Hall factor $\gamma_H \equiv \mu_H/\mu_D$ is equal to unity. However, the ratio μ_H/μ_D is $1.1 \sim 1.3$ at temperatures between 77 and 300 K. In a precise analysis of the scattering mechanisms, the difference between the Hall mobility and the drift mobility cannot be neglected.

In this chapter, the author shows theoretical calculations of the electron Hall mobility and Hall factors of $In_{1-x}Ga_xAs$ and $InAs_{1-x}P_x$. Theoretical and experimental results are discussed, taking $In_{0.53}Ga_{0.47}As$ as an example.

7-2. SOLUTION OF THE BOLTZMANN EQUATION BY ITERATIVE METHOD

The iterative method of solution of the Boltzmann equation by D. L. Rode[1] is applied to the calculations in this chapter.

Non-parabolicity of the conduction band at $\vec{k}=(0,0,0)$ with the spin-orbit splitting $\Delta=0$ is expressed by the sub-parabolic E-k relation:

$$E = E_o + (\alpha - 1)\frac{1}{2}E_g$$

---

* Y. Takeda and A. Sasaki, Japan. J. Appl. Phys. (submitted)

where E is the energy measured upward from the conduction band edge at $\vec{k}=(0,0,0)$, E_o is equal to $\hbar k^2/2m_o$, m_o is the free-electron mass, $\alpha^2 = 1 + 4E_o(m_o - m^*)/m^*E_g$, m^* is the electron effective mass at $\vec{k}=(0,0,0)$, and E_g is the effective-mass energy gap[2]. The p-function admixture in the electron wave function is expressed by the coefficient c of the p-function through the relations in the Δ=0 approximation:

$$2a^2 = 1 + 1/\alpha, \quad a^2 + c^2 = 1$$

where a is the coefficient of the s-function. The effective-mass energy gap is temperature dependent:

$$E_g(T) = E_g(0) - 3\ell T \left(\frac{\partial E_g}{\partial P}\right)_T / K$$

where ℓ is the linear coefficient of thermal expansion, $\left(\frac{\partial E_g}{\partial P}\right)_T$ is the rate of change of the band gap with pressure, and K is the compressibility. Experimentally determined electron effective mass ($0.043 m_o$) [3,4], energy gap at 0 K (0.810 eV) [5], lattice parameter (5.868 Å), and the linear coefficient of thermal expansion (5.66×10^{-6} K^{-1})[6] of $In_{0.53}Ga_{0.47}As$ are used. Other parameters are assumed to be a linear function of composition. Temperature dependence of the lattice parameter and the effective-mass energy gap are taken into account, but other parameters are assumed to be independent of temperature.

The scattering mechanisms included are polar-optical phonon, acoustic phonon, piezoelectric, ionized impurity, and alloy scattering. There have been many interpretations and expressions of the alloy scattering, but it is still in question. The alloy scattering by Brooks[7] is tentatively used here, taking the potential difference $\Delta U = 1.072$ eV.

The distribution function in the presence of a small electric field $\vec{F}$ is given by

$$f(\vec{k}) = f_o(k) + x\,g(k)$$

where x is the cosine of the angle between $\vec{k}$ and $\vec{F}$, $f_o(k)$ is the equilibrium Boltzmann distribution, and $g(k)$ is the perturbation distribution. The drift mobility μ_D is by definition:

$$\mu_D = \frac{\vec{j}}{en\vec{F}} = \frac{1}{n}\frac{V}{3\pi^2}\int_0^\infty \frac{\hbar k^3}{Fm_o d} g(k)dk$$

$$n = \frac{2V}{8\pi^3}\int f(\vec{k})d\vec{k} = \frac{V}{4\pi^3}\int f_o(\vec{k})d\vec{k}, \quad d = 1 + (m_o - m^*)/m^*\alpha$$

With the normalization condition $\int f_o d\vec{k} = 1$, μ_D is written as

$$\mu_D = \frac{4\pi}{3}\frac{\hbar}{m_o}\int_0^\infty \frac{g(k)}{Fd} k^3 dk$$

$g(k)$ is obtained by the iterative method as shown below. The total scattering rate S_o is

$$S_o = S_{opo} + S_{ac} + S_{pe} + S_{al} + S_{ii}$$

where S_{opo} is the isotropic part (in momentum space) of the scattering rate due to polar-optical phonon scattering, S_{ac} due to acoustic phonon scattering, S_{pe} due to piezoelectric scattering, S_{al} due to alloy scattering, and S_{ii} due to ionized impurity scattering. The perturbation distribution function g is

$$g(k) = \frac{S^+_{ipo} g(k^+) + S^-_{ipo} g(k^-) - \frac{eF}{\hbar}\frac{\partial f_o}{\partial k}}{S_o}$$

In the equation, + and - corresponds to scattering-in from the differential element $d\vec{k}$ by phonon absorption and by phonon emission, respectively. $S^{\pm}_{ipo}$ is the scattering-in rate and $\pm$ signifies that S_{ipo} is evaluated at $k^{\pm}$.

The perturbation distribution can be found by numerical

iteration. The zeroth-iteration $g_o(k)$ is zero for all k. Then, the first-iteration becomes

$$g_1(k) = -\frac{eF}{\hbar S_o}\frac{\partial f_o}{\partial k} \qquad \text{----------(*)}$$

and in general

$$g_{i+1} = \frac{S^+_{ipo}\, g_i(k^+) + S^-_{iop}\, g_i(k^-) - \frac{eF}{\hbar}\frac{\partial f_o}{\partial k}}{S_o}$$

(*) is the usual result for a relaxation approximation. With increasing number of iterations, the perturbation distribution approaches to the correct distribution. In the calculations here 10 ∿ 12 iterations are carried out and the results are within 0.1% error.

The distribution function in the presence both of a small electric field $\vec{F}$ and magnetic field $\vec{B}$ is given by

$$f(\vec{k}) = f_o(k) + x\, g(k) + y\, h(k)$$

where y is the direction cosine from $\vec{B}\times\vec{F}$ to $\vec{k}$. $g(k)$ and $h(k)$ are written as

$$g(k) = \frac{S^+_{ipo}\, g(k^+) + S^-_{ipo}\, g(k^-) - \frac{eF}{\hbar}\frac{\partial f_o}{\partial k} + \frac{eB}{\hbar^2}\frac{\partial E}{\partial k}\frac{h(k)}{k}}{S_o}$$

$$h(k) = \frac{S^+_{ipo}\, h(k^+) + S^-_{ipo}\, h(k^-) - \frac{eB}{\hbar^2}\frac{\partial E}{\partial k}\frac{g(k)}{k}}{S_o}$$

The iterative method is used again to obtain numerical results. The zeroth iterations $g_o(k)=0$ and $h_o(k)=0$ for all k. The first iterations are

$$g_1(k) = -\frac{eF}{\hbar S_o}\frac{\partial f_o}{\partial k} \quad , \quad h_1(k) = 0$$

and the second-iteration of $h_2(k)$

$$h_2(k) = - \frac{eB}{\hbar^2 S_o} \frac{\partial E}{\partial k} \frac{g_1(k)}{k}$$

In general

$$g_{i+1}(k) = \frac{S^+_{ipo}\, g_i(k^+) + S^-_{ipo}\, g_i(k^-) - \frac{eF}{\hbar}\frac{\partial f_o}{\partial k} + \frac{eB}{\hbar^2}\frac{\partial E}{\partial k}\frac{h_i(k)}{k}}{S_o}$$

$$h_{i+1}(k) = \frac{S^+_{ipo}\, h_i(k^+) + S^-_{ipo}\, h_i(k^-) - \frac{eB}{\hbar^2}\frac{\partial E}{\partial k}\frac{g_i(k)}{k}}{S_o}$$

The x-component j_x and y-component j_y of currnet $\vec{j}$ are derived using the perturbation distributions g and h as follows:

$$j_x = \int e v_x f(\vec{k})\, d\vec{k} = \frac{V}{3\pi^3}\frac{e\hbar}{m_o F} \left[\langle g \rangle F_x - \langle h \rangle F_y \right]$$

$$j_y = \int e v_y f(\vec{k})\, d\vec{k} = \frac{V}{3\pi^3}\frac{e\hbar}{m_o F} \left[\langle g \rangle F_y + \langle h \rangle F_x \right]$$

With the condition $j_y=0$, j_x becomes

$$j_x = \frac{V}{3\pi^3}\frac{e\hbar}{m_o F} \left[\langle g \rangle + \frac{\langle h \rangle^2}{\langle g \rangle} \right] F_x$$

$$\equiv \sigma F_x$$

and by definition,

$$R_H \equiv \frac{F_y}{j_x B} = - \frac{3\pi^3 m_o F}{e\hbar V} \frac{\langle h \rangle}{\langle g \rangle^2 + \langle h \rangle^2} \frac{1}{B}$$

where $\langle\ \rangle = \int (k^3/d)dk$

Then, by definition

$$\mu_H \equiv R_H \sigma = - \frac{\langle h \rangle}{\langle g \rangle} \frac{1}{B}$$

and

$$\gamma_H \equiv \mu_H/\mu_D \ .$$

7-3. COMPOSITION DEPENDENCE OF μ_D, μ_H, AND γ_H

Composition dependence of the drift mobility and Hall mobility, and the Hall factors of the intrinsic and extrinsic ($N_d=1\times10^{17}$ cm^{-3}) $InAs_{1-x}P_x$ and $In_{1-x}Ga_xAs$ at 300 K are shown in Fig. 7-1 and Fig. 7-2, respectively. The mobility *vs.* composition curves are concave in the virtual-crystal approximation because the mobility limited by the polar-optical phonon scattering, which is dominant at RT, is roughly proportional to $m^{*\,-3/2}$. In the intrinsic alloys the difference between μ_D and μ_H is the largest. In the extrinsic alloys

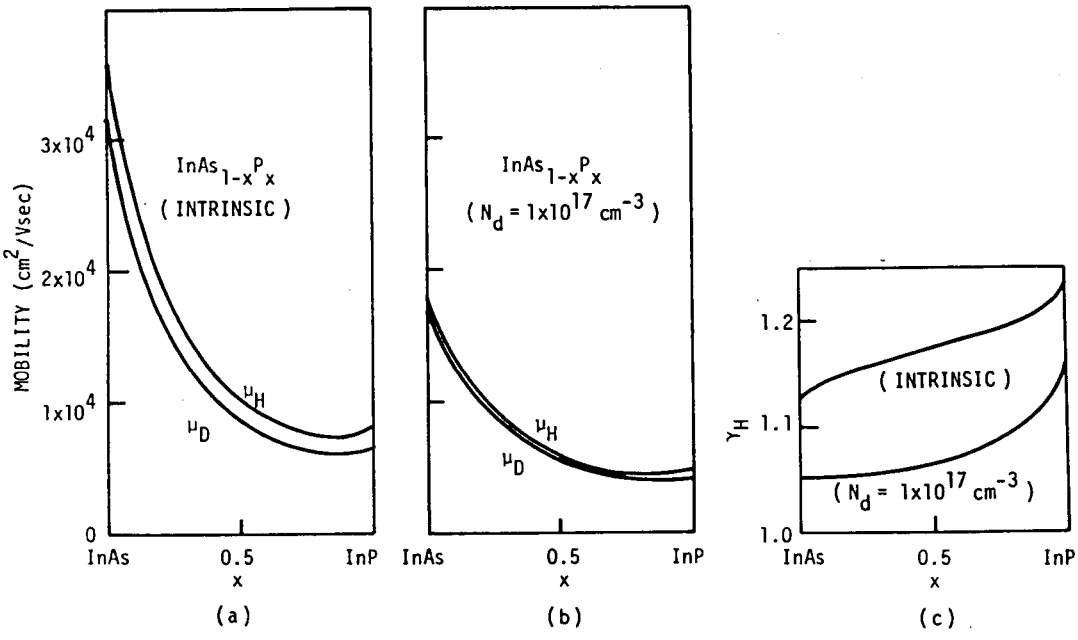

Fig. 7-1 Composition dependence of mobility and Hall factors of $InAs_{1-x}P_x$. (a) μ_D and μ_H of intrinsic $InAs_{1-x}P_x$, (b) μ_D and μ_H of extrinsic $InAs_{1-x}P_x$ with donor concentration 1×10^{17} cm^{-3} and no compensation, and (c) Hall factors of intrinsic and extrinsic $InAs_{1-x}P_x$.

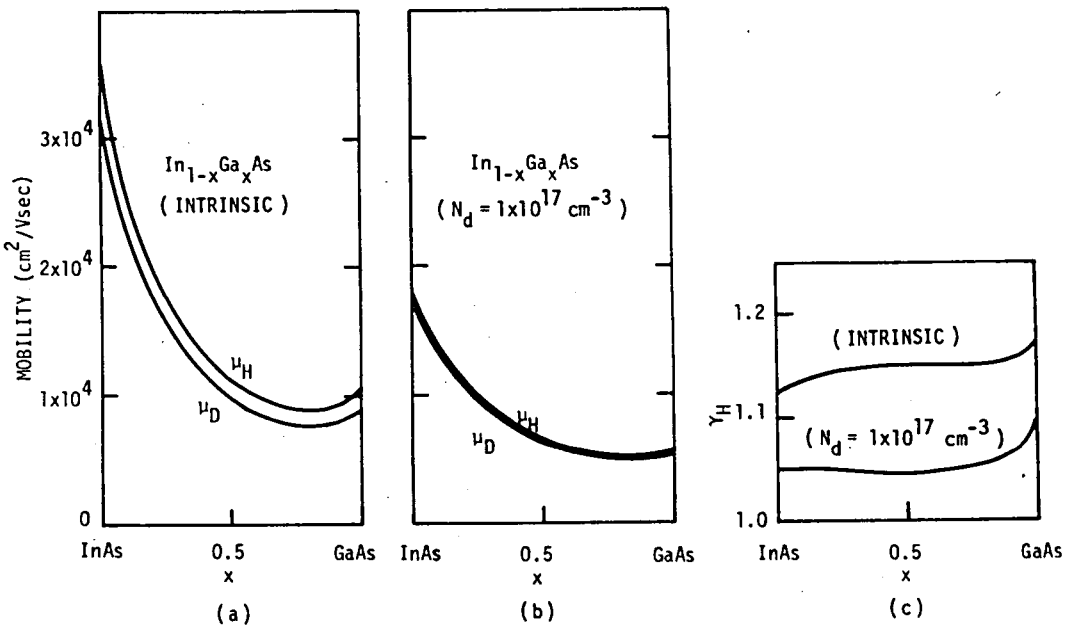

Fig. 7-2 Composition dependence of mobility and Hall factors of $In_{1-x}Ga_xAs$. (a) μ_D and μ_H of intrinsic $In_{1-x}Ga_xAs$, (b) μ_D and μ_H of extrinsic $In_{1-x}Ga_xAs$ with donor concentration 1×10^{17} cm^{-3} and no compensation, and (c) Hall factors of intrinsic and extrinsic $In_{1-x}Ga_xAs$.

the difference is smaller because the momentum dependence of the polar-optical phonon scattering and the ionized impurity scattering tends to cancel each other at around RT. When the scattering rate is independent of momentum, γ_H is known to be equal to unity.

In the temperature dependence of γ_H, it has the maximum at approximately $T_{po}/2$ (T_{po} is the polar-phonon Debye temperature) since the polar-optical phonon scattering is a rapidly varying function at this energy[1,8]. At higher temperatures than T_{po}, γ_H approaches to unity because the polar scattering is weakly momentum-dependent[8]. Thus, γ_H of a polar crystal which has a lower T_{po} is smaller at 300 K ($T_{po}/2$ is lower than 300 K in most III-V compounds). The T_{po}'s of InAs, GaAs, and InP are 350, 420, and 501 K, respective-

ly[8]. Therefore, in the alloys of $InAs_{1-x}P_x$ and $In_{1-x}Ga_xAs$, γ_H increases with x.

7-4. TEMPERATURE DEPENDENCE OF μ_H AND γ_H IN $In_{0.53}Ga_{0.47}As$

Temperature dependences of the electron Hall mobility which is limited by a combination of the polar-optical phonon, acoustic phonon, piezoelectric, and/or alloy scattering are shown in Fig. 7-3. Alloy scattering and no alloy scattering indicated in the figure denote that the alloy scattering by Brooks is included in the calculation and not included, respectively. With the alloy scattering included the mobility becomes weakly temperature-dependent, which is the usual observation in the experiments (see Chapter VIII). Numerical results of the mobility at 300 and 77 K with and without the alloy scattering are listed in Table 7-1.

The electron effective mass $m^*=0.043m_o$ is used in the calculation, but there is another report that the effective mass is $0.041m_o$ [6]. The numerical results calculated with this value are also listed in the same table.

Experimentally determined effective mass varies with carrier concentration because of the non-parabolicity and band filling. On the other hand, in the calculation the effective mass at the band edge $\vec{k}=(0,0,0)$ is used here. Thus, experimental determination of m^* in a purer sample is necessary. Other physical parameters, which are obtained from the assumed linear composition-dependence here, should be determined experimentally.

Temperature dependence of the Hall factors due to the acoustic phonon (γ_{ac}) , piezoelectric (γ_{pe}) , ionized impurity (γ_{ii}) , and alloy (γ_{al}) scattering are shown in Fig. 7-4. The Hall factor due to the polar-phonon scattering alone varies with temperature very similarly to the curve shown in Fig. 7-5 with no alloy scattering.

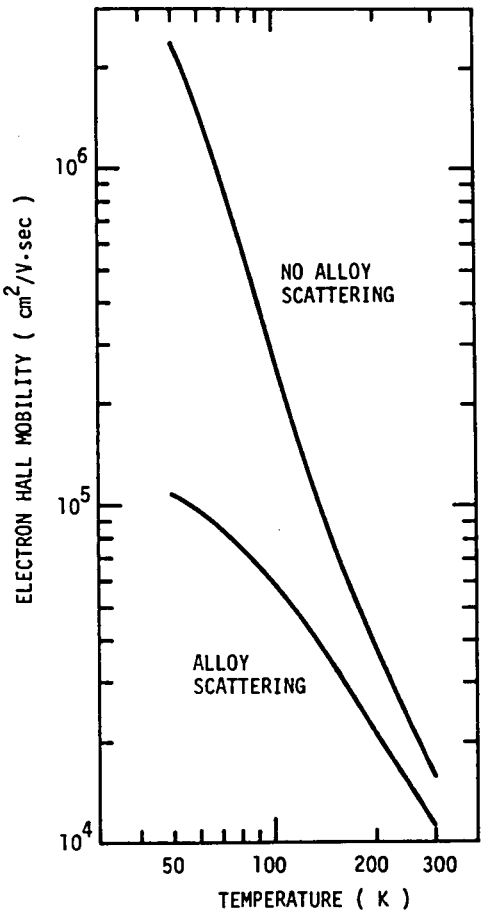

Fig. 7-3 Electron Hall mobility *vs.* temperature. Intrinsic $In_{0.53}Ga_{0.47}As$ with and without alloy scatterig.

	μ_D (cm^2/Vsec)		μ_H (cm^2/Vsec)	
	300 K	77 K	300 K	77 K
no alloy	14 000	631 000	16 000	672 000
alloy ($m^* = 0.043m_o$)	9 980	69 000	11 470	79 100
no alloy	15 100	685 000	17 200	729 000
alloy ($m^* = 0.041m_o$)	10 900	77 300	12 500	88 400

Table 7-1 Numerical results of μ_D and μ_H at 300 and 77 K. Two values are reported for the electron effective mass.

In a parabolic conduction-band approximation, $\gamma_{ac} = \gamma_{al} = 3\pi/8 = 1.18$, $\gamma_{pe} = 45\pi/128 = 1.10$, and $\gamma_{ii} = 315\pi/512 = 1.93$ [9], and are temperature-independent as shown in standard textbooks. When the non-parabolicity is taken into account, they become temperature-dependent mainly due to the contribution of the higher energy electrons excited by the thermal energy to the Hall factors. The higher energy electrons have heavier effective mass due to the non-parabolicity. γ_{ii}'s in the figure are calculated using the Brooks-Herring model[10]. They are dependent on temperature, carrier concentration, and impurity concentration because the screening effect of the scattering potential is taken into account in the model.

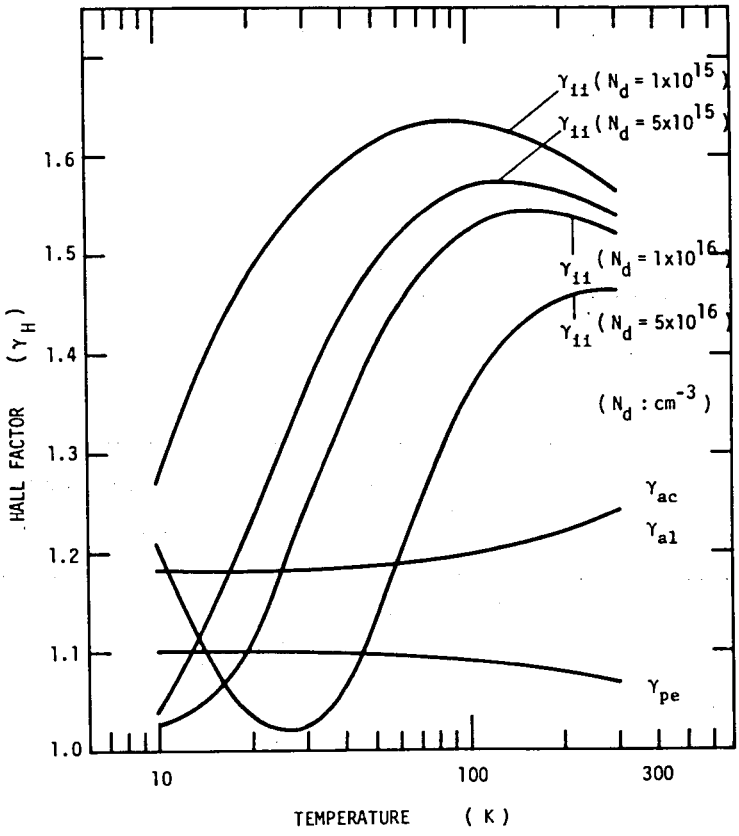

Fig. 7-4 Hall factors due to individual scattering mechanisms. γ_{ii}: ionized impurity scattering, γ_{ac}: acoustic phonon scattering, γ_{al}: alloy scattering, and γ_{pe}: piezoelectric scattering.

Fig. 7-5 shows the temperature dependence of the Hall factors in the intrinsic $In_{0.53}Ga_{0.47}As$ with the alloy scattering included and not included. At around 200 K, the Hall mobility is greater by 20∿30% than the drift mobility. The temperature dependence of γ_H of intrinsic $In_{0.53}Ga_{0.47}As$ without alloy scattering is very similar to that of GaAs[1]. At temperatures lower than ∿170 K the alloy scattering is so dominant that the γ_H with the alloy scattering included comes close to 1.18 which is the Hall factor of the alloy scattering alone. From Fig. 7-5 it is seen that the Hall factor is not approximated to be unity through all tempertures when we investigate the temperature dependence of mobility.

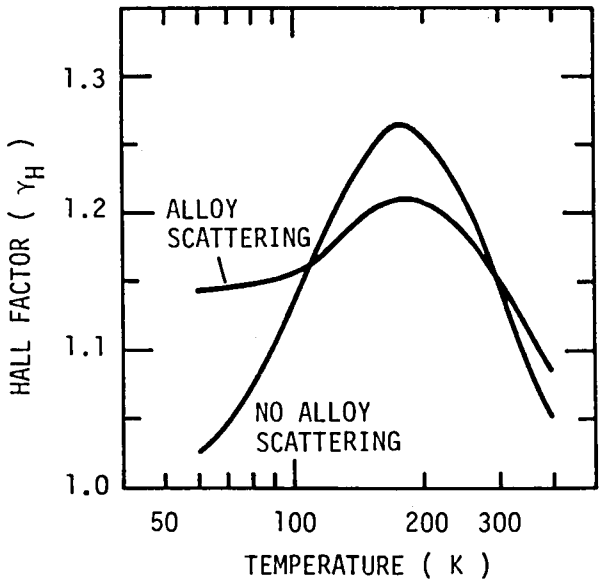

Fig. 7-5 Hall factor *vs.* temperature. Intrinsic $In_{0.53}Ga_{0.47}As$ with and without alloy scattering.

7-5. DONOR-CONCENTRATION DEPENDENCE OF μ_H

Fig. 7-6 shows the donor concentration (N_d) dependence of the Hall mobility with no compensation and a slight compensation ($N_a=0.2N_d$ which is often observed in our experiments). Here, N_a is the acceptor concentration. Some of the experiment-

al results reported recently[11-13] are plotted in the figure. It is interesting that the experimental values of the room-temperature mobility are coming close to the theoretical values without alloy scattering, but those of the liquid-nitrogen Hall mobility are on the lines with alloy scattering included.

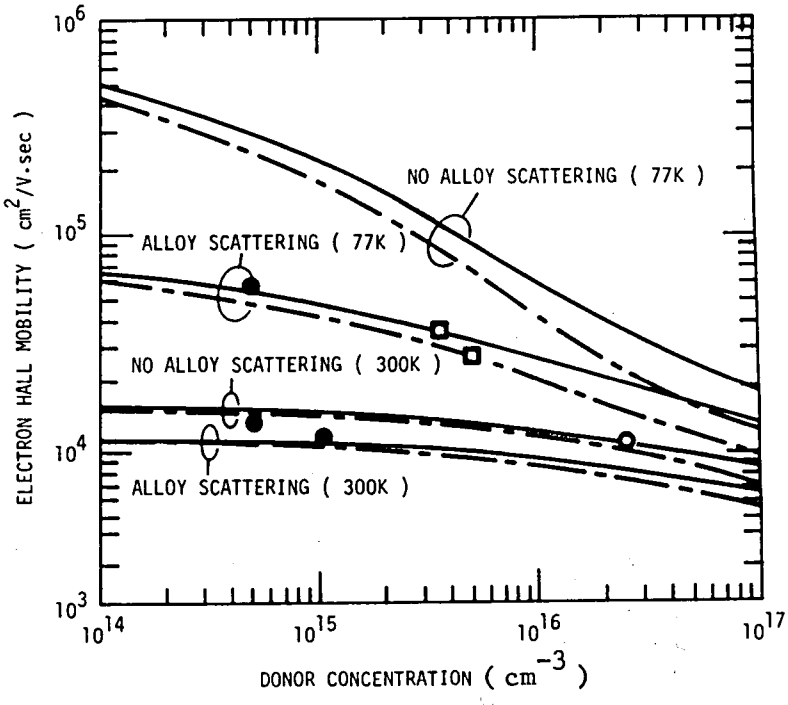

Fig. 7-6 Electron Hall mobility *vs.* donor concentration, with and without alloy scattering, and with no compensation (solid line) and with a slight compensation($N_a=0.2\,N_d$) (broken line). Experimental values are found in □ Ref. 11, o Ref. 12, and ● Ref. 13.

7-6. DISCUSSION

It has been very often assumed that the Hall factor $\gamma_H \equiv \mu_H/\mu_D$ is equal to unity. It may be sufficient to estimate roughly the mobility values by a simple calculation neglecting γ_H. However, when the pure material is obtained and the mobility is greatly

improved to reach the ultimate value, the difference cannot be neglected. The neglect will lead to mis-evaluation of the rate of scattering in the analysis of the mobility.

Fig. 7-7 is an experimental result of the temperature dependence of the electron Hall mobility of $In_{0.53}Ga_{0.47}As$. A part of it has been reported in Ref. 11. By the curve fitting to this experimental result using μ_D and μ_H, the fitting parameters, CAL($\equiv \tau_{alloy}/\tau_{Brooks}$), N_d, and N_a are derived. The results are listed in Table 7-2. The difference in the CAL is thought to be large and to affect the considerations on the origin of the potential difference of the alloy scattering.

The experimental results of the electron mobility are further discussed in Chapter VIII.

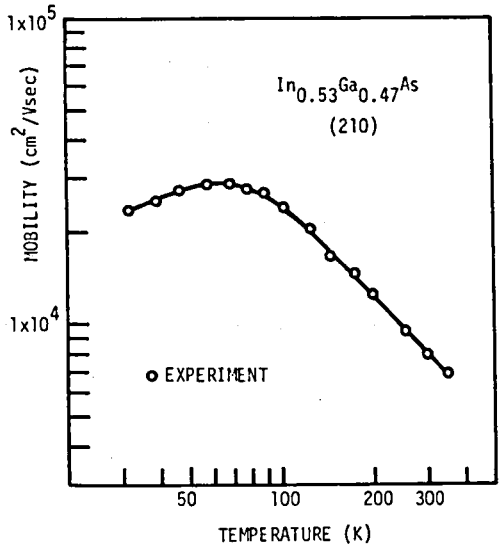

Fig. 7-7 An experimental result of temperature dependence of Hall mobility.

	CAL	Nd	Na
μ_D	1.2 ~ 1.4	6.0 ~ 6.5x10^{15}	1.0 ~ 1.5x10^{15}
μ_H	1.6 ~ 1.8	5.0 ~ 6.0x10^{15}	0.2 ~ 1.0x10^{15}

$CAL=\tau_{alloy}/\tau_{Brooks}$, Nd, Na (cm^{-3})

Table 7-2 Values of parameters obtained from the curve fitting using μ_D and μ_H.

7-7. SUMMARY

1) Hall factor, Hall mobility and drift mobility of ternary alloys have been calculated by the iterative method taking the polar-optical phonon, acoustic phonon, piezoelectric, ionized impurity, and/or alloy scattering into account.

2) Simplifying assumption such as the summation of the inverse μ limited by each scattering, the relaxation-time approximation and the parabolic band approximation have not been used in the calculation.

3) The Hall factors have been found to become smaller with increasing, but moderate, ionized impurity concentration.

4) The temperature dependences of the Hall mobility and Hall factor of n-$In_{0.53}Ga_{0.47}As$ have been shown.

5) The Hall mobility has been found to be higher by 20$\sim$30% than the drift mobility at $\sim$200 K.

6) The donor concentration dependences of the Hall mobility of n-$In_{0.53}Ga_{0.47}As$ at 300 and 77 K have been calculated and compared with the experimental data.

7) The influence of the difference of the Hall and drift mobility on the analysis of scattering mechanisms has been demonstrated taking n-$In_{0.53}Ga_{0.47}As$ as an example.

References

[1] D. L. Rode, phys. stat. sol., (b) 55, 687 (1973)

[2] H. Ehrenreich, J. Phys. Chem. Solids, 2, 131 (1957); 9, 129 (1959)

[3] M. B. Thomas and J. C. Woolley, Canad. J. Phys., 49, 2052 (1971)

[4] E. H. Perea, E. Mendez, and C. G. Fonstad, 21st Electron. Mater. Conf., Boulder, 1979, L-4

[5] Extrapolated from our results at 77 K (J. Electrochem. Soc., 125, 130 (1978) and Chapter III) and at 293 K (Ref. 11)

[6] T. P. Pearsall, R. Bisaro, P. Merenda, G. Laurencin, R. Ansel, J. C. Portal, C. Houlbert, and M. Quillec, in *Gallium Arsenide and Related Compounds*, 1978 Conference, Series 45 (Institute of Physics, Bristol and London, 1979) p. 94

[7] The Brooks' expression for the alloy scattering-limited mobility is shown in J. Phys. Chem. Solids, 34, 487 (1973) by L. Makowski and M. Glicksman

[8] D. L. Rode, Phys. Rev., B2, 1012 (1970)

[9] D. L. Rode and S. Knight, Phys. Rev., B3, 2534 (1971)

[10] H. Brooks, "Theory of the electronic properties of germanium and silicon," in *Advances in Electronics and Electron Physics* (Academic Press, New York, 1956) Vol. 7, and for the notation, see C. M. Wolfe, G. E. Stillman, and W. T. Lindley, J. Appl. Phys., 41, 3088 (1970)

[11] Y. Takeda, A. Sasaki, Y. Imamura, and T. Takagi, J. Appl. Phys., 47, 5405 (1976)

[12] R. F. Leheny, A. A. Ballman, J. C. DeWinter, R. E. Nahory, and M. A. Pollack, 21st Electron. Mater. Conf., Boulder, 1979, L-3

[13] J. D. Oliver, Jr., and L. F. Eastman, *ibid.* L-7

VIII. HALL MOBILITY OF n-$In_{0.53}Ga_{0.47}As$*

8-1. INTRODUCTION

Several workers have investigated the epitaxial growth of $In_{1-x}Ga_xAs$ on GaAs[1,2] and Al_2O_3[3]. However, the electron mobility of the alloy crystals, especially around middle composition, has been much lower than those of GaAs and bulk $In_{1-x}Ga_xAs$ grown by the Czochralski method[4] or the horizontal Bridgman method[5,6]. The reason could be due to the crystal imperfection such as strain, a large number of dislocations and/or microcracks caused by the lattice mismatch between the grown layer and the substrate.

Better results have been obtained with vapor phase epitaxy (VPE) avoiding the lattice-mismatch problem by a continuous grading of composition between the substrate and the desired final composition. Electron mobility of 5 900 cm^2/Vsec at 300 K and 13 000 cm^2/Vsec at 77 K has been reported for $In_{0.477}Ga_{0.523}As$ grown by this way[7].

It has been recognized that the electron mobility is affected by the crystal quality through the scattering of electron by the ionized impurity and other crystal imperfections. It is seen from the above-stated facts that the elimination of the lattice mismatch is essential to improve the electron mobility in the hetero-epitaxial layer. On the other hand, it has been reported that $In_{1-x}Ga_xAs$ ($x \simeq 0.5$) can be grown directly on InP substrate by LPE[8].

In this chapter, a great improvement of the electron mobility of n-$In_{1-x}Ga_xAs$($x \simeq 0.5$), especially $In_{0.53}Ga_{0.47}As$, using InP as a substrate is described. Growth-temperature dependence of the mobil-

---

* A. Sasaki, Y. Takeda, N. Shikagawa, and T. Takagi, Proc. 8th Conf. (1976 International) on Solid State Devices, Tokyo, 1976; Japan. J. Appl. Phys., 16 (1977) Suppl. 16-1, p.239
Y. Takeda, A. Sasaki, Y. Imamura, and T. Takagi, J. Appl. Phys., 47, 5405 (1976)

ity and the scattering mechanisms in $In_{0.53}Ga_{0.47}As$ are also described.

8-2. EXPERIMENTS

Growth procedures are the same as described in Chapter II and Chapter III, §3-2-1. The experimental method for the electrical evaluations is described here.

The method of van der Pauw[9] is used to determine the resistivity and the Hall coefficient, from which the Hall mobility and the carrier concentration are derived. For a practical use the equations in Ref. 9 are modified as follows:

$$\rho = d\,(R_{AB,CD} + R_{BC,DA})\,f \cdot 2.27 \times 10^{-4} \qquad (\Omega cm)$$

$$n = \frac{B}{d\,\Delta R_{BD,AC}} \cdot 6.24 \times 10^{17} \qquad (cm^{-3})$$

$$\mu_H = \frac{1}{B} \cdot \frac{\Delta R_{BD,AC}}{R_{AB,CD} + R_{BC,DA}} \cdot \frac{1}{f} \cdot 4.41 \times 10^{4} \qquad (cm^2/Vsec)$$

where ρ is the resistivity in Ωcm, d the thickness in μm, n the carrier concentration in cm^{-3}, B the magnetic field in kG, and μ_H the Hall mobility in $cm^2/Vsec$. $R_{AB,CD}$, $R_{BC,DA}$, and $\Delta R_{BD,AC}$ are defined in Ref. 9 and they are in unit of Ω. f is a function of the ratio of $R_{AB,CD}$ and $R_{BC,DA}$, and its values are tabulated in Ref. 10.

Typical sample dimensions for the measurements are 4×4 mm^2 and the thickness of the epitaxial layers varies from 3 to 24 μm. Pure In dots (usually about 300 μm in diameter) are alloyed for contact electrodes at the corners of the grown layers in a flowing hydrogen atmosphere at 450°C for 1 min. Prior to the alloying, the surface is lightly etched with a 1% Br:methanol solution.

The sample temperature can be varied from 4.2 K (immersed in liquid helium) to 400 K and controlled to be stable within ± 0.5 K. The temperature is detected by the Au - Au·Co thermocouple, and it is calibrated at four standard temperatures, *i.e.*, 273.16 K (0°C), 77.35 K (liquid nitrogen at 360 mmHg), 63.14 K (triple point of nitrogen at 94 mmHg), and 4.2 K (liquid helium at 360 mmHg). The source current is 20 or 100 μA, depending on the sample resistance, and the magnetic field for the Hall coefficient measurement is 5 kG.

8-3. RESULTS

8-3-1. Growth-Temperature Dependence of Hall mobility

The highest electron Hall mobility values at different growth temperatures are listed in Table 8-1 along with the electron concentrations and compositions. Note here that all the compositions are not 0.47 since the alloys are grown from the liquidus with the solidus composition 0.50 as described in Chapter III.

T_G	X	SAMPLE NO.	300 K		77 K	
			μ_H	n	μ_H	n
550	0.44	183	5240	6.3	7400	5.3
600	0.46	180	6590	3.2	11700	2.7
650	0.47	177	8240	2.3	15400	2.0
700	0.47	158	7670	1.6	15000	1.5
750	0.47	173	8500	1.3	22100	1.1

T_G: GROWTH TEMPERATURE (°C)

X : GaAs MOLE FRACTION

μ_H: HALL MOBILITY ($cm^2/Vsec$)

n : ELECTRON CONCENTRATION ($10^{16} cm^{-3}$)

Table 8-1 Composition and electrical properties of InGaAs grown at different temperatures. The sample which shows the highest mobility at each growth temperature is listed.

All the grown alloys are n-type with excess carrier concentrations of the order of 10^{16} cm^{-3}. The author's experiments indicate the general tendency that the mobility increases while the concentration decreases with increasing growth temperature. The former is illustrated in Fig. 8-1. An observation similar to this has been made in the case of InP grown at temperatures between 540° and 780°C by LPE on InP[25]. It seems from the table and the figure that better alloys (with higher mobility and lower electron concentration) can be grown at higher temperatures. But the epitaxial layer is nonuniform at high temperatures due to the thermal etching of the substrate surface. Invariably, the mobility of the alloys increases with decreasing lattice temperature to ∿77 K as shown in Fig. 8-2, in contrast to Conrad's[1] and Baliga's[2] data. Both 8 500 cm^2/Vsec at 300 K and 22 100 cm^2/Vsec at 77 K of sample #173 are significantly high in the epitaxial $In_{1-x}Ga_xAs$($x \simeq 0.5$)[1,2,7] and comparable to those of bulk grown alloys[4-6].

Recently, Sankaran *et al.*[11] have reported mobility values of 10 030 cm^2/Vsec at 300 K and 34 620 cm^2/Vsec at 77 K in

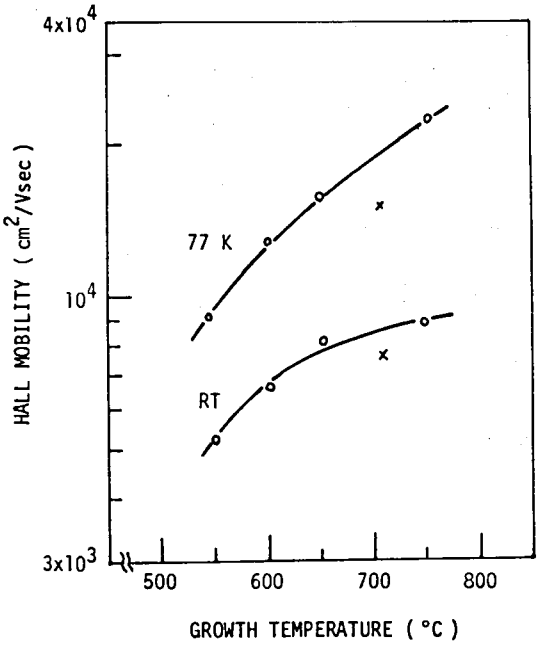

Fig. 8-1 Growth temperature dependence of room-temperature and liquid-nitrogen Hall mobility.

$In_{0.53}Ga_{0.47}As$ grown at 650°C by LPE on InP substrate, using In, Ga, and As for the melt material which was baked at 725°C for 22 h. With In, Ga, and InAs as the melt constituents they have obtained 5 540 cm^2/Vsec at 300 K and 8 430 cm^2/Vsec at 77 K. Using almost the same purity In, Ga, and InAs, the author has obtained mobility values of about 8 000 cm^2/Vsec at 300 K in $In_{0.53}Ga_{0.47}As$ grown between 650° and 750°C by baking In and Ga at 800°C for only 3 h.

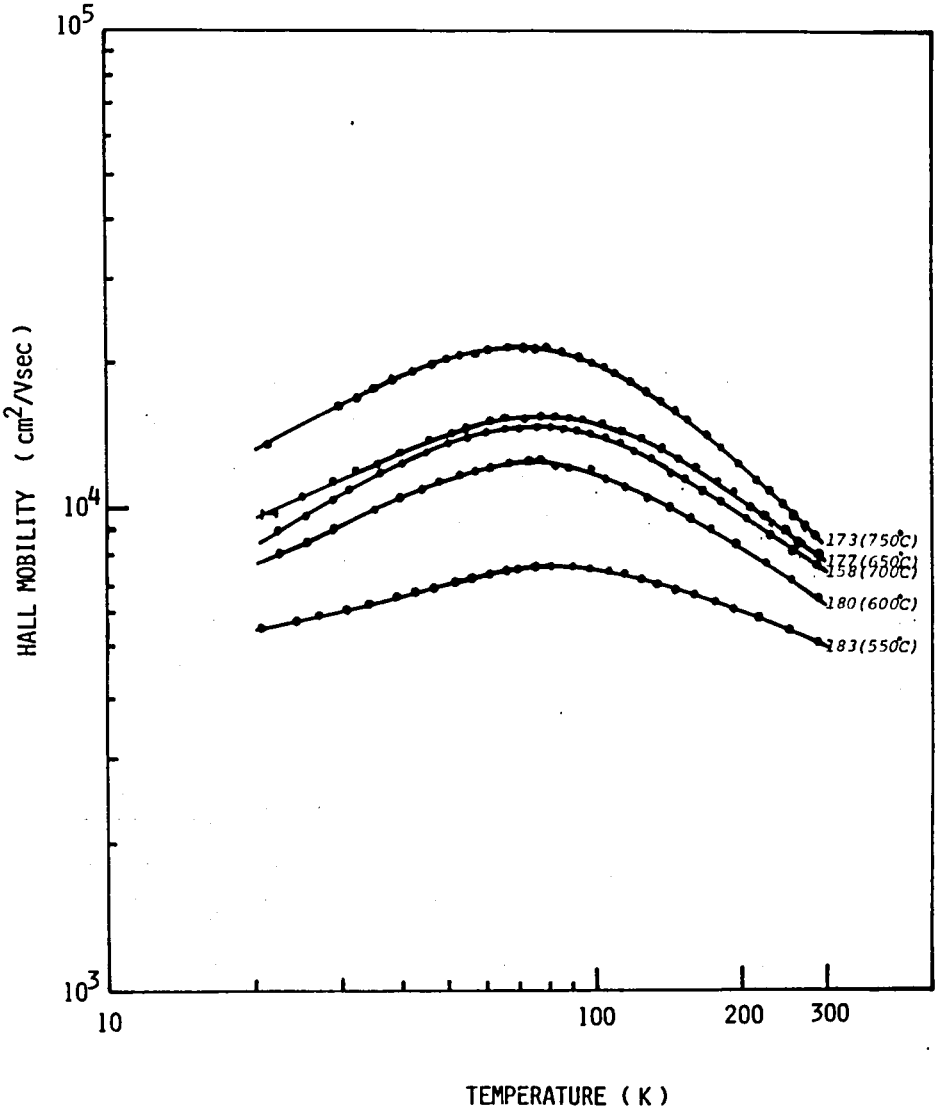

Fig. 8-2 Lattice-temperature dependence of Hall mobility.

8-3-2. Hall Mobility of GaAs and $In_{0.53}Ga_{0.47}As$

In Table 8-2, the data of GaAs grown in the same system at 800°C are shown for comparison. The mobility about 7 000 cm^2/Vsec of GaAs at 300 K is fairly good and the system is considered to be in a good condition.

The values of Hall mobility of $In_{0.53}Ga_{0.47}As$ at RT and 77 K are plotted in Fig. 8-3-a and b, respectively. The data are from the Table 8-1 and other experimentally obtained ones by the author. In the figures the Hall mobility of GaAs is shown for comparison The curve in Fig. 8-3-a gives the highest mobility of GaAs at each concentration[12] and the curves in Fig. 8-3-b are for the highest and the lowest mobility reported for GaAs[12]. It is clearly seen from Fig. 8-3-a that all the mobility values of $In_{0.53}Ga_{0.47}As$ exceed those of GaAs at RT. However, at 77 K all the mobility is equal to or lower than the lowest mobility of GaAs as shown in Fig. 8-3-b. It should be noted here that the electron concentration of $In_{0.53}Ga_{0.47}As$ is unintentionally obtained value, *i.e.*, being doped under uncontrolled growth conditions. Still better results would be obtained with the careful intentional doping of specific donor impurity atoms.

GaAs	300 K		77 K	
	μ_H	n	μ_H	n
GG204	6 780	2.0×10^{14}	49 200	1.9×10^{14}
GG211	6 870	2.8×10^{14}	43 300	2.5×10^{14}

μ_H : cm^2/Vsec, n : cm^{-3}

Table 8-2 Electrical properties of GaAs grown in the same growth system as for InGaAs.

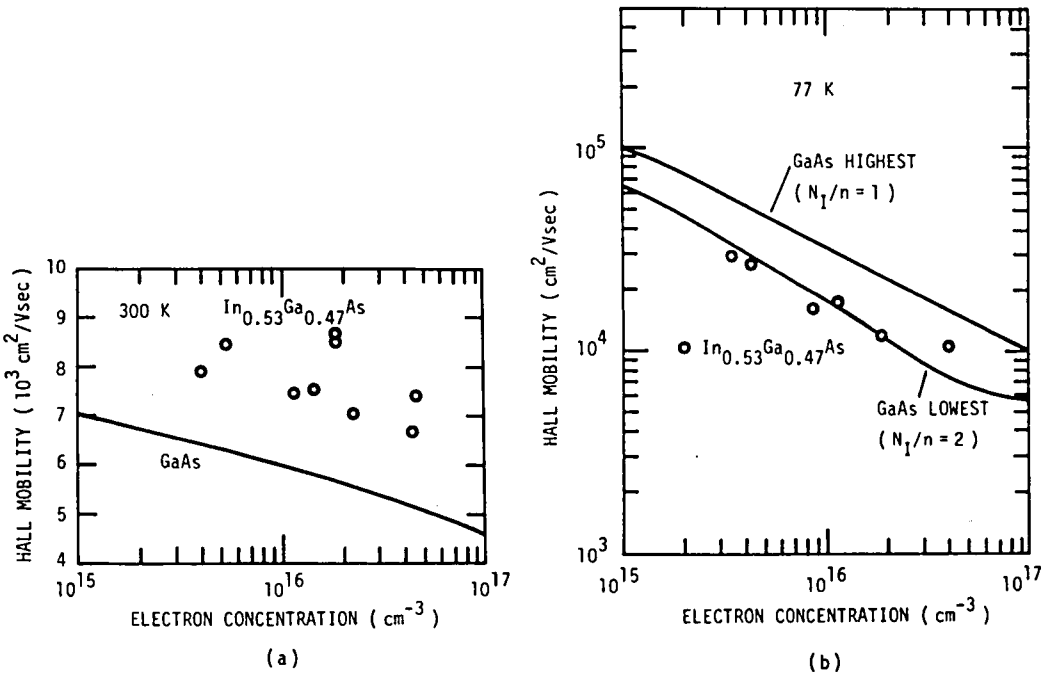

Fig. 8-3 Comparison of mobility of $In_{0.53}Ga_{0.47}As$ with those of GaAs: (a) at RT and (b) at 77 K. In (a) the curve for GaAs is the highest mobility at each concentration, and in (b) the curves are for the highest and the lowest mobility of GaAs.

In Fig. 8-4 are shown examples of the temperature dependence of the mobility of $In_{0.53}Ga_{0.47}As$(#210) and GaAs(#GG204) grown in the same growth system. The temperature dependence of the alloy is weak in comparison with that of GaAs, suggeting the existence of an additional scattering in the alloy as reported by Makowski *et al.* [13]. Its temperature dependence is not described by a combination of polar optical phonon, acoustic phonon, piezoelectric, and ionized impurity scattering, but well described by adding to them the alloy scattering which is shown in Ref. 13. However, the scattering time due to the "alloy" is varied to fit the experimental data from the calculated value of Brooks' formula [13]. This problem is discussed

in the next section.

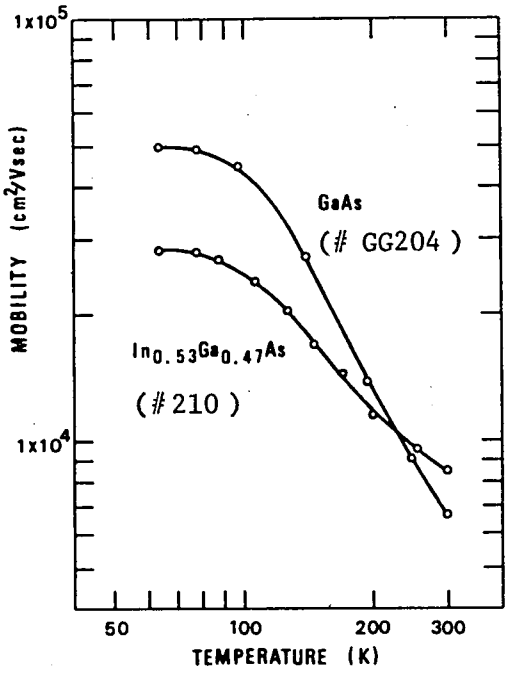

Fig. 8-4 Examples of temperature dependence of mobility of $In_{0.53}Ga_{0.47}As$ and GaAs grown in the same growth system.

8-4. DISCUSSION

At the beginning of this section, an important confirmation is given. It has been reported that anomalously high mobility may be obtained by van der Pauw's method in inhomogeneous semiconductors which contain many metal inclusions and that the anomaly is found out by the magnetic-field dependence of the mobility[14]. In the author's experiments, the magnetic-field dependence of the mobility is tested at 300 and 77 K from 0.9 to 7 kG. Inclusions in the grown layer and the interface are not found under a microscope or not detected by the EPMA (2 μm resolution). From the results, it is confirmed that the high mobility values are not due to the anomalous effect.

8-4-1. Observed Mobility in Other $In_{1-x}Ga_xAs$ ($x \simeq 0.5$) than $In_{0.53}Ga_{0.47}As$ on InP

In the hetero-epitaxial $In_{1-x}Ga_xAs$ grown directly on GaAs[1,2] the mobility was reported to decrease with decreasing lattice-temperature, *i.e.*, positive temperature dependence of the mobility. Conrad *et al.* found no explanation for the scattering mechanism responsible for the temperature dependence and they suspected that the alloy formation *per se* may be responsible in part for the low mobility[1]. The present author believes, comparing his results with Conrad's and Baliga's, that the alloy crystals grown with a large lattice-mismatch are much degraded due to the crystal imperfection such as strain, a large number of dislocations and/or microcracks caused by the lattice mismatch. Precise lattice-matching is essential to obtain a high mobility in the alloy.

In the bulk-grown $In_{1-x}Ga_xAs$, which is free from lattice mismatch with a substrate, positive temperature-dependence of mobility is found[6]. The mobility at around middle compositions is high and comparable to the data obtained here. The mobility values and its temperature-dependence of the bulk InGaAs cannot be explained by any combination of polar-optical phonon, acoustic phonon, piezoelectric, alloy, space-charge, and ionized impurity scattering. The only explanation to be left is the anomalous effect due to the inhomogeneity in the bulk $In_{1-x}Ga_xAs$.

In the VPE-grown $In_{0.477}Ga_{0.523}As$, avoiding the lattice mismatch by a continuous grading of composition between the GaAs substrate and the final alloy layer, the electron mobility values of 5 900 cm^2/Vsec at 300 K and 13 000 cm^2/Vsec at 77 K have been obtained [7].

With the author's results of mobility obtained in §8-3-1 and those of the VPE-grown $In_{0.477}Ga_{0.523}As$, it is concluded that the negative temperature-dependence of mobility is the essential proper-

ty of high quality $In_{1-x}Ga_xAs$ in a temperature range higher than ∿77 K.

8-4-2. Scattering Mechanisms in $In_{0.53}Ga_{0.47}As$

Scattering mechanisms in $In_{0.53}Ga_{0.47}As$ are analysed with relation to the growth temperature (T_G). To find a general tendency in the T_G-dependence, some simplifications are made. The mobility which is limited by a combination of polar-optical phonon, acoustic phonon, and piezoelectric scattering is approximated by the equation:

$$\mu_p = 2.89\times10^2 T^{\frac{1}{2}} [\ \exp(430/T - 1)]$$

The equation is determined to fit well the rigorously calculated mobility shown in Fig. 7-3 with no alloy scattering at higher temperatures than ∿77 K. The mobility limited by the ionized impurity scattering is, in the Born approximation, expressed by the equation:

$$\mu_I = \frac{4e}{3\sqrt{\pi}\, m^*} \int_0^\infty \tau(x)\, x^{\frac{3}{2}} \exp(-x)\, dx$$

$$\frac{1}{\tau(x)} = 2.4149 [(2N_a + n)/\varepsilon_r^{\,2})(\frac{m^*}{m_o})^{\frac{1}{2}} g (n', T, x) x^{-\frac{3}{2}} T^{-\frac{3}{2}}$$

where $x = E/k_BT$, N_a is the acceptor concentration, and n the free electron concentration. Definition of n' and g(n', T, x) is given in Ref. 15. It is known that the Born approximation becomes invalid in a higher concentration sample and at lower temperature[16]. In the sample measured here, the free electron concentrations are $1 \sim 7\times10^{16}$ cm^{-3} and the discrepancy between the calculated and experimental mobility is found to be larger at lower temperatures than ∿70 K. Thus, the analysis is made in the temperature range between 77 and 300 K. The alloy scattering limited mobility is known to be proportional to $T^{-\frac{1}{2}}$. In Brooks' formula [13]:

$$\mu_A = \frac{(2\pi)^{\frac{1}{2}} e \hbar^4 N_o}{3(m^*)^{\frac{5}{2}}(k_B T)^{\frac{1}{2}} x(1-x)\ \Delta U^2}$$

where N_o is the number of atoms per unit volume, ΔU is the potential difference for the scattering. In the analysis, μ_A is expressed by

$$\mu_A = D\, T^{-\frac{1}{2}}$$

where D is a fitting parameter. The combined mobility is approximated by the equation:

$$\frac{1}{\mu} \simeq \frac{1}{\mu_p} + \frac{1}{\mu_I} + \frac{1}{\mu_A}$$

that is Mathiessen's rule. Mathiessen's rule in not applicable to semiconductors and the rigorous calculation shown in Chapter VII should be used. However, the approximation is still useful to find the general tendency in the growth-temperature dependence of the mobility. From the curve fitting N_d, N_a, and D are determined at the best fit to the experimental data by the method of least squares.

Figure 8-5-a shows an example that when the experimental mobility of sample #173 is fitted by a combination of μ_P and μ_I at a low temperature, the discrepancy is great at higher temperatures. It is well fitted by a combination of μ_P, μ_I, and μ_A as shown in Fig. 8-5-b. Other examples of mobility combinations are shown in Figs. 8-6-a and b.

The results determined from the curve fitting are shown in Figs. 8-7 and 8-8. Fig. 8-7 is the ionized impurity concentration, *i.e.*, $N_I = N_d^+ + N_a^- = n + 2N_a$, as a function of growth temperature.

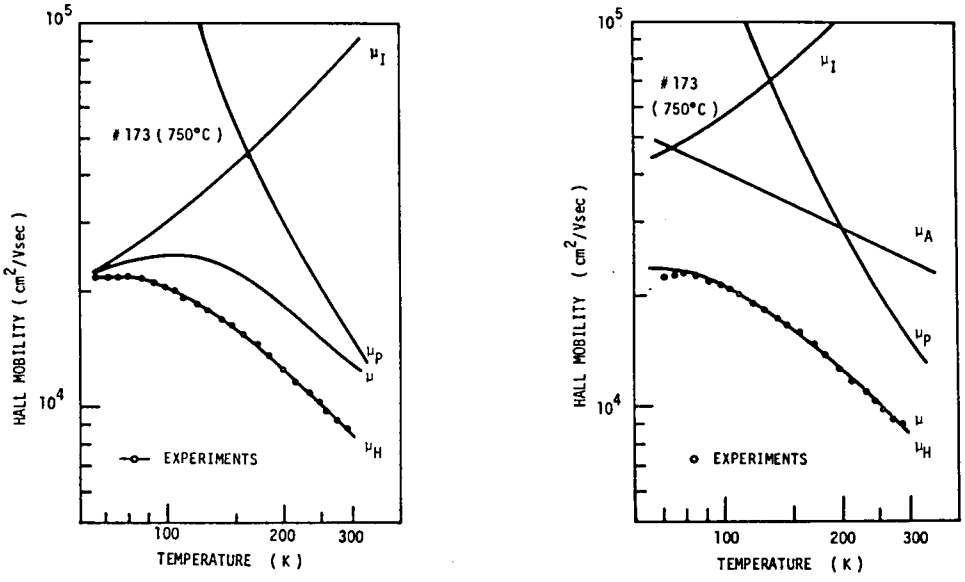

Fig. 8-5 Curve fitting to the experimental mobility with a combination of μ_P and μ_I is impossible (a), but with a combination of μ_P, μ_I, and μ_A the fitting is good (b).

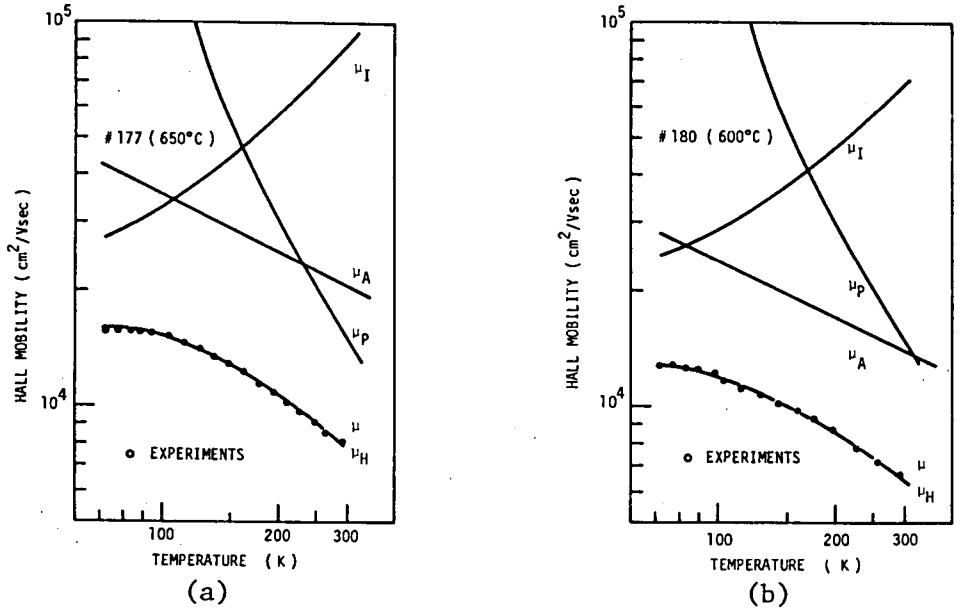

Fig. 8-6 Other examples of the curve fitting with a combination of the three kinds of μ's. (a) For sample #177 grown at 650° C and (b) for sample #180 grown at 600°C.

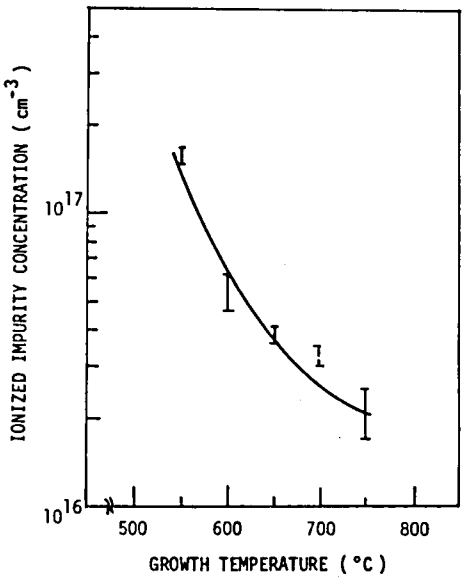

Fig. 8-7 Growth temperature dependence of the ionized impurity concentration derived from the curve fitting.

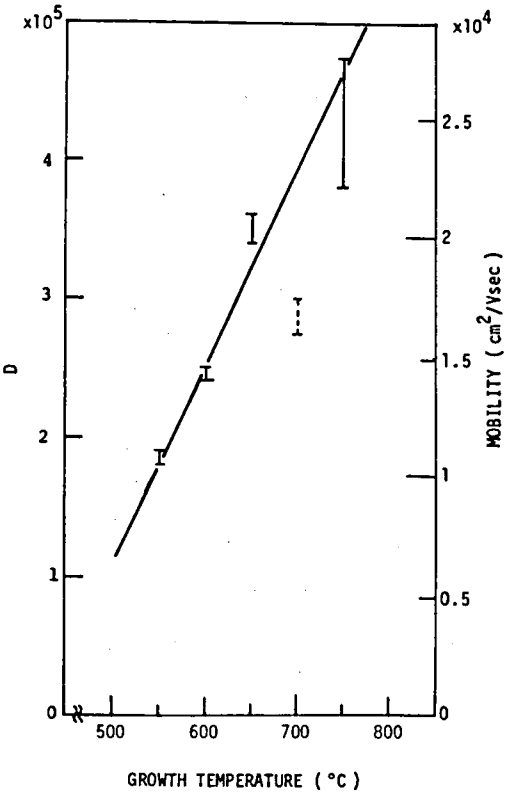

Fig. 8-8 Growth temperature dependence of the coefficient D and the alloy-scattering limited mobility derived from the curve fitting.

There is a clear tendency that N_I decreases whereas D increases with increasing T_G.

Note here that the alloy scattering of Brooks' model has a definite value at a fixed composition and does not vary with growth-temperature as shown in Fig. 8-8. In addition, Brooks' alloy scattering is considered in a complete disorder of constituent atoms. From the ordering point of view, the complete disorder is thought to give the lowest mobility (the mobility which is limited by Brooks' alloy scattering is 47 600 cm^2/Vsec in $In_{0.53}Ga_{0.47}As$ at 300 K). For example, if the In and Ga atom are arranged perfectly one after another in $In_{0.50}Ga_{0.50}As$, the alloy scattering vanishes since the alloy is a completely ordered new material. In the virtual-crystal approximation[17] the alloy scattering also vanishes, since the virtual-crystal itself is a completely ordered new (but virtual) material. Therefore, another scattering mechanism which gives lower mobility than Brooks' alloy scattering and varies with growth conditions must be thought out.

The author suspects two scattering mechanisms: one is the scattering due to clustered atoms, and the other is the space-charge scattering. Both have already been proposed for the ternay alloys: the former by F. Osaka *et al.*[18] and the latter by T. Katoda *et al.*[19], but they are re-examined using new experimental results obtained here. The mobility which is limited by these scatterings are known to be proportional to $T^{-\frac{1}{2}}$.

Statistical thermodynamics shows that at high temperatures atoms tend to be randomnized by the thermal energy. From the "quasi-chemical" point of view[20], the interaction (attractive or repulsive) between atoms is a function of temperature and interaction parameter; at very high temperatures the atoms will be in complete random and at lower temperatures the similar or dissimilar atoms gather depending on the value and sign (+ of -) of the interaction parameter between atoms. Hence, at lower growth temperatures the

mobility which is limited by the scattering due to the clustered atoms would be lower. Fig. 8-8 appears to suggest this tendency. However, in the author's sample wich is grown at 600°C with a different growth condition (this is discussed later) shows a high mobility 8 480 cm^2/Vsec at RT. In addition, very high mobility values are reported for $In_{0.53}Ga_{0.47}As$ grown at around 650°C[21-23]. Thus, the clustering of atoms, if it is a function of the growth temperature, would not be the scattering center for the μ_A here.

Next, the space-charge scattering is considered. The space-charge scattering was discussed by E. M. Conwell and M. O. Vassell to explain the lower mobility of GaAs than the combined mobility due to polar-optical phonon, acoustic phonon, and ionized impurity scattering[24] and by T. Katoda *et al.*[19] for VPE-grown $In_{1-x}Ga_xAs$ on GaAs. In the experiments of growth-temperature dependence of the electron mobility here, only the growth temperature was varied as described in Chapter III. InAs was added after cooling the In and Ga melt. The author suspects that the baking of InAs during the saturation period effects the purity and crystal quality of the grown alloys. Polycrystalline InAs, which is etched and rinsed just prior to loading, does not seem to be so clean as that after being baked in a flowing Pd-diffused hydrogen. The melt materials including InAs will be better purified at higher temperatures. The decrease of the ionized impurity concentration with increasing growth temperature, as shown in Fig. 8-7, would be caused by this effect of baking. The space-charge region, probably a region of gathering impurity atoms, is thought to be larger in an impurer sample.

To confirm the baking effect of InAs on the mobility, In, Ga, and InAs are baked at 800°C for 3 h, and the alloy is grown at 600°C as shown in Fig. 8-9. The mobility values obtained are 8 480 cm^2/Vsec at 300 K and 19 900 cm^2/Vsec at 77 K, with $n=1.8\times10^{16}$ cm^{-3} at 300 K (sample #206). Since the melt materials are thermally equilibrated at 600°C, the clustering effects discussed above would not act here.

The author believes that the purification of the melt materials yielded here the high mobility in the sample grown at the lower temperature(600°C).

It is expected from the discussion that still better crystals, with higher mobility and lower excess carrier concentration, can be obtained by purifying the melt materials and probably the substrate, together with a close lattice matching.

Although some simplifying assumptions have been made in the analysis, it provides a good insight for obtaining still better alloys. For a quantitative analysis of the scattering rates, the Hall mobility both theoretical and experimental should be used, as shown and discussed in Chapter VII, although it consumes a great deal of computation time of the computor.

Very recently, very high mobility values are observed at RT in LPE-grown $In_{0.53}Ga_{0.47}As$ on InP; 15 000 cm^2/Vsec by T. P. Pearsall *et al.*[21], 13 500 cm^2/Vsec by J. D. Oliver, Jr. and L. F. Eastman[22],

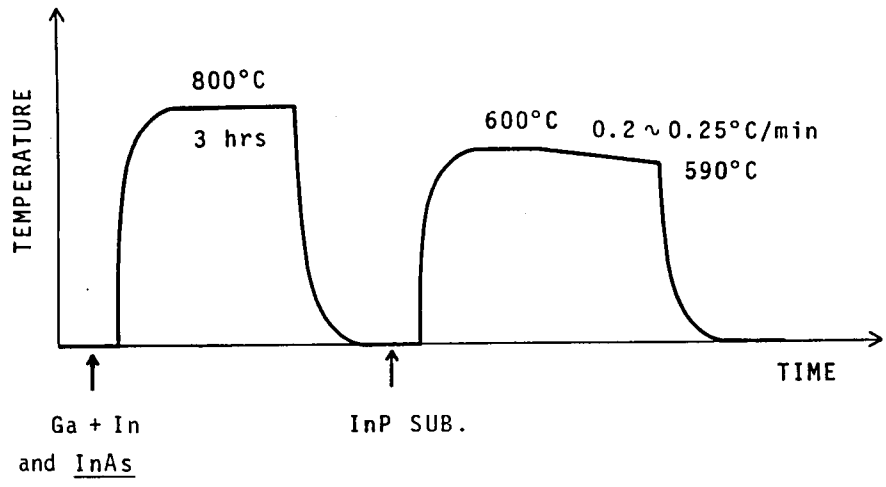

Fig. 8-9 Temperature cycle for the growth at 600°C. In, Ga, and InAs are baked before growth.

and 11 000 cm^2/Vsec by R. F. Leheny *et al.*[23]. Although the experimental data had been behind the progress of the theoretical arguments on the mobility, the theory is now, in turn, being challenged. For example, as shown in Chapter VII, Fig. 7-6, the experimental Hall mobility at 300 K are on the calculated lines without alloy scattering, but those at 77 K are on the lines with the alloy scattering included. The theory and experiments are stimulating each other for further improvements.

8-5. SUMMARY

1) High mobility values (>8 000 cm^2/Vsec) have been obtained in $In_{0.53}Ga_{0.47}As$ on InP grown at 650∿750°C.
2) In the experiments on InGaAs here, the electron mobility increases and the electron concentration decreases with increasing growth-temperature.
3) The lattice-temperature dependence of the mobility of $In_{0.53}Ga_{0.47}As$ is found to be weaker than that of GaAs.
4) The electron mobility increases on cooling from 300 to 77 K in all samples. This is the essential property of high quality $In_{1-x}Ga_xAs$.
5) Scattering mechanisms in $In_{0.53}Ga_{0.47}As$ on InP have been discussed with relation to growth-temperature.
6) It has been suggested that still better crystals can be obtained by the purification of melt materials.

References

[1] R. W. Conrad, P. L. Hoyt, and D. D. Martin, J. Electrochem. Soc., 114, 164 (1967)

[2] B. J. Baliga and S. K. Ghandhi, J. Electrochem. Soc., 122,

683 (1975)

[3] H. M. Manasevit and W. I. Simpson, J. Electrochem. Soc., 120, 135 (1973)

[4] John W. Wagner, J. Electrochem. Soc., 117, 1193 (1970)

[5] M. S. Abrahams, R. Braunstein, and F. D. Rosi, J. Phys. Chem. Solids, 10, 204 (1959)

[6] T. V. Dzhakhutashvili, A. A. Mirtskhulava, L. G. Sakvarelidze, A. L. Shkol'nik, and M. S. Matinova, Sov. Phys.-Semicond., 5, 190 (1971)

[7] R. E. Enstrom, D. Richman, M. S. Abrahams, J. R. Appert, D. G. Fisher, A. H. Sommer, and B. F. Williams, in *Gallium Arsenide and Related Compounds*, 1970 Conference, Series 9 (Institute of Physics, London, 1971) p. 30

[8] A. Sasaki, M. Mohri, T. Takagi, and T. Tanaka, Abstracts of the 4th Int'l. Conf. Cryst. Growth, Tokyo, 1974, p. 237

[9] L. J. van der Pauw, Philips. Res. Rep., 13, 1 (1958)

[10] G. Kusumoto, Oyo-butsuri, 42, 756 (1973) (in Japanese)

[11] R. Sankaran, R. L. Moon, and G. A. Antypas, J. Cryst. Growth, 33, 271 (1976)

[12] S. M. Sze and J. C. Irvin, Solid-State Electron., 11, 599 (1968)

D. L. Rode, " Low-Field Electron Transport," in *Semiconductors and Semimetals* edited by R. K. Willardson and A. C. Beer (Academic Press, New York, 1975) Vol. 10, chapter 1

[13] L. Makowski and M. Glicksman, J. Phys. Chem. Solids, 34, 487 (1973)

[14] C. M. Wolfe and G. E. Stillman, Appl. Phys. Lett., 18, 205 (1971) and

C. M. Wolfe and G. E. Stillman, " Apparaent Mobility Enhancement in Inhomogeneous Crystals," in *Semiconductors and Semimetals* (Academic Press, New York, 1975) Vol. 10, chapter 3

[15] H. Brooks, "Theory of the electronic properties of germanium and silicon," in *Advances in Electronics and Electron Physics* (Academic Press, New York, 1956) Vol. 7, and for the notation, see C. M. Wolfe, G. E. Stillman, W. T. Lindley, J. Appl. Phys., 41, 3088 (1970).

[16] F. J. Blatt, J. Phys. Chem. Solids, 1, 262 (1957)

[17] L. Nordheim, Ann. Physik, 9, 607 and 641 (1931)

[18] F. Oosaka, T. Sugano, Y. Okabe, and Y. Okada, Japan. J. Appl.

[19] T. Katoda, F. Osaka, and T. Sugano, Japan. J. Appl. Phys., 13, 561 (1974)

[20] E. A. Guggenheim, *Mixtures* (Oxford Press, London, 1952)

[21] T. P. Pearsall, R. Bisaro, P. Merenda, G. Laurencin, R. Ansel, J. C. Portal, C. Houlbert, and M. Quillec, in *Gallium Arsenide and Related Compounds,* 1978 Conference, Series 45 (Institute of Physics, Bristol and London, 1979) p. 94

[22] J. D. Oliver, Jr. and L. F. Eastman, 21st Electron. Mater. Conf., Boulder, 1979, L-7

[23] R. F. Leheny, A. A. Ballman, J. C. DeWinter, R. E. Nahory, and M. A. Pollack, 21st Electron. Mater. Conf., Boulder, 1979, L-3

[24] E. M. Conwell and M. O. Vassell, Phys. Rev., 166, 797 (1968)

[25] M. G. Astles, F. G. H. Smith, and E. W. Williams, J. Electrochem. Soc., 120, 1750 (1973)

IX. HIGH-FIELD TRANSPORT PROPERTIES OF n-$In_{0.53}Ga_{0.47}As$*

9-1. INTRODUCTION

Silicon is a semiconductor which is commonly used for devices such as diodes, transistors, and thyristors. However, it is not satisfactory in an electron mobility and a maximum velocity for transistors to operate in a microwave frequency region or at a very high switching speed. Thus, GaAs which has a higher mobility (about six times) and a higher maximum velocity (about twice) compared with silicon is normally used for microwave FET's (field-effect transistors). Today (1975), GaAs MESFET's (metal-semiconductor FET's) have shown the highest frequency operation ($\sim$80 GHz) and the fastest switching speed (speed-power product = 4 pJ) of all transistors[1].

InSb and InAs have very high mobility such as 78 000 and 33 000 cm^2/Vsec at room temperature[2], respectively. However, these materials cannot be used for transistors at room temperature, because of very narrow energy gaps, 0.18 and 0.356 eV, respectively. The alloy of InAs and GaAs can be expected to yield a higher mobility than GaAs and a wider energy gap than InAs. Near a half composition ($x \simeq 0.5$), the energy gap, E_g, becomes 0.75 eV at which the extrinsic carrier concentration ($>10^{15}$ cm^{-3}) is not affected by the variation of the intrinsic carrier concentration ($\sim 10^{11}$ cm^{-3}). Further, the difference, ΔE, between the central and satellite valleys in the conduction band becomes wider with the increase of the composition rate of InAs. This tends to make a maximum velocity higher by suppressing the transferred-electron effect. Near $x=0.5$, ΔE was expected to equal E_g[3].

---

* A. Sasaki, Y. Takeda, N. Shikagawa, and T. Takagi, Proc. 8th Conf. (1976 International) on Solid State Devices, Tokyo, 1976; Japan. J. Appl. Phys., 16 (1977) Suppl. 16-1, p. 239
Y. Takeda, N. Shikagawa, and A. Sasaki, Solid-State Electron., (submitted)

On the other hand, it becomes possible to apply a high electric field to $In_{0.53}Ga_{0.47}As$ for the first time in the world, since uniform and high quality crystals have been obtained in this study.

In this chapter, the experimental procedures, the velocity-field characteristics, and the phenomena related to the transferred-electron effect are described.

9-2. EXPERIMENTS

9-2-1. Device Fabrication

The $In_{0.53}Ga_{0.47}As$ layers were grown on Cr-doped ($\rho > 10^3$ Ωcm) and Fe-doped ($\rho > 10^6$ Ωcm) semi-insulating InP substrates by LPE using similar procedures described in Chapter II. Coplanar and H-shaped devices are delineated by conventional photo-lithographic techniques and sawed into the shapes as shown in Fig. 9-1-a. A photograph of a H-shaped GaAs device is shown in Fig. 9-1-b. To eliminate the electric influence of the Cr-doped substrate which has a relatively low resistivity, the substrate is lapped to 100 μm thickness. The dimensions of the active region are $\sim$200×(150$\sim$400)×(5$\sim$10) μm^3 (length×width×thickness) and $\sim$200×70×(5$\sim$10) μm^3 for the

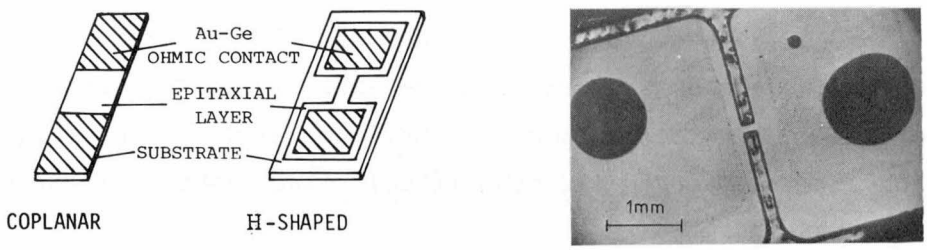

(a) (b)

Fig. 9-1 Device structure for the velocity-field measurements: (a) schematic drawings and (b) a photograph of the H-shaped GaAs device.

coplanar and H-shaped devices, respectively. Ohmic contacts are formed onto the end portions of the device by evaporating Au-Ge (88: 12 in weight) and Ni and alloying at 480°C for 1 min in a flowing hydrogen gas. Typical device resistances are 50 Ω for the coplanar and 200 Ω for the H-shaped devices. Similar devices are fabricated using GaAs as reference devices.

The electron concentration and Hall mobility of the $In_{0.53}Ga_{0.47}As$ wafers are listed in Table 9-1 along with those of GaAs used in the experiments.

	WAFER NO.	n (cm^{-3})	μ_H(cm^2/Vsec)
$In_{0.53}Ga_{0.47}As$	# 206	1.81×10^{16}	8 630
	# 210	5.18×10^{15}	8 450
	# 211	3.95×10^{15}	7 580
	# 220	2.29×10^{16}	7 070
	# 237	4.04×10^{16}	6 690
GaAs	1N447	2.65×10^{15}	6 600
	N4372	9.28×10^{15}	6 420

Table 9-1 The electrical properties of $In_{0.53}Ga_{0.47}As$ and GaAs used in the experiments.

9-2-2. $v - E$ Characteristics

Time of flight[4] and microwave heating[5] techniques have been used for the measurement of the velocity-field ($v - E$) characteristics of a semiconductor which has the negative differential resistivity(NDR) region. If the $v - E$ characteristic does not have the NDR region, much simpler technique can be employed. In the

author's experiments, the $v-E$ characteristics below the threshold field and the maximum drift velocity are derived from the current-voltage (I - V) characteristics which are obtained using 2 μsec pulse bias voltage (33 Hz repetition) in a conventional 50 Ω resistive circuit as shown in Fig. 9-2. The drift velocity is calculated from the measured current, the cross-sectional area of the active region, the elecron charge, and the electron concentration measured from the Hall effect. The device is mounted on a copper stud to prevent from temperature rise, and the device and the resistances are contained in a copper package as shown in Fig. 9-3.

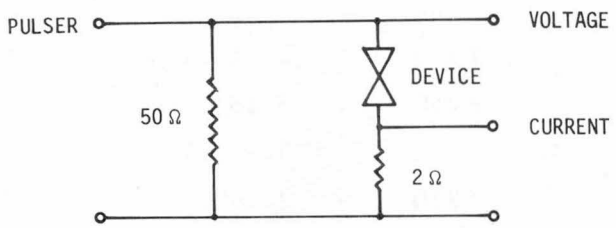

Fig. 9-2 50 Ω resistive circuit for the current-voltage measurement.

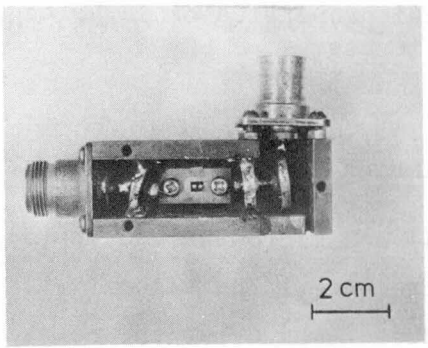

Fig. 9-3 A photograph of the copper package.

9-2-3. Measurement of Average Current beyond Threshold

Beyond threshold, current instabilities are observed by the oscilloscope. The Boxcar integrator[i)] is used to measure the average current with sampling the current flow during the applied pulse voltage. The measurement apparatus is shown in Fig. 9-4. Pulse voltage, current, and gate position of the Boxcar integrator are monitored by the oscilloscope.

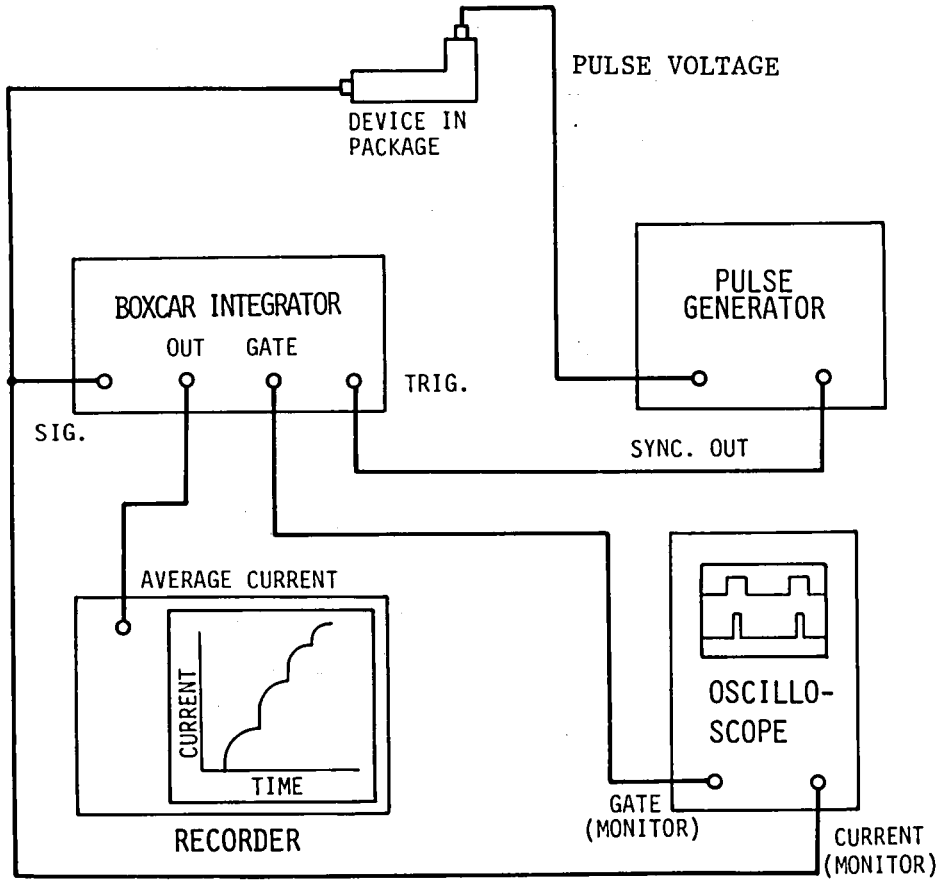

Fig. 9-4 Apparatus for the average current measurement.

i) BX-530A, NF Circuit Design Block Co., LTD.

9-2-4. Spectrum Analysis beyond Threshold

To make it clear whether the current instability is the transferred-electron oscillation or not, the spectrum is observed by the spectrum analyser[i)]. The measurement apparatus is similar to that shown in Fig. 9-4, but the current signal is supplied to the spectrum analyser. No resonant circuit is used.

9-3. RESULTS

9-3-1. $v-E$ Characteristics below Threshold

The velocity - field curves are shown in Fig. 9-5 to each one of $In_{0.53}Ga_{0.47}As$ and GaAs devices, and the velocity - field points beyond which the current instabilities are observed are plotted to the other devices. The letters I and G denote the InGaAs and GaAs device, respectively. The subscripts C and H are for coplanar type and H-shaped type, respectively. Note that the electric field is calculated simply from the applied voltage divided by the electrode

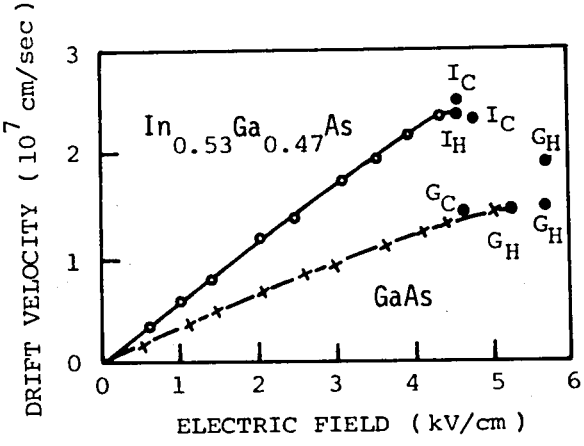

Fig. 9-5 Derived v-E curves and points for $In_{0.53}Ga_{0.47}As$ and GaAs.

i) 851B, 8551B Spectrum Analyser, Hewlett Packard

distance. The correction to the electric field is discussed in §9-4.

9-3-2. Average Current beyond Threshold

Figures 9-6-a, b, and c show current *vs.* voltage characteristics below threshold (solid line) and average current *vs.* voltage characteristics beyond threshold (dashed line) for three $In_{0.53}Ga_{0.47}As$ devices with different electron concentrations. In Fig. 9-6-a, a decrease in the average current is observed for the device which has the lowest electron concentration among the three devices. Steep increase in the average current is observed beyond threshold in Figs. 9-6-b and c. The pulse of 0.5 μsec width is also used and no difference is found in the characteristics from those observed using the pulse of 2 μsec width.

The average I - V characteristics are measured for the GaAs devices as shown in Figs. 9-7-a, b, and c. The dependence of the beyond-threshold characteristics of the GaAs devices with 200 μm-electrode distance on the electron concentration is very similar to those observed for the $In_{0.53}Ga_{0.47}As$ devices. With the same electron concentration (made from the same wafer N 4372) the decrease in the average current beyond threshold is clearly seen for the device which has a shorter electrode distance (100 μm). Compare Fig. 9-7-b with c.

Figures 9-6-a∿c and 9-7-a∿c are illustrated in next two pages.

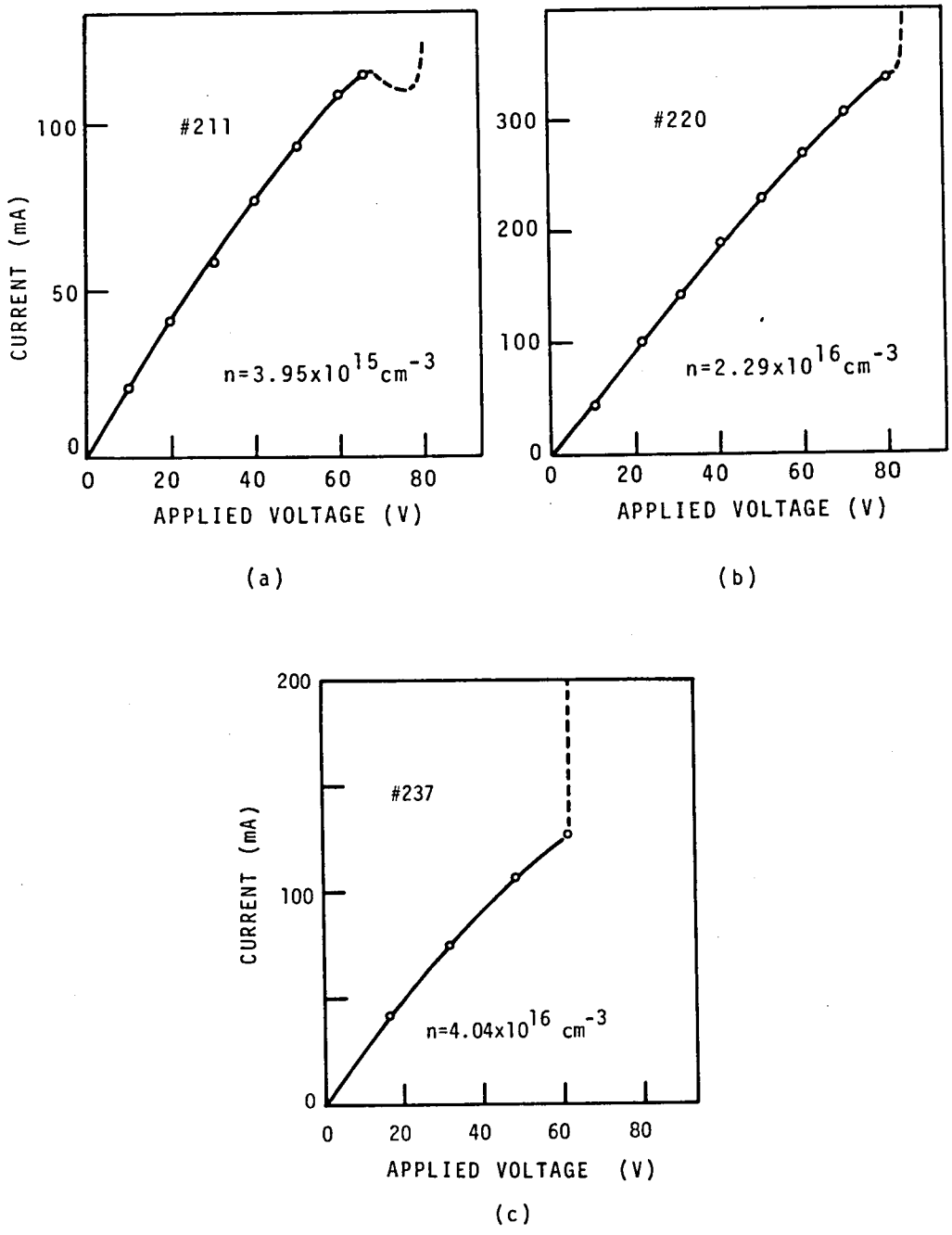

Fig. 9-6 Current below threshold (solid line) and average current beyond threshold (dashed line) observed in $In_{0.53}Ga_{0.47}As$ devices with the same electrode distance but different electron concentration: (a) $n = 3.95\times10^{15}$ cm^{-3}, (b) $n = 2.29\times10^{16}$ cm^{-3}, and (c) $n = 4.04\times10^{16}$ cm^{-3}.

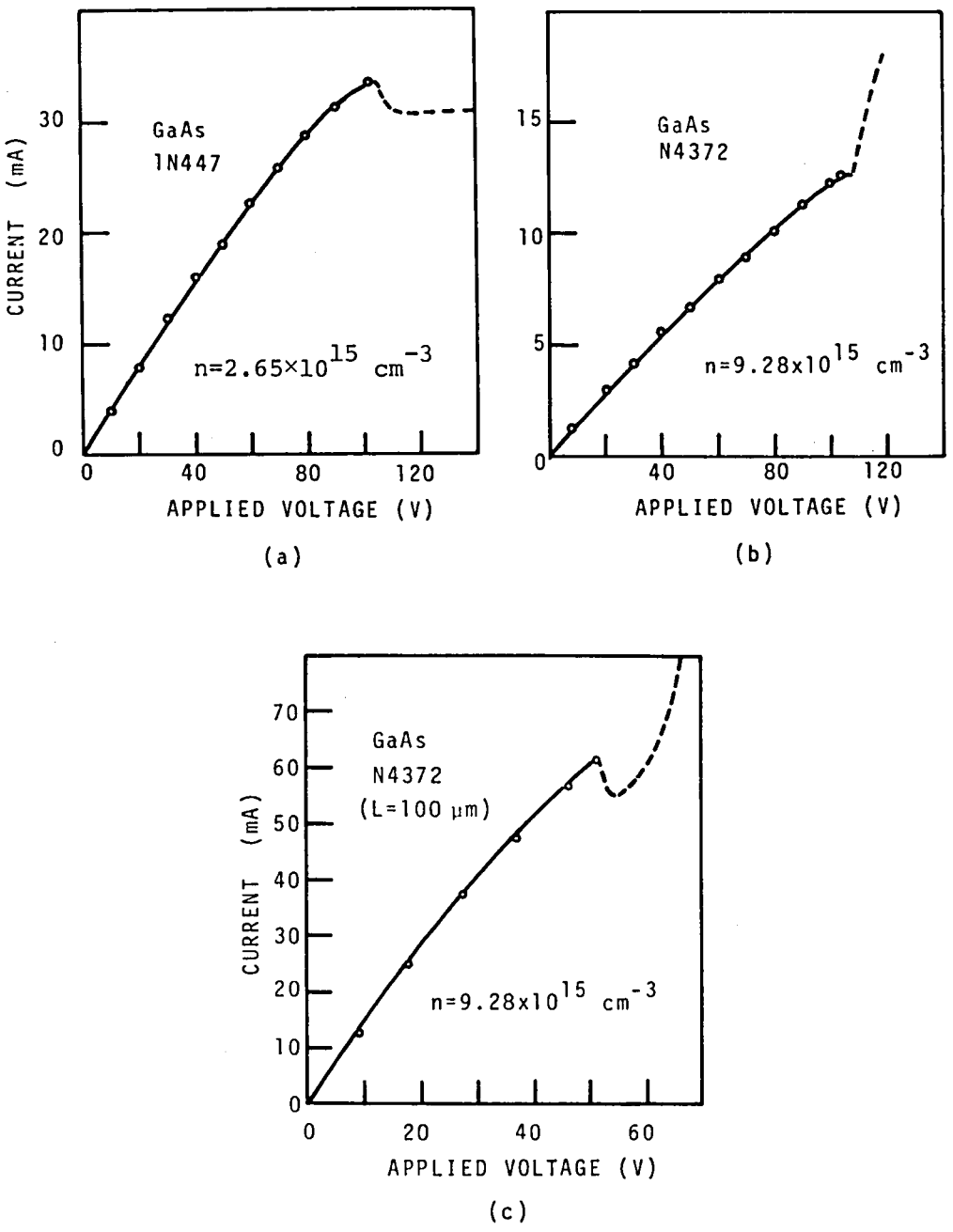

Fig. 9-7 Current below threshold (solid line) and average current beyond threshold (dashed line) observed in GaAs devices. (a) The electrode distance is 200 μm and n is 2.65×10^{15} cm^{-3}. (b) The distance is 200 μm and n is 9.28×10^{15} cm^{-3}. (c) The n is the same as that in (b), but the electrode distance is 100 μm.

9-3-3. Oscillation Spectrum

Observations of the current instabilities by the oscilloscope and the spectrum analyser are shown in Figs. 9-8-a∿c, and Figs. 9-9-a∿c, respectively: (a)'s for GaAs, and (b)'s and (c)'s for $In_{0.53}Ga_{0.47}As$. The instability in the GaAs device is due to the Gunn oscillation and has a sharp peak at 1.32 GHz in the oscillation spectrum. In the $In_{0.53}Ga_{0.47}As$ devices, broader but definite peaks are observed at 1.33 and 1.8 GHz as shown in Figs. 9-9-b and c. In the device made of the wafer #237 which has the highest electron concentration, no definite peak is found in the spectrum.

9-4. DISCUSSION

The following three points are discussed here: correction to the $v-E$ curve using the low field mobility values and Hall factors, comparison of the $v-E$ curve with that of other materials, and the origin of the current instabilities beyond threshold.

9-4-1. Correction to $v-E$ Curve

In the calculation to obtain the $v-E$ curve from the I-V curve, the electron concentration measured from the Hall effect has been used. As is well known, the electron concentration (n) is related to the Hall coefficient (R_H) through the equation:

$$n = \frac{\gamma_H}{e R_H}$$

where e is the electron charge and γ_H is the Hall factor. If n' is calculated from $1/e R_H$, n' is smaller by a factor of γ_H than the real concentration n:

$$n' = n/\gamma_H$$

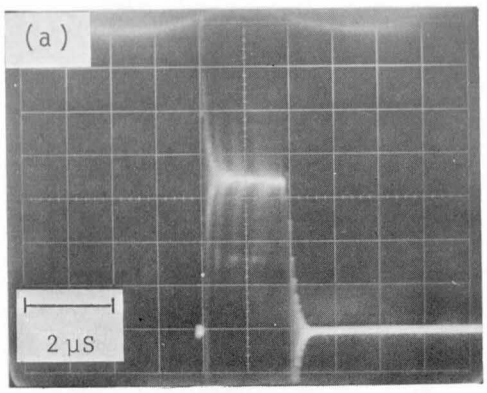

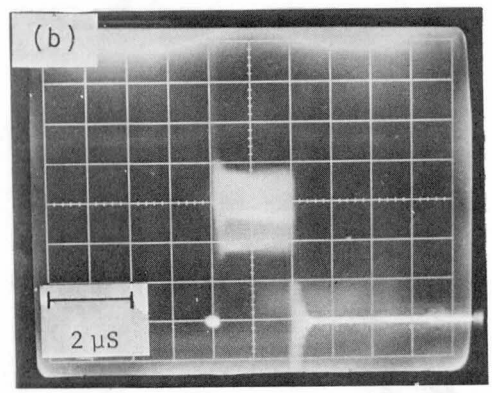

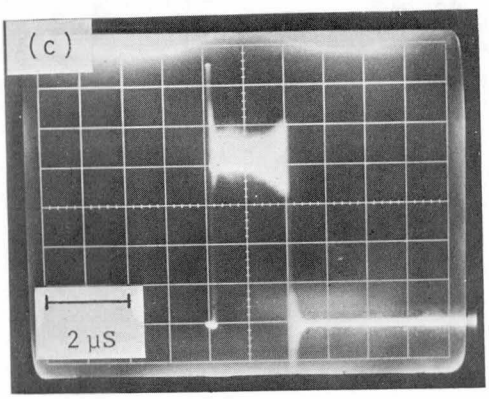

Fig. 9-8 Oscilloscope observation of current beyond threshold. (a) GaAs(1N447) at 104 V, (b) InGaAs(#211) at 92 V, and (c) InGaAs(#220) at 60 V.

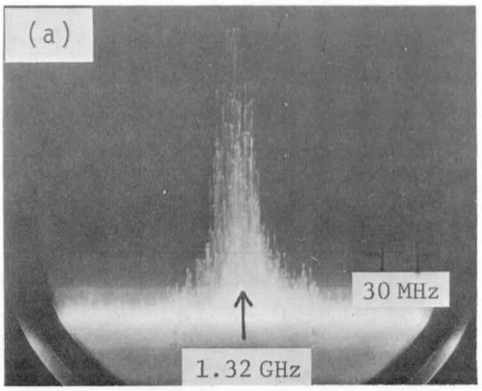

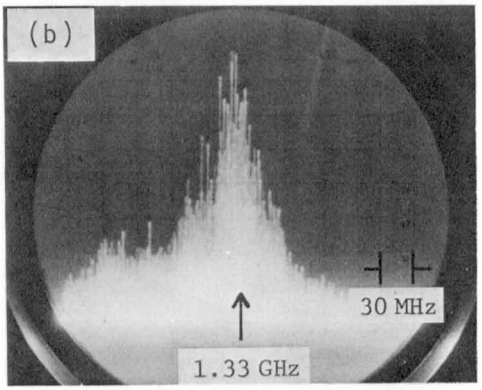

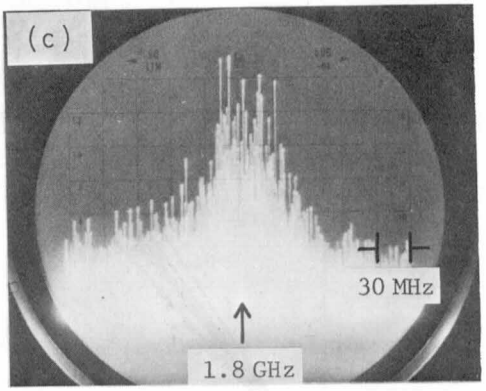

Fig. 9-9 Spectrum observation of current oscillation. (a) GaAs(1N447) at 104 V, (b) InGaAs(#211) at 92 V and (c) InGaAs(#220) at 60 V.

The drift velocity derived from the current density using n' is

$$v' = \gamma_H v \qquad (\because j = e n v = e n' v')$$

where v is the real drift velocity.

In Fig. 9-10, the $v' - E'$ curve where E' is the electric field calculated from the applied bias voltage divided by the electrode distance (Δ), the $v - E'$ curve which is obtained by dividing v' by

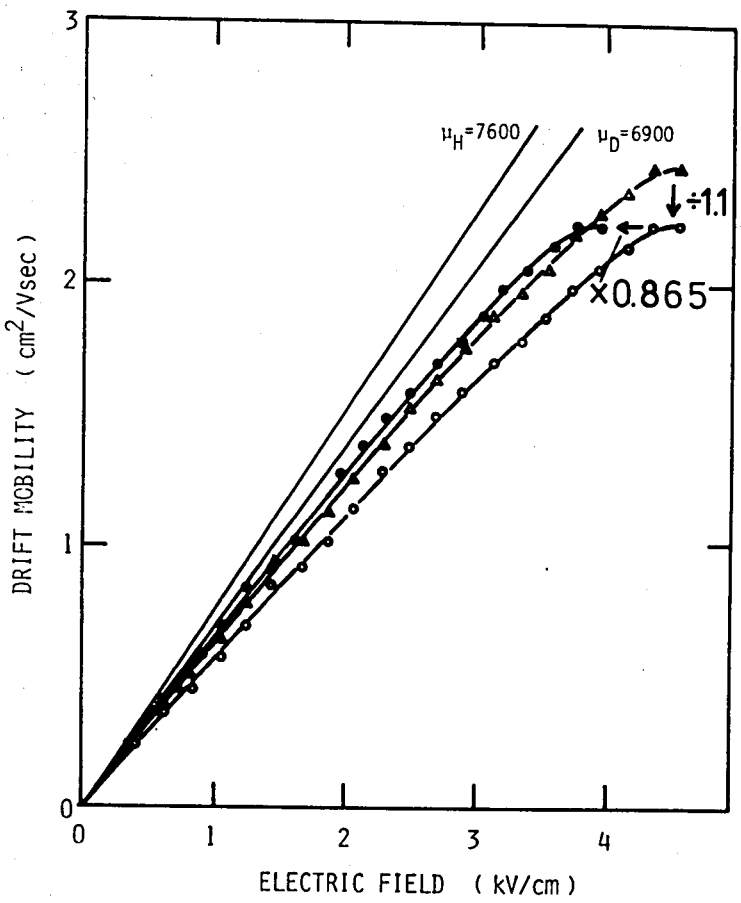

Fig. 9-10 Correction to the $v - E$ curve using the Hall mobility, drift mobility, and the Hall factor.

γ_H (= 1.10 in this device which was calculated using the same method described in Chapter VII) (o), and the final $v-E$ curve in which the electric field is reduced from E' by a factor of 0.856 to fit the low field drift mobility μ_D = 6 900 cm^2/Vsec which has been calculated from the measured Hall mobility μ_H = 7 650 cm^2/Vsec using the same γ_H = 1.10 (●) are shown.

The corrected final $v-E$ curve has the maximum drift velocity of 2.22×10^7 cm/sec at the electric field of 4.0 kV/cm.

On the other hand, M. A. Littlejohn *et al.* have calculated the $v-E$ curve of $In_{0.50}Ga_{0.50}As$ with the Monte Carlo method[6]. They assumed three kinds of the alloy scattering potential and have shown that the scattering affects the $v-E$ characteristics. As shown in Fig. 9-11, the curve calculated with the electron affinity

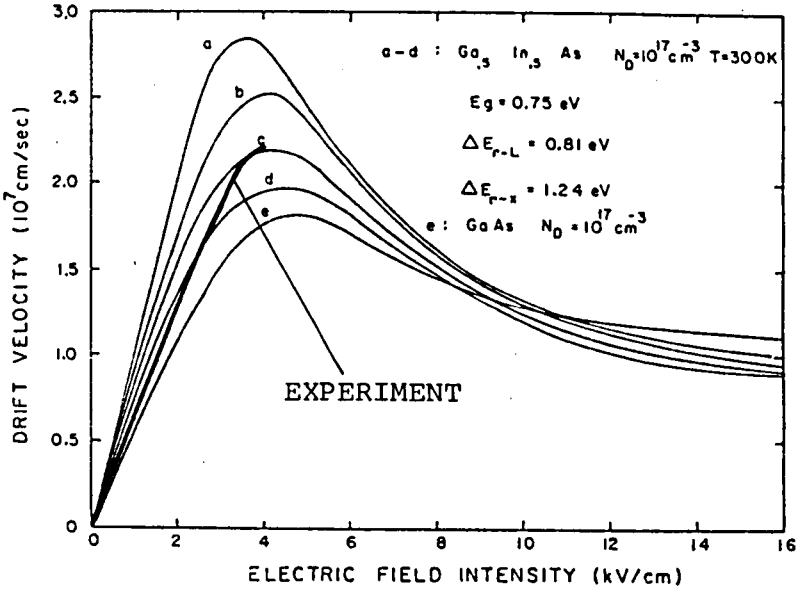

Fig. 9-11 Comparison of the final v-E curve with the calculated curves. Curves (a) ∿ (d) are for $In_{0.50}Ga_{0.50}As$ with different scattering potentials. Curve (e) is for GaAs. The donor concentration is 1×10^{17} cm^{-3} in (a) ∿ (e). For other notations see Ref. 6.

difference as the scattering potential agrees fairly well at the maximum drift velocity with the final $v-E$ curve in Fig. 9-10.

Similar procedures for the curve correction have been conducted for GaAs. The result shown in Fig. 9-12 agrees fairly well with the reported curve[7,8].

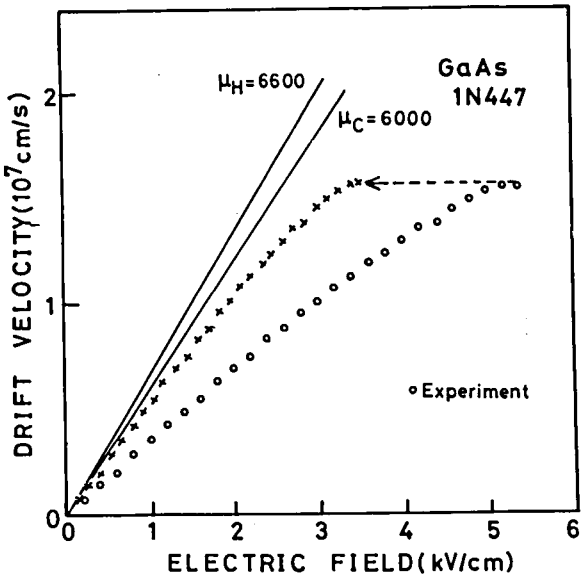

Fig. 9-12 Correction to the $v-E$ curve for GaAs.

9-4-2. Comparison of $v-E$ Curve with That of Other Materials

In Fig. 9-13, the $v-E$ curves for GaAs[7], InP[8], and $In_{0.53}Ga_{0.47}As$ are shown for comparison. The characteristics should be compared at the same doping level, since both the maximum drift velocity and the low field mobility are affected by the ionized impurity scattering. It has been shown in Chapter VII that at the same carrier concentration the mobility of $In_{0.53}Ga_{0.47}As$ is higher by a factor of $\sim$1.5 than that of GaAs. The maximum drift velocity of the alloy is higher by $\sim$30% than that of GaAs. The $v-E$ curve

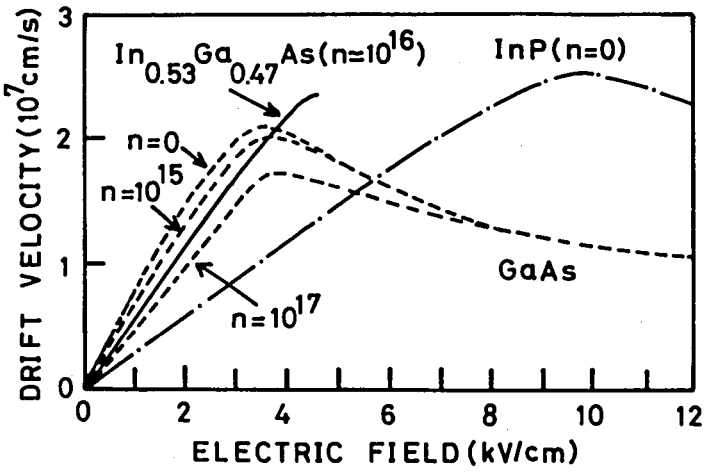

Fig. 9-13 The $v-E$ curves for GaAs, InP, and $In_{0.53}Ga_{0.47}As$ are compared.

of pure InP is shown in the figure, and the maximum velocity is about 2.4×10^7 cm/sec. At the same impurity concentration, $In_{0.53}Ga_{0.47}As$ would have the same or a higher maximum drift velocity than InP. However, the mobility of InP is much lower ($3\,000\sim4\,000$ cm^2/Vsec) and the threshold field is much higher than those of $In_{0.53}Ga_{0.47}As$. Thus, $In_{0.53}Ga_{0.47}As$ would be better suited to the high frequency FET's and high speed switching devices than GaAs and InP.

9-4-3. FET Model Calculations

The low field mobility and the maximum drift velocity are the two of the most essential parameters which predict the highest operating frequency of a relatively long channel FET. Some of the FET characteristics can be predicted by a simple scaling process as shown below.

An equivalent circuit of a MESFET is shown in Fig. 9-14[9]. The notations in the intrinsic FET model represents as follows:

$(C_{dg} + C_{gs})$; the total gate-to-channel capacitance,
C_{dc} ; the capacitance of the dipole layer,
R_i and R_{ds} ; the effects of the channel resistance,
i_{ds} ; the voltage-controlled current source,
g_m ; the transconductance, and
τ_o ; a phase delay reflecting the carrier transit time in the channel section.

The extrinsic (parasitic) elements are:

R_s ; the source resistance,
R_d ; the drain resistance,
R_g ; the gate-metal resistance, and
C_{ds} ; the substrate capacitance.

Some of the electrical properties and the equivalent-circuit parameters used for a GaAs-MESFET[11] and $In_{0.53}Ga_{0.47}As$-MESFET model calculation with 1 μm-gate length and 500 μm-gate width are listed in Table 9-2. In the estimation of the parameters for $In_{0.53}Ga_{0.47}As$, R_i and R_{ds} are reduced by a factor of 5/7.5 which is the ratio of

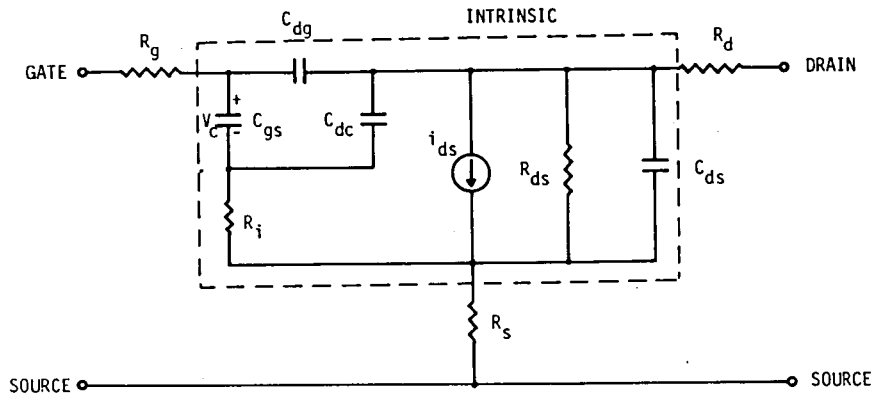

Fig. 9-14 The equivalent circuit for operation of a MESFET in the saturated current region in common-source configuration.

mobility values (μ_H's), C_{gs}, C_{dg}, and C_{dc} are increased by 11.38/10.9 which is the ratio of dielectric constants (ε_o's), and C_{ds} is reduced by 9.52/10.9 which is the ratio of ε_o's of the substrates (InP and GaAs). τ_o is reduced by a factor of 1.7/2.22 which is the ratio of the maximum drift velocities (v_{max}'s). g_m is calculated with the Lehovec and Zuleeg model[12], using the ratios of ε_o,

	GaAs		$In_{0.53}Ga_{0.47}As$	
n	$1x10^{17}$	cm^{-3}	"	
a	0.8	μm	"	
ℓ	1	μm	"	
W	500	μm	"	
v_{max}	$1.7x10^7$	cm/sec	$2.22x10^7$	cm/sec
μ_H	5 000	cm^2/Vsec	7 500	cm^2/Vsec
ε_o	10.9		11.38	
R_d	3	Ω	"	
R_g	2.9	Ω	"	
R_s	2.0	Ω	"	
R_i	2.6	Ω	1.73	Ω
R_{ds}	400	Ω	267	Ω
C_{gs}	0.62	pF	0.647	pF
C_{dg}	0.014	pF	0.0146	pF
C_{dc}	0.02	pF	0.021	pF
C_{ds}	0.12	pF	0.10	pF
τ_o	5.0	psec	3.8	psec

a: active layer thickness, ℓ: gate length, W: gate width

Table 9-2 Fundamental electrical properties and device dimensions of MESFET's are listed in the upper half , and the equivalent-circuit parameters are tabulated in the lower half of the table.

μ_H, and v_{max}. R_d, R_g, and R_s are assumed to be the same as those of GaAs. R_d and R_s would be smaller in $In_{0.53}Ga_{0.47}As$, since they contain sheet resistance of the semiconductor which is smaller in $In_{0.53}Ga_{0.47}As$.

The transconductance g_m, the frequency at unity current gain f_T, and the maximum frequency of oscillation f_u are calculated using the equivalent-circuit parameters in Table 9-2. The results are listed in Table 9-3. They are the predicted values for an $In_{0.53}Ga_{0.47}As$-MESFET on InP substrate with the same dimensions, carrier concentration and contact resistances as those for a GaAs-MESFET. The frequencies are increased with the mobility and the maximum drift velocity, but some what decreased with the increase of the dielectric constants. The transconductance g_m benefits the increases of all ε_o, μ_H, and v_{max}. The frequencies would be still higher if the contact resistances R_d and R_s are correctly evaluated.

From these model calculations based on the experimentally determined parameters, it can be expected that $In_{0.53}Ga_{0.47}As$ has a potential for higher frequency and higher switching speed devices than GaAs and probably than InP.

	GaAs	$In_{0.53}Ga_{0.47}As$
g_m	53 mmho	74.6 mmho
f_T	13.6 GHz	18.4 GHz
f_u	45.6 GHz	53.4 GHz

Table 9-3 g_m, f_T, and f_u derived from the equivalent-circuits are compared between a GaAs- and $In_{0.53}Ga_{0.47}As$-MESFET.

9-4-4. Origin of Current Instability beyond Threshold

In GaAs it is well known that beyond threshold the oscillation occurs due to the transferred-electron effect, *i.e.*, the Gunn oscillation under certain conditions[10-12]. In addition, at the same n_o the maximum electric field in the domain (E_m) is higher with the longer L when biased at threshold[13], and further, at the same applied external voltage the E_m is higher with the larger n_oL product [14], where n_o is the constant equilibrium value of electron concentration and L the length of the active region. If the maximum domain field is high enough, current increase rather than saturation is observed due to the impact ionization of carriers in the high field domain[15].

The phenomena observed in the GaAs devices are just the same as described above: the decreased current region is wider in the lower electron concentration device and the decrease of the current is clearly observed in a shorter length device. In addition, in the corrected $v-E$ curve the threshold field is about 3.5 kV/cm which is common in GaAs[4,5,11,12]. Thus, it can be stated that in the GaAs devices the Gunn oscillation starts beyond threshold and then the impact ionization due to the created high field domains follows.

In the $In_{0.53}Ga_{0.47}As$ devices, very similar phenomena to GaAs are observed in the average I - V characteristics. Moreover, the definite peak is observed in the oscillation spectrum, and from the frequency the domain velocity is estimated to be $2 \sim 3 \times 10^7$ cm/sec or less. It can be considered from these observations that the transferred-electron oscillation occurs in $In_{0.53}Ga_{0.47}As$ beyond threshold and then the impact ionization follows.

At the beginning when we started the research on InGaAs, we had considered vaguely that the transferred-electron effect would be suppressed in $In_{0.53}Ga_{0.47}As$ by the wide energy separation (ΔE) between the central and satellite valleys, since it had been pre-

dicted from a simple consideration on the band structure that in $In_{0.53}Ga_{0.47}As$ the ΔE is equal to or larger than the energy gap and that the transferred-electron effect will not occur at this composition[3,16]. In Ref. 3, the E_g of $In_{0.53}Ga_{0.47}As$ was assumed to be 0.86 eV and equal to ΔE, since in the calculation the linear dependence of the energy gap and separation on composition was used. However, the E_g of $In_{0.53}Ga_{0.47}As$ has been determined accurately to be 0.75 eV at RT as described in Chapter VI. Moreover, the transferred-electron oscillation is observed in this alloy as opposed to the prediction. Thus, further consideration should be given to the band structure.

In GaAs it has been believed that the second lowest conduction-band minima are at X(1,0,0). However, since the Schottky-barrier electro-reflectance measurements using synchrotron radiation[17,18], the evidence has been accumulated which indicates Γ-L-X conduction band ordering for GaAs[19]. The band structure of InAs is shown in Fig. 9-15-a and that of GaAs in Fig. 9-15-c. The $E_{L-\Gamma}$ and $E_{X-\Gamma}$ for InAs and GaAs are found in Ref. 16 and Aspnes' reports[20,21], respectively. The quadratic composition dependence of energy expressed by the Thompson-Woolley formula[22]:

$$E(x) = E_1 + (E_2 - E_1)x + \frac{0.3}{\sqrt{0.5(E_2 + E_1)}}(x^2 - x)$$

gives 0.78 eV for the E_g of $In_{0.53}Ga_{0.47}As$ and is more appropriate than the simple linear composition dependence. In the formula, E_1 and E_2 denote the energy gaps for two end materials. Van Vechten and Bergstresser[23] have theoretically calculated the bowing parameter, *i.e*, the coefficient of $(x^2 - x)$ in the quadratic composition dependence, but it is applicable to the energy gap at $\vec{k} = (0,0,0)$. It is not examined that the Thompson-Woolley formula can be used for the indirect gaps. However, the formula is expressed with the energy gaps of two end materials and is convenient for the first order approximation of the energy gap calculation of ternary alloys.

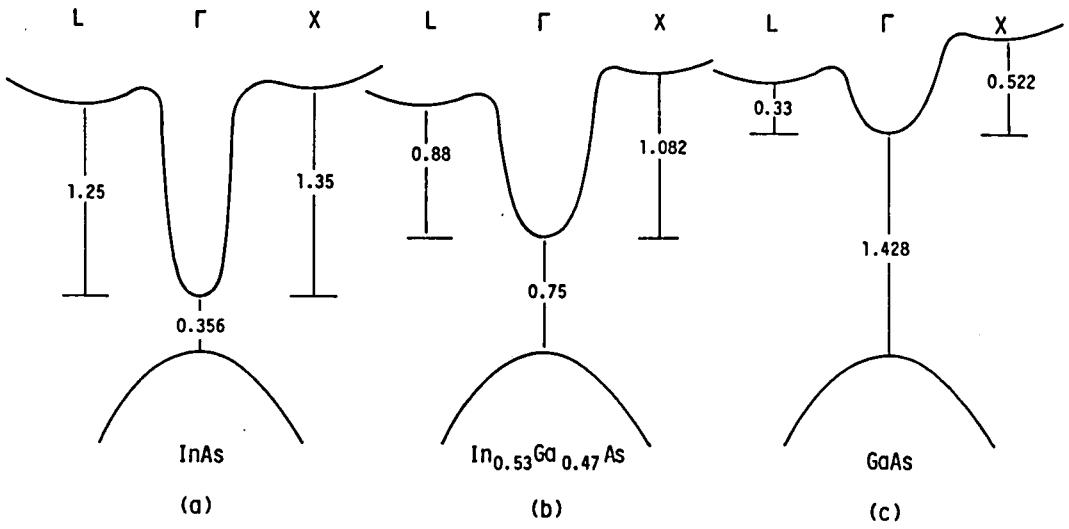

Fig. 9-15 The band structure of InAs, $In_{0.53}Ga_{0.47}As$ and GaAs. The values indicated in the figure are in units of eV.

A predicted band structure of $In_{0.53}Ga_{0.47}As$ is shown in Fig. 9-15-b. The values of $E_{L-\Gamma}$ and $E_{X-\Gamma}$ are calculated from the Thompson-Woolley formula. From the figure, it is seen that the energy separation $E_{L-\Gamma}$ is larger than the energy gap and seems that the transferred-electron effect is suppressed in this alloy. However, it has been shown that the energy as large as about 1.5 times of the energy gap is necessary to impact-ionize the electron-hole pair across the energy gap[24]. The threshold energy for the impact ionization in $In_{0.53}Ga_{0.47}As$ is calculated to be about 1.13 eV (= 1.5×0.75 eV). Thus, it is possible to predict from this band structure that the electron transfer occurs before the impact ionization starts in a low electron concentration $In_{0.53}Ga_{0.47}As$. If the energy separation in the actual $In_{0.53}Ga_{0.47}As$ is smaller than 0.88 eV, the possibility is still higher.

Investigations of the impact-ionization coefficients for electron and hole, the coupling constants between the central and

satellite valleys, and the electron effective masses at the satellite valleys are left for further study.

The avalanche breakdown due to the impact ionization is undesirable for the FET applications, since at a deep gate bias or at a high source-drain voltage the electric field in the channel can be so high as to induce impact ionization. The predominance of the transferred-electron effect is one of the merits of this material for the FET applications.

9-5. SUMMARY

A high electric field has been applied to the $In_{0.53}Ga_{0.47}As$ planar devices, since uniform and high quality crystals have been grown. The results obtained in this chapter are listed below.

1) The velocity-field curve has been derived for $In_{0.53}Ga_{0.47}As$ below threshold.

2) The current instabilities have been observed beyond threshold.

3) The instabilities have been found to be caused by the transferred-electron effect and that the impact-ionization follows.

4) The transferred-electron oscillation peak has been observed by the spectrum analyser.

5) The corrected v-E curve using the Hall factor and the drift mobility agrees fairly well with the curve calculated by the Monte Carlo method.

6) A model calculation based on the experimentally determined parameters predicts a larger transconductance and higher operation frequencies for an $In_{0.53}Ga_{0.47}As$-MESFET than a GaAs-MESFET with the same dimensions and carrier concentration.

References

[1] C. A. Liechti, IEEE IEDM Technical Digest, 1975, p. 6

[2] M. Neuberger, *III-V Semiconducting Compounds*, Handbook of Electronic Materials (IFI/Plenum, New York, 1971) Vol. 2

[3] W. Fawcett, C. Hilsum, and H. D. Rees, Electron. Lett., 5, 313 (1969)

[4] J. G. Ruch and G. S. Kino, Appl. Phys. Lett., 10, 40 (1967)

[5] G. A. Acket and J. De Groot, IEEE Trans. Electron Devices, ED-14, 505 (1967)

[6] M. A. Littlejohn, J. R. Hauser, T. H. Glisson, D. K. Ferry, and J. W. Harrison, Solid-State Electron., 21, 107 (1978)

[7] J. G. Rush and W. Fawcett, J. Appl. Phys., 41, 3843 (1970)

[8] W. Fawcett and D. C. Herbert, J. Phys. C, 7, 1641 (1974)

[9] C. A. Liechti, IEEE Trans. Microwave Theory and Techinque, MTT-24, 279 (1976)

[10] J. B. Gunn, Solid State Commun., 1, 88 (1963)

[11] J. B. Gunn, IBM J. Res. Develop., 8, 141 (1964)

[12] For example, IEEE Trans. Electron Devices, ED-13 (1966), Special Issue on Semiconductor Bulk-Effect and Transit-Time Devices

[13] A. Sasaki, Radio and Electronics Engineer, 39, 81 (1970)

[14] B. G. Bosch and R. W. H. Engelmann, *Gunn-Effect Electronics* (Pitman Publishing, London, 1975) p. 52

[15] P. D. Southgate, J. Appl. Phys., 38, 4589 (1967). We also observed in the experiments at 77 K.

[16] P. J. Bulman, G. S. Hobson, and B. C. Taylor, *Transferred Electron Devices* (Academic Press, London, 1972) pp. 360∿362

[17] D. E. Aspnes, C. G. Olson, and D. W. Lynch, Phys. Rev. Lett., 37, 766 (1976)

[18] D. E. Aspnes, Phys. Rev., B14, 5331 (1976)

[19] M. A. Littlejohn, J. R. Hauser, and T. H. Glisson, J. Appl. Phys., 48, 4587 (1977) and references therein.

[20] D. E. Aspnes, IEEE Trans. Electron Devices, ED-23, 1256 (1976)

[21] D. E. Aspnes and M. Cardona, Bull. Am. Phys. Soc., 22, 410 (1977)

[22] A. G. Thompson and J. C. Woolley, Canad. J. Phys., 45, 255 (1967)

[23] J. A. Van Vechten and T. K. Bergstresser, Phys. Rev., B1, 3351 (1970)

[24] A. G. Chynoweth, in *Semiconductors and Semimetals* edited by R. K. Willardson and A. C. Beer (Academic Press, New York, 1968) Vol. 4, chapter 4

X. PROPERTIES OF Zn-DOPED p-$In_{0.53}Ga_{0.47}As$ ON InP AND APPLICATION TO P-N JUNCTION*

10-1. INTRODUCTION

Although interest is being focused on the applications of $In_{0.53}Ga_{0.47}As$ for optoelectronic devices such as DH lasers[1,2] and APD's[3], there are few reports on the properties of p-type $In_{0.53}Ga_{0.47}As$. P-type layers play a very important role in optoelectronic devices which utilize p-n junction.

In this chapter, electrical and optical properties of Zn-doped p-type $In_{0.53}Ga_{0.47}As$ grown on InP substrates by liquid phase epitaxy, and their application to p-n junction are described.

10-2. EXPERIMENTS

10-2-1. Growth of p-$In_{0.53}Ga_{0.47}As$

The temperature cycle for the growth is similar to Fig. 2-4. After cooling the melts to room temperature, the InP substrate, polycrystalline InAs, and dopant Zn (five 9's pure) are introduced into the boat. The saturation period at 650°C is 30∿40 min. The cooling interval is 5°C with a cooling rate of 0.2∿0.25°C/min. It deposits about 2 μm thickness of the layer. Zn is etched with the H_2O_2:HCl (20:1 in volume) solution for 10 sec at RT. Other materials preparation is similar to those described in Chapter II.

10-2-2. Electrical Properties of p-$In_{0.53}Ga_{0.47}As$

Carrier concentration, resistivity, and Hall mobility are

---

* Y. Takeda, M. Kuzuhara, and A. Sasaki, Japan. J. Appl. Phys. (to be published)

measured by van der Pauw's method[4]. The magnetic field is 5 kG. The contact electrodes are made with pure In dots alloyed at 450°C for 1 min in a flowing hydrogen atmosphere. Semi-insulating InP substrates facilitate electrical evaluations of the grown layers.

10-2-3. Growth of p-n Junction

A temperature cycle for the growth of p-n junction is shown in Fig. 10-1. The substrate surface is etched by the pure In for 10∿15 sec just prior to the growth of InP buffer layer. The n^+-InP buffer layer, non-doped n-$In_{0.53}Ga_{0.47}As$, and p^+-$In_{0.53}Ga_{0.47}As$ layers are successively grown. The growth from 640° to 625°C gives 7∿8 μm thickness of the InP layer. Since the Sn-doped InP epitaxial layer tends to grow non-uniformly[5], Te is used as a dopant for the n^+-InP buffer layer. Starting from 625°C, the cooling intervals of 5°C and 6∿7°C give ∿2 μm and ∿3 μm thickness of $In_{0.53}Ga_{0.47}As$, respectively. Typical carrier concentrations are $n \simeq 2\times10^{16}$ cm^{-3} and $p \simeq 2\times10^{18}$ cm^{-3}. The substrate is Sn-doped n^+-InP ($n \sim 2\times10^{18}$ cm^{-3}) and (111)B-oriented. A cross section of the p-n junction is shown in Fig. 10-2. The creaved cross section

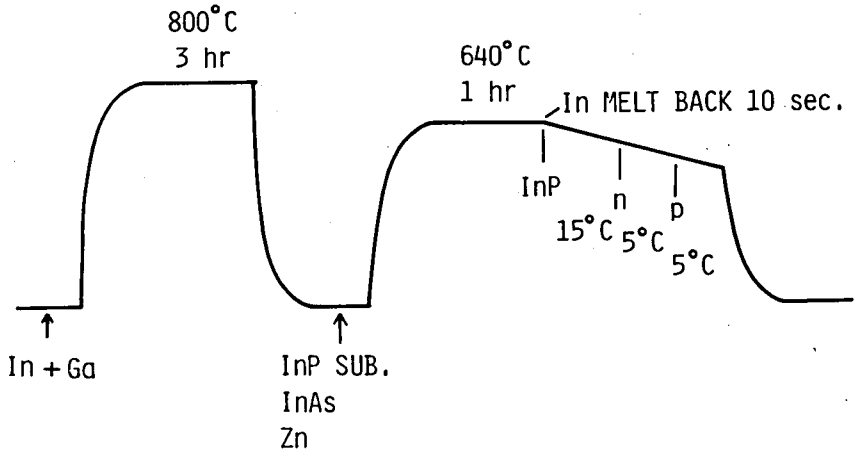

Fig. 10-1 Temperature cycle for the growth of p-n junction.

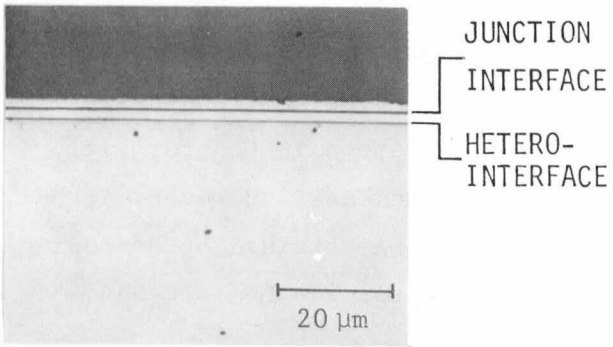

Fig. 10-2 A cleaved and etched cross section of the $In_{0.53}Ga_{0.47}As$ homojunction diode on InP.

has been etched with the A-B solution[6] at 50°C for several sec. The interfaces are seen to be planar.

10-2-4. SEM and EBIC Observation

The SEM (scanning electron microscope) of the Auger electron microscope[i)] is used for the secondary-electron and EBIC (electron-beam induced current) mode observation of the junction. With the secondary-electron mode the heterojunction interface and/or the p-n junction interface are delineated without chemical etching, since the emission rate of the secondary-electron depends on the materials or material characteristics. In the EBIC mode the brightness of the CRT display is modulated by the EBIC intensity. At the same excitation, the intensity varies with the distance from the junction interface, the diffusion length, the defects, and any mechanism which affects the flow rate of the created minority carriers through the p-n junction. For a general description of the SEM and EBIC used for characterizations of semiconductor devices, see Ref. 7.

10-3. RESULTS AND DISCUSSION

---

i) JAMP-3, JEOL LTD.

10-3-1. Zn-Doping

Undoped layers of $In_{0.53}Ga_{0.47}As$ are n-type with carrier concentration $n = 1 \sim 2\times10^{16}$ cm^{-3}, resistivity $\rho \simeq 0.08$ Ωcm, and Hall mobility $\mu_H = 7\,000 \sim 8\,000$ $cm^2/Vsec$ at RT as shown in Chapter VIII. Ge and Zn are commonly used as an acceptor in GaAs. However, it has been reported that p-type $In_{1-x}Ga_xAs$ cannot be obtained by Ge-doping for $x < 0.9$[8]. Since Zn is used as an acceptor in InAs, it was decided to investigate Zn-doping in $In_{0.53}Ga_{0.47}As$.

Zn is quite volatile and R. E. Nahory *et al.*[9] used graphite plugs capping the melt wells to reduce Zn evaporation. Graphite caps are used in our boat, anticipating dopant loss during the saturation period. However, noticeable dopant loss is not observed in our growth at 650°C which is much lower than those of Nahory *et al.* ($\geq$ 800°C). This is confirmed by repeating the growth using the same melt and the same temperature cycle. The hole concentrations and Hall mobility values are the same between the first and the second wafer.

Fig. 10-3 shows the hole concentration as a function of the atomic fraction of Zn in the solution, n_{Zn}^{ℓ}. The hole concentration is proportional to the square root of n_{Zn}^{ℓ}, *i.e.*, $p \propto (n_{Zn}^{\ell})^{\frac{1}{2}}$.

In GaAs the same relationship has been observed[10]. From a simple theory which assumes growth from a dilute solution and equilibrium between the bulk of the solid and the liquid solution, the dopant concentration in the solid n^s is proportional to the square root of the dopant atomic fraction in the liquid n^{ℓ} when $n^s >> n_i$. Here, n_i is the intrinsic carrier concentration in the solid at the growth temperature. Since in GaAs $n_i = 10^{16} \sim 10^{17}$ cm^{-3} at the usual LPE growth temperatures of $800 \sim 900$°C, the extrinsic approximation is appropriate for the usual doping of interest[10]. In addition, Zn is a fast diffusing dopant and the equilibrium is thought to be established for the moderate growth rate[10].

The intrinsic carrier concentration of $In_{0.53}Ga_{0.47}As$ at 650°C is $\sim 3\times10^{17}$ cm^{-3}[11], and it can be considered to be extrinsic for the doping range in Fig. 10-3. The growth velocity is $\sim 10^{-7}$ cm/sec in $In_{0.53}Ga_{0.47}As$ on (111)B-oriented InP substrate. Both extrinsic and equilibrium conditions may be satisfied, and thus p is proportional to $(n_{Zn}^{\ell})^{\frac{1}{2}}$. In $In_{0.15}Ga_{0.85}As$, the hole concentration is proportional to n_{Zn}^{ℓ}[9]. In their case it would be considered that the Zn evaporation affected the relationship.

The same n_{Zn}^{ℓ} gives higher hole concentration in $In_{0.53}Ga_{0.47}As$ than in GaAs. This tendency is agreeable with the prediction from the Schottky barrier effect[10,12]. In liquid phase epitaxy, the melt is a liquid metal and the growing solid is a semiconductor. In this case, the Schottky barrier is formed at the interface. This

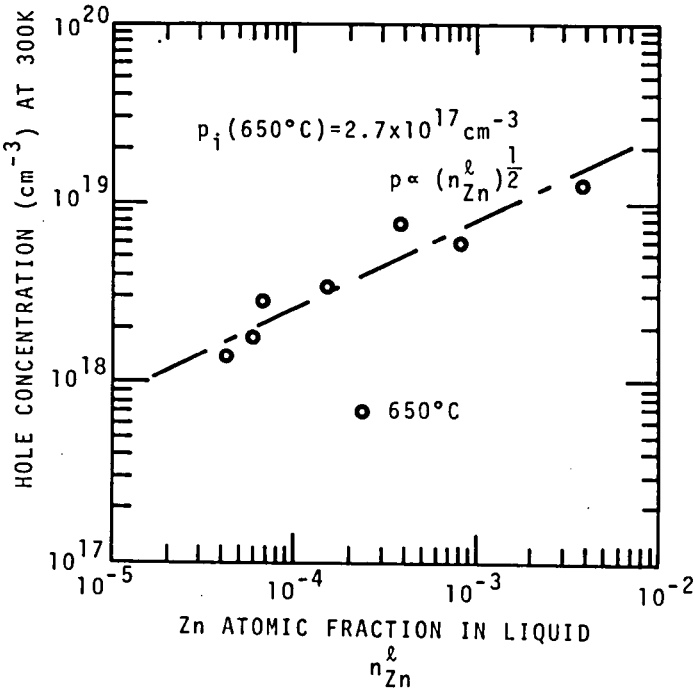

Fig. 10-3 Hole concentration in $In_{0.53}Ga_{0.47}As$, grown at 650°C, as a function of atomic fraction of Zn in melt. The line drawn through the data points has a slope of -1/2.

Schottky barrier modifies the growth behavior of liquid phase epitaxy. The variation of growth rate with the crystal orientation is explained by the barrier-height dependence on the orientation. Although the barrier heights of the liquid Ga:GaAs contact and the liquid (In + Ga):$In_{0.53}Ga_{0.47}As$ are not known, it would be reasonable to assume that $In_{0.53}Ga_{0.47}As$ has a lower barrier height than GaAs [13]. The distribution coefficient $k(T)$ is expressed as:

$$k(T) = k_o(T) \exp(- \phi_B / k_B T)$$

where $k_o(T)$ is a concentration independent term and ϕ_B is the Schottky barrier height[10]. The equation shows that at a lower barrier height the distribution coefficient is larger and thus the hole concentration is higher at the same n^s.

10-3-2. Resistivity and Hall Mobility

The variations in the room-temperature resistivity and Hall mobility of Zn-doped $In_{0.53}Ga_{0.47}As$ are shown in Figs. 10-4 and 10-5 together with those of Zn-doped $In_{0.15}Ga_{0.85}As$[9]. The solid circles are for $In_{0.53}Ga_{0.47}As$ and open circles are for $In_{0.15}Ga_{0.85}As$. There is seen to be very little difference between them. Zn-doped InAs gives room-temperature Hall mobility of 150 cm^2/Vsec at $p \simeq 2\times 10^{17}$ cm^{-3} and 100 cm^2/Vsec at $p \simeq 7\times 10^{18}$ cm^{-3}[14]. These mobility values are slightly higher than those of alloys. Nahory *et al.*[9] found no difference in the resistivity and Hall mobility between $In_{0.15}Ga_{0.85}As$ and GaAs grown in the same growth system.

In relatively highly doped p-type $In_{1-x}Ga_xAs$ as shown here, there seems to be no strong variation in the room-temperature electrical properties with composition. On the other hand, in n-type $In_{1-x}Ga_xAs$, electron mobility is greatly dependent on composition[15]. Effects of disorder on electrical properties in purer

p-type $In_{1-x}Ga_xAs$ will be interested. Theoretical calulation and extensive review of hole mobility of III-V compounds are given by J. D. Wiley[16].

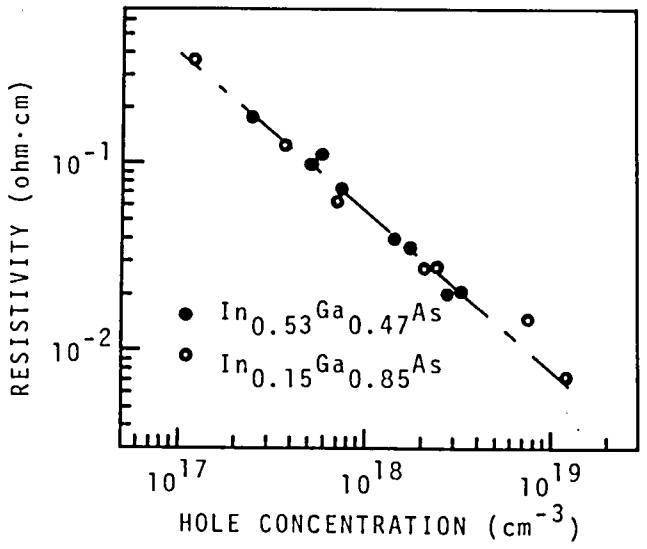

Fig. 10-4 Room-temperature resistivity *vs.* hole concentration. The solid circles are for $In_{0.53}Ga_{0.47}As$. The open circles represent the reported data for $In_{0.15}Ga_{0.85}As$.

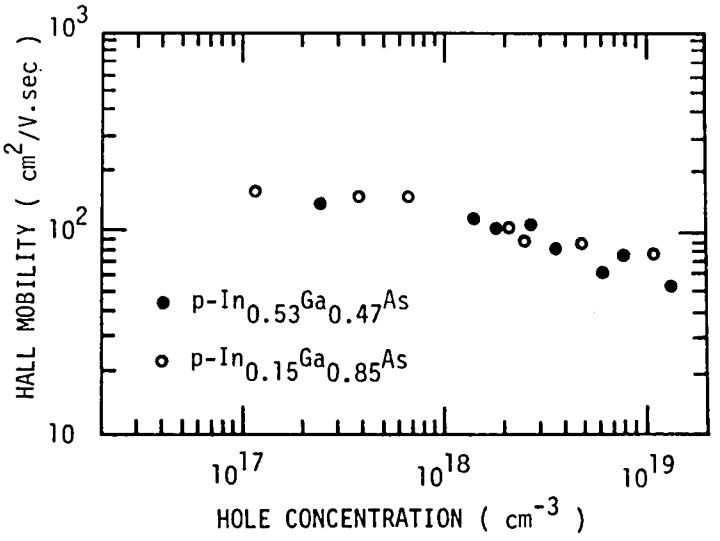

Fig. 10-5 Room-temperature Hall mobility *vs.* hole concentration. The solid circles give data for $In_{0.53}Ga_{0.47}As$ and the open circles are for the reported data for $In_{0.15}Ga_{0.85}As$.

10-3-3. Photoluminescence

Photoluminescence experiments are similar to those described in Chapter III, but samples are not angle-lapped. Fig. 10-6 shows hole concentration dependence of the energy at peak PL intensity. A slight decrease in energy is observed both at 300 and 77 K. In Zn-doped GaAs, distinct decrease of the photon energy at peak was observed, and this is explained as a shrinkage of band gap due to heavy doping[17].

The full width at half maximum (FWHM) of the PL spectra increases with hole concentration as shown in Fig. 10-7 and the dependence in $In_{0.53}Ga_{0.47}As$ is weaker than in GaAs[17]. The FWHM of undoped $In_{0.53}Ga_{0.47}As$ is 12∿13 meV at 77 K and 40∿45 meV at 300 K.

10-3-4. SEM and EBIC Observation of Cleaved Cross Section

Figure 10-8-a shows the SEM observation of the cleaved cross section in the secondary-electron mode. The p-n junction interface is clearly delineated without staining. Fig. 10-8-b shows the EBIC micrograph of the same portion as Fig. 10-8-a. The width and brightness of the white portion along the junction are uniform. It

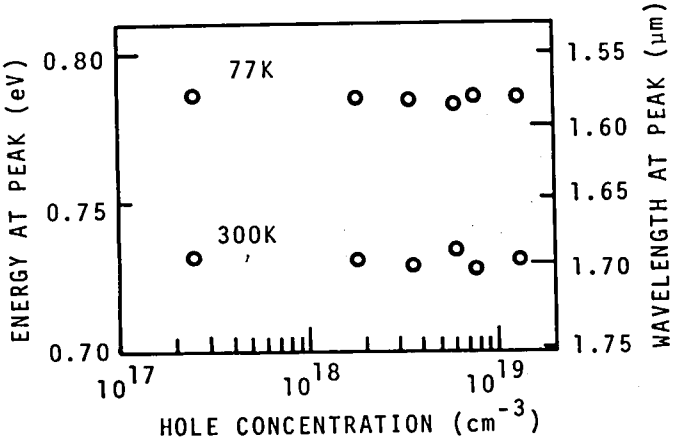

Fig. 10-6 The energy at peak PL intensity at 77 and 300 K as a function of hole concentration. A slight decrease in photon energy is observed.

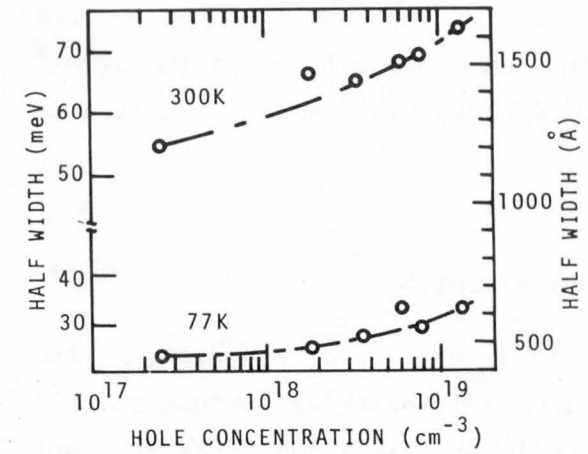

Fig. 10-7 The FWHM of the PL spectra at 77 and 300 K as a function of hole concentration.

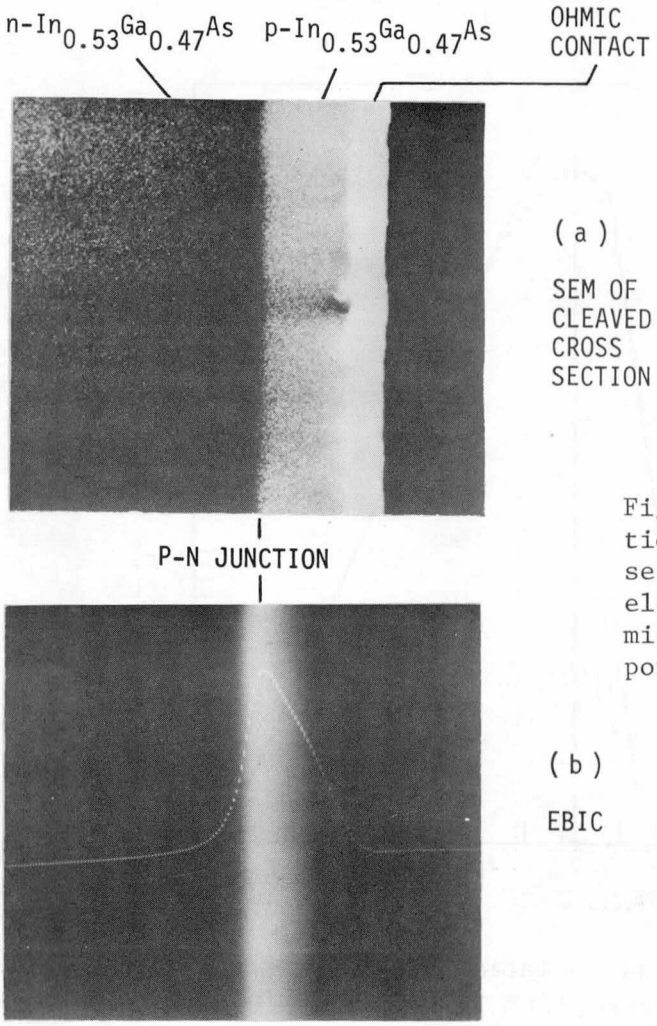

Fig. 10-8 (a) SEM observation of the cleaved cross section in the secondary-electron mode. (b) The EBIC micrograph of the same portion as (a).

(#330)

can be considered from the figure that both the diffusion lengths of the electron and hole are constant along the p-n junction interface, indicating uniform crystal quality and doping level in the alloy layers. A line scan of the EBIC intensity across the junction is superimposed in Fig. 10-8-b.

10-3-5. Minority-Carrier Diffusion Length

The EBIC intensity (I_E) is a function of the distance from the p-n junction interface (d), minority-carrier diffusion length (L), and surface-recombination velocity (v_s), when the excitation

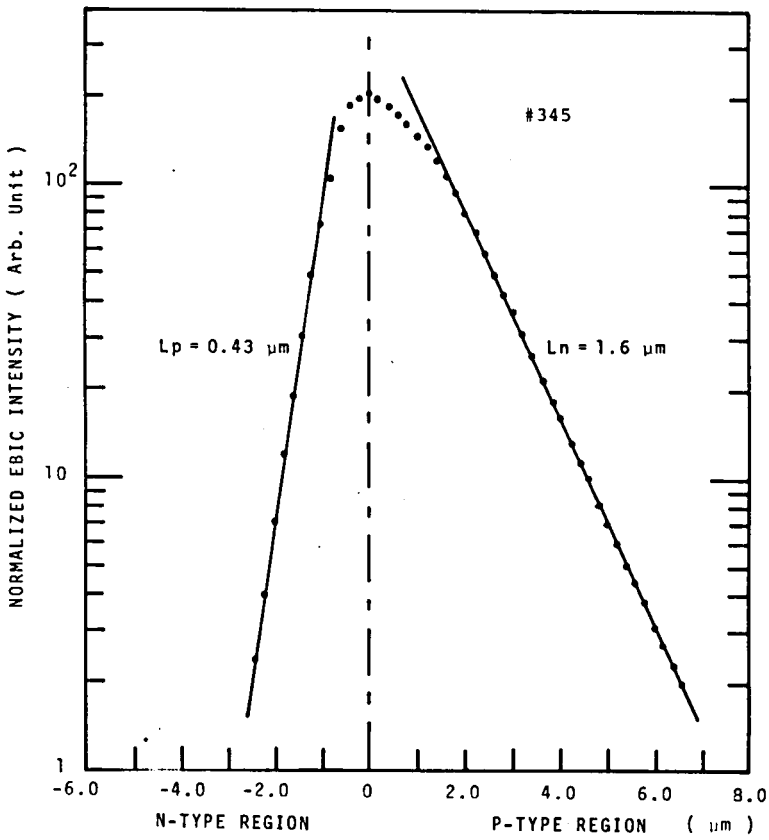

Fig. 10-9 The EBIC intensity variation with distance from the junction interface. From the slopes, minority-carrier diffusion lengths are derived.

is constant in a normal material. However, it has been shown that when $d > 2L$, $I_E \propto \exp(-d/L)$ and independent of v_s[18].

Figure 10-9 is an example of the EBIC intensity variation with distance from the p-n junction interface. The acceleration voltage of the electron beam is 20 kV and the beam current is 1×10^{-10} A.

In the figure the distance is longer than 2L in both n- and p-type layer. From the slopes, minority-carrier diffusion lengths L_n (for the electron in the p-type region) $\sim$1.6 μm and L_p (for the hole in the n-type region) $\sim$0.43 μm are derived. The L_n is comparable to that observed in $In_{0.14}Ga_{0.86}As$ homojunction[19]. With the measurements in other junctions, the L_n and L_p are found to be $1.3\sim4.3$ μm and $0.39\sim0.65$ μm, respectively. The dependence of the diffusion length on the majority-carrier concentration, which is observed in GaAs[20], is not clear, and left for further study.

10-4. SUMMARY

1) Zn has been found to be a useful dopant as an acceptor for $In_{0.53}Ga_{0.47}As$ and it has been found that the hole concentration is proportional to $(n_{Zn}^{\ell})^{\frac{1}{2}}$.
2) Noticeable influence of Zn evaporation has not been observed at 650°C.
3) The variation of resistivity and Hall mobility of Zn-doped $In_{0.53}Ga_{0.47}As$ at RT is essentially the same as those of Zn-doped $In_{0.15}Ga_{0.85}As$ and GaAs.
4) The photon energy at peak intensity and full width at half maximum of the PL spectra vary with the hole concentration in the same manner as GaAs, but the dependence is weaker than GaAs.
5) $In_{0.53}Ga_{0.47}As$ homojunction has been formed on InP substrate utilizing the Zn-doping.
6) Minority-carrier diffusion lengths have been derived using the

distance dependence of the EBIC intensity. The results are that L_n is 1.3∿4.3 μm and that L_p is 0.39∿0.65 μm.

References

[1] H. Nagai and Y. Noguchi, Appl. Phys. Lett., 32, 234 (1978)

[2] S. Akiba, K. Sakai, and T. Yamamoto, Japan. J. Appl. Phys., 17, 1899 (1978)

[3] T. P. Pearsall and R. W. Hopson, Jr., J. Electron. Mater., 7, 133 (1978)

[4] L. J. van der Pauw, Philips Res. Rep., 13, 1 (1958)

[5] T. Fukui and T. Kobayashi, 25th Spring Meet. Japan. Soc. Appl. Phys. and Related Socs., Tokyo, March 1978, 28a-K-8

[6] M. S. Abrahams and C. J. Buiocchi, J. Appl. Phys., 36, 2855 (1965)
G. H. Olsen and M. Ettenberg, J. Appl. Phys., 45, 5112 (1974)

[7] For example, L. J. Balk, E. Kubalek, and E. Menzel, IEEE Trans. Electron Devices, ED-22, 707 (1975)

[8] M. Kurihara, T. Moriizumi, and K. Takahashi, Solid-State Electron., 16, 7631 (1973)

[9] R. E. Nahory, M. A. Pollack, and J. C. DeWinter, J. Appl. Phys., 46, 775 (1975)

[10] H. Kressel and H. Nelson, "Properties and Applications of III-V Compound Films Deposited by Liquid Phase Epitaxy," in *Physics of Thin Films* edited by G. Hass, M. H. Francombe, and R. W. Hoffman (Academic Press, New York, 1973) Vol. 7, and references therein.

[11] Extrapolated from the author's calculation. Y. Takeda, A. Sasaki, and T. Takagi, Rept. Tech. Group Electron Devices ED76-65 (1976-10), IECE Japan (in Japanese), and Chapter VI of this thesis.

[12] K. H. Zschauer and A. Vogel, in *Gallium Arsenide and Related Compounds*, 1970 Conference, Series 9 (Institute of Physics, London, 1971) p. 100

[13] C. A. Mead and W. G. Spitzer, Phys. Rev.,134, A713 (1964)

[14] O. G. Folberth and H. Weiss, Z. Naturforsch., 9A, 954 (1954)

[15] T. Katoda, F. Osaka, and T. Sugano, Japan. J. Appl. Phys., 13, 561 (1974)

[16] J. D. Wiley, in *Semiconductors and Semimetals* edited by R. K.

Willardson and A. C. Beer (Academic Press, New York, 1975) Vol. 10, p. 91

[17] J. I. Pankove, *Optical Processes in Semiconductors* (Prentice-Hall, New Jersey, 1971) pp. 134∿137, and references therein.

[18] C. van Opdorp, Philips. Res. Rep., 32, 192 (1977)

[19] T. Ota, K. Oe, and M. Yamaguchi, J. Appl. Phys., 56, 3674 (1975)

[20] H. C. Casey, Jr., B. I. Miller, and E. Pinkas, J. Appl. Phys., 44, 1281 (1973)

XI. INFRARED PHOTODETECTOR*

11-1. INTRODUCTION

In the optical fiber transmission system at the wavelength of 0.85 μm, those of the optical source of GaAs laser, the transmission line of silica fiber, and the detector of Si-APD (avalanche photodiode) are used. The fabrication technology of the GaAs DH (double heterojunction) laser is well established, and the Si-APD is a very reliable detector. The transmission system at 0.85 μm is an epoch-making one and superior to the conventional microwave system in many respects[1,2].

However, for a higher capacity and longer distance (*e.g.*, > 50 km) transmission, the wavelength of ∿1.3 μm is best suited to the silica fiber. It is because at this wavelength the transmission loss is as low as 0.47 dB/km[3] and the material dispersion is zero [4].

The InGaAsP/InP DH laser is well developed for an optical source at ∿1.3 μm[5] and has a fairly long life at cw operation at room temperature[6]. The detector for this wavelength is now being developed. The Ge-APD is the only device which can be used at present. However, the Ge-APD suffers a high leakage current and a large avalanche noise[7,8]. Many materials such as InGaAs/InP[9], InGaAsP/InP[10], AlGaSb/GaSb[11], and AlGaAsSb/GaSb[12] are now being investigated, and the Ge-APD is being refined.

On the other hand, a silica fiber which has an extremely low loss at the wavelength of 1.55 μm as low as 0.20 dB/km has been fabricated very recently[13]. It is expected that with this fiber a longer distance than 100 km transmission is available without any

---

* Y. Takeda and A. Sasaki, Rept. Tech. Group Electron Devices, ED78-62 (1978-10) IECE Japan (in Japanese)
Y. Takeda and A. Sasaki, 1979 Nat. Conv. Rec., IECE Japan. S3-19

repeater. Among those materials mentioned above, InGaAs/InP and/or AlGaSb/GaSb would be suited to the detector at this wavelength, since they cover the wavelength as long as ∿1.6 μm. The InGaAs/InP photodiode covers the low loss region of the silica fiber as shown in Fig. 11-1. The wavelength dependence of the photoresponse of the diode is shown in §11-3-2.

Since high quality of $In_{0.53}Ga_{0.47}As$ layers on InP substrate are obtained and it has the energy gap of 0.75 eV (corresponding to 1.65 μm wavelength) at room temperature, an infrared photodetector has been fabricated with this material.

In this chapter, the electrical and optical characteristics of the $In_{0.53}Ga_{0.47}As$ homojunction diodes, and the APD-operation are described.

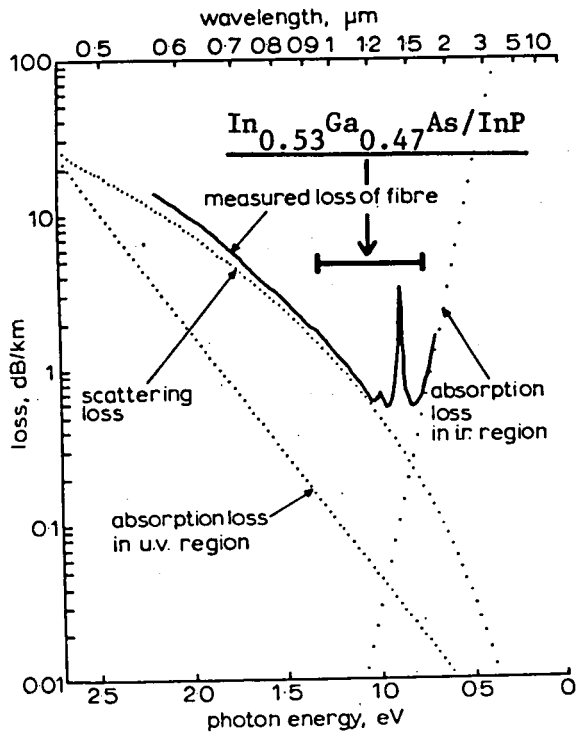

Fig. 11-1 The $In_{0.53}Ga_{0.47}As$/InP photodiode covers the low loss region of the silica fiber.

11-2. EXPERIMENTS

11-2-1. Fabrication of Diode

The growth procedures for the p-n junction are described in Chapter X. The InP surface of the wafer in which p-n junction is formed is lapped and polished to the thickness of 150∿200 μm. Ohmic contact materials, Au-Sn (90:10 in weight) for n^+-InP and Au-Zn (90:10 in weight) for p^+-$In_{0.53}Ga_{0.47}As$, are evaporated onto the wafer surfaces on which contact patterns are delineated by a conventional photolithographic technique. The photoresist is used as an evaporation mask. After removing the photoresist (the contact materials which are evaporated directly onto the semiconductor surfaces remain keeping the contact pattern after removal), the contacts are alloyed at 450°C for 1 min in a flowing hydrogen atmosphere.

The wafer is etched to form mesa-shaped diodes, as shown in Fig. 11-2, with a solution of H_2SO_4:H_2O_2:H_2O (3∿5:1:1 in volume) or HF:HNO_3:H_2O (1:1:1 in volume) at room temperature. Both solutions etch InGaAs selectively, since the etching rate for InP is much lower than for InGaAs. The diode is mounted with In solder on the copper plate which has an aperture for the incident light. The ohmic contact of the p^+-layer is connected with an electrode by a microprobe under a microscope.

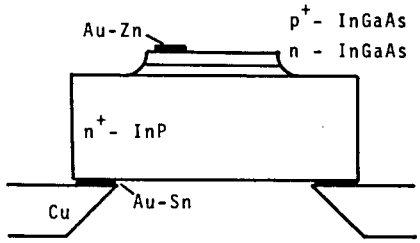

Fig. 11-2 A schematic drawing of the mesa-shaped diode. It is mounted on a copper plate which has an aperture.

11-2-2. Capacitance - Voltage (C - V) Characteristics

The C - V characteristics of the diodes are measured with a conventional capacitance meter[i] by changing the reverse bias voltage.

11-2-3. Photoresponse

The photoresponse of the diode, *i.e.*, the wavelength-dependence of the short-circuit current, is measured by irradiating the diode surface with a monochromatic light whose wavelength is varied continuously by a monochromator[ii]. The optical source is a tungsten lamp.

The relative intensity *vs.* wavelength characteristics of the incident beam on the diode surface is measured by a PbS photoconductive cell whose responsivity is known. It is shown in Fig. 11-3.

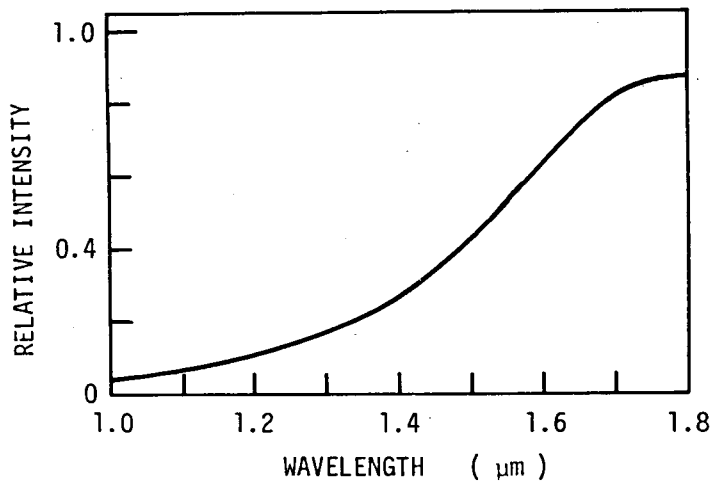

Fig. 11-3 Spectral distribution of the excitation light for the photoresponse measurement.

i) LCR meter 4332A, Yokogawa Hewlett Packard

ii) G-250, Nippon Kogaku Kogyo K.K.

11-2-4. Current - Voltage (I - V) Characteristics

The I - V characteristics of the diodes are measured by the X - Y recorder or the electrometer[i] and microvoltmeter[ii].

11-2-5. Measurement of Avalanche Multiplication

The reverse voltage dependence of the avalanche multiplication is measured by a lock-in technique using the apparatus shown in Fig. 11-4. The photo-carriers are generated by a YAG laser[iii] beam

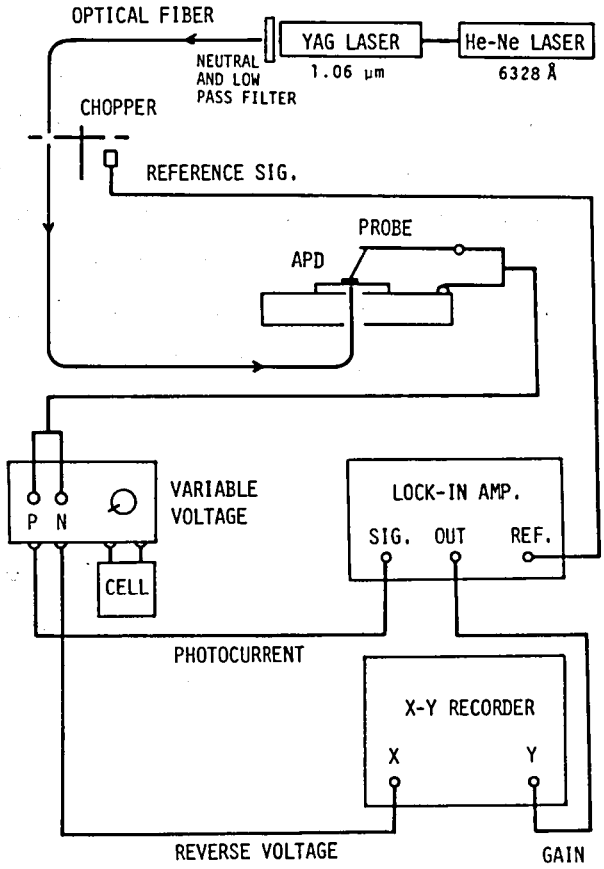

Fig. 11-4 Schematic diagram of the apparatus for the measurement of avalanche multiplication.

i) VIBRATING REED ELECTROMETER, TR-48M, TAKEDA RIKEN
ii) Model AM-1001, OHKURA ELECTRIC Co.
iii) YAG-TWO, general photonics corp.

(1.06 μm wavelength) which is attenuated by neutral filters to give a photocurrent of 1∿2 μA at the bias-voltage of zero. With the lock-in technique the increase of the DC dark current at the reverse bias is eliminated from the measurement of photocurrent which is induced by the chopped laser beam, since only a synchronized current with the chopped beam is detected by this technique.

11-3. RESULTS AND DISCUSSION

11-3-1. C - V Characteristics

The characteristics of $1/C^2$ *vs.* voltage at low reverse voltage are shown in Fig. 11-5. The capacitance is normalized to the area of 1 cm^2. All the data are on the straight lines, indicating the abrupt junction being formed. Since the n-layer has lower carrier concentrations by about two orders of magnitude than the p-layer ($p \simeq 2\times10^{18}$ cm^{-3}), the junction is the one-sided abrupt junction. In the one-sided abrupt junction the shape of the electric field distribution is a right-angled triangle. This is the simplest

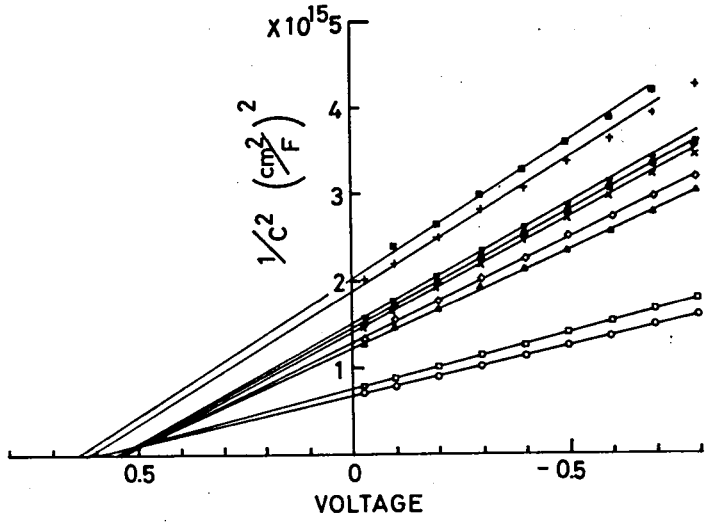

Fig. 11-5 Capacitance-voltage characteristics at low voltage. $1/C^2$ values are plotted against V to confirm the abrupt junction in the diodes.

and convenient for the analysis of the behavior of carriers in the field. The built-in voltage at the junction is seen to be about 0.6 V.

Figure 11-6-a shows a $1/C^2 - V$ characteristic of a diode in a wider range of reverse voltage, as high as -18 V. It is seen to have two different slopes; at the lower voltage the slope corresponds to $N_d = 1.9\times10^{16}$ cm^{-3} and at the higher voltage $N_d = 2.7\times10^{16}$ cm^{-3}. The donor concentrations are calculated from the well-known equation

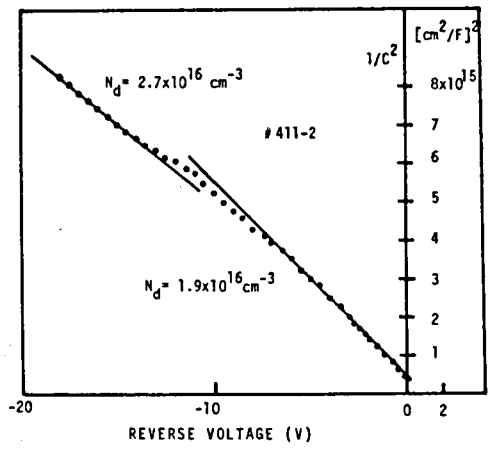

(a)

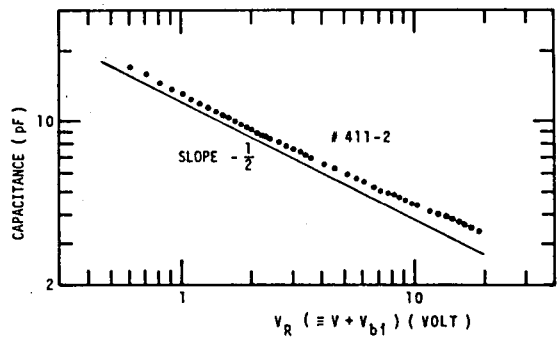

(b)

Fig. 11-6 (a) $1/C^2 - V$ characteristic in a wide range of reverse voltage. (b) The same data are plotted in log C *vs.* log V_R to find the slope variation.

for the one-sided abrupt-junction:

$$\frac{d\,(1/C^2)}{dV} = \frac{2}{e\,\varepsilon_o\,\varepsilon_r\,N_d}$$

The deviation from the abrupt junction at higher reverse voltage is more clearly seen in Fig. 11-6-b. The abscissa is $(V+V_{bi})$ and the ordinate is the capacitance. Here, V is the applied voltage and V_{bi} is the built-in voltage. At lower voltages than $\sim$5 V, the data are on the straight line which has the slope of -1/2, but at higher voltages the slope varies and appears to approach to -1/2 again. At -18 V the width of the depletion region is calculated to be $\sim$1.3 μm. The donor concentration variation in the 1.3 μm thickness of undoped n-type $In_{0.53}Ga_{0.47}As$ might be due to the growth behavior of the alloy in the temperature lowering growth method, or to the compensation of donors near the interface by the Zn-dopant in the p-layer.

The capacitance of the diode with a diameter of 200 μm is 3.45 pF at -18 V.

11-3-2. Photoresponse

Relative intensity of short-circuit current as a function of wavelength (being called here as photoresponse) is shown in Fig. 11-7. The light beam is incident on the InP surface. The intensity is normalized by the peak at around 1.65 μm. The intensity at 1.3 μm is 75% and at 1.55 μm is 96% of the peak intensity. The curve is very similar to that reported by T. P. Pearsall[9].

The photoresponse is calculated with the absorption coefficient, minority carrier diffusion lengths, and thicknesses of n, p, and depletion layers, using Terman's equation[14] and taking the generation of carriers in the depletion layer into account. A wavelength dependence of the absorption coefficient for undoped

$In_{0.53}Ga_{0.47}As$ is shown in Fig. 11-8. This is measured and calculated with the same way as described in Chapter VI. The minority carrier diffusion lengths, L_n and L_p, are measured using the EBIC as described in Chapter X.

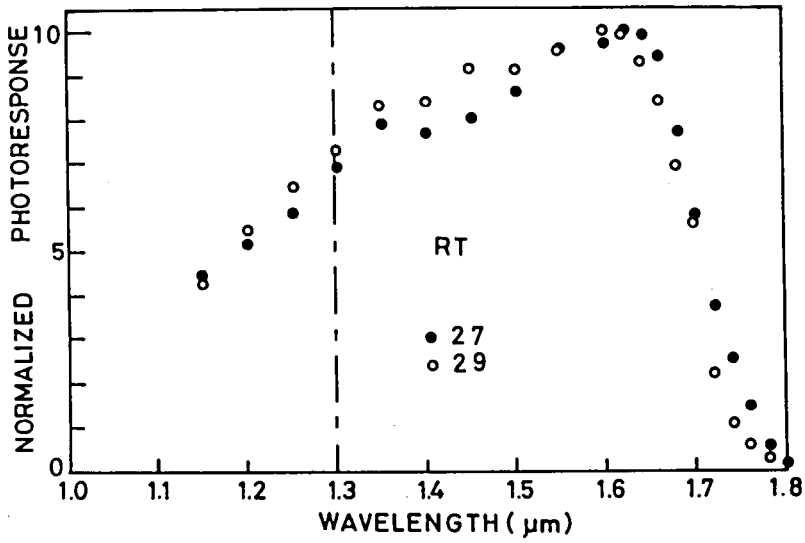

Fig. 11-7 Photoresponse of $In_{0.53}Ga_{0.47}As$ homojunction diodes on InP.

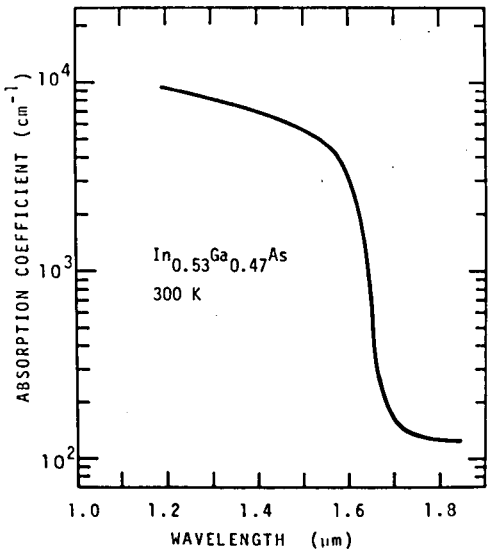

Fig. 11-8 Wavelength dependence of the absorption coefficient of undoped $In_{0.53}Ga_{0.47}As$.

A calculated result is compared with the experimental data in Fig. 11-9. The thickness of the n-layer (D_n), p-layer (D_p) and depletion layer (D), and the diffusion lengths of electron and hole are indicated in the figure. It is seen that they fit fairly well with each other. At the shorter wavelength, the discrepancy is larger. In this wavelength region the measured signals of the photoresponse and the light transmission (for the measurement of the absorption coefficient as described in Chapter VI) become small, because of the strong absorption of the incident light by the alloy layer. The discrepancy would be caused by the errors in the measurements of the photoresponse and the absorption coefficient.

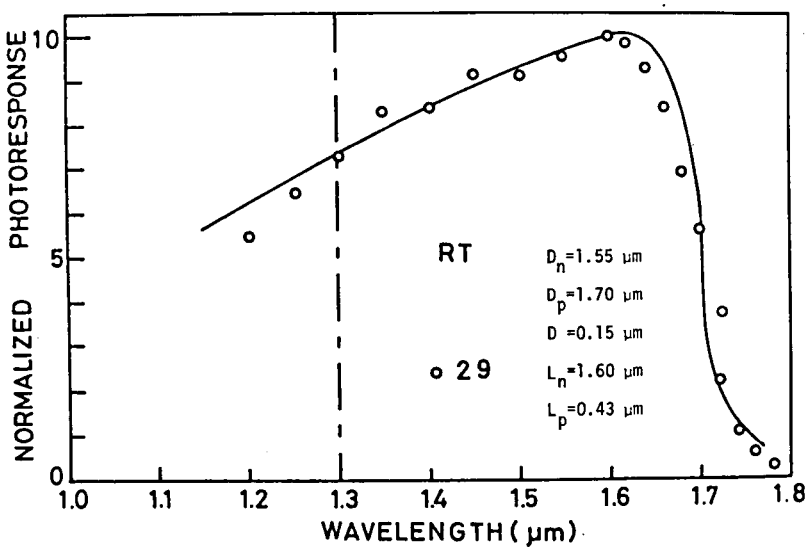

Fig. 11-9 A calculated curve is compared with the experimental data.

The photoresponse of the $In_{0.53}Ga_{0.47}As$ and Ge[7] photodiodes are shown in Fig. 11-10. It is clear that the $In_{0.53}Ga_{0.47}As$ photodiode is better suited to the 1.55 μm wavelength detection than Ge photodiode. At 1.55 μm, the absorption coefficient of Ge is $\sim 3\times10^2$ cm^{-1}[15] and that of $In_{0.53}Ga_{0.47}As$ is $\sim 5\times10^3$ cm^{-1}. A smaller

absorption coefficient results in a wider region of the photo-carrier generation in semiconductor. A wide absorption region causes a slow response of the diode due to the long transit-time of the generated carrier.

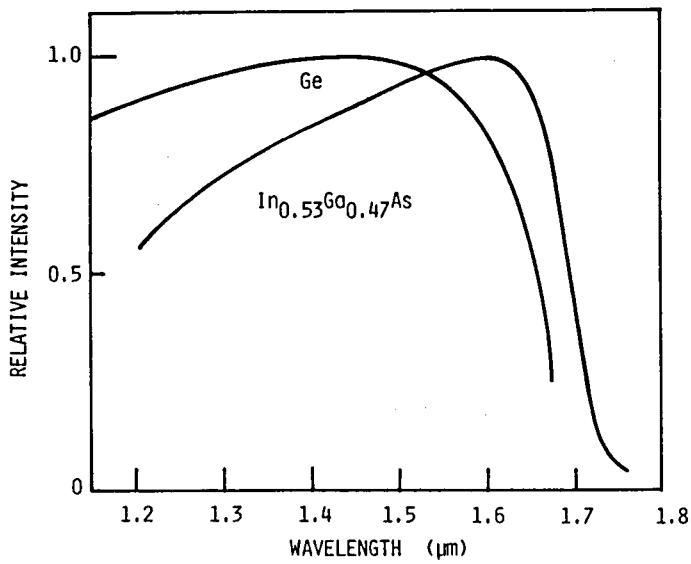

Fig. 11-10 Photoresponse of $In_{0.53}Ga_{0.47}As$ and Ge diodes. Both are normalized at peak intensities. The Ge diode has a high response only in a direct transition region($\lambda \lesssim 1.55\ \mu m$).

11-3-3. I - V Characteristics

A high crystal quality and high device technology are necessary for the fabrication of the APD's, since leakage current as low as possible and a sharp and uniform breakdown characteristics at a deep reverse bias are essential to the operation of the APD.

With the InP substrate which has a high etch pit density (EPD) ($>5\times10^5\ cm^{-2}$) it was impossible to increase the breakdown voltage above $\sim$10 V. Low EPD portion ($<1\times10^4\ cm^{-2}$) was found out

by etching the whole polished substrate with the A-B solution[16] at 60∿70°C for 10 min. An I - V curve of the mesa-diode on the low EPD substrate is shown in Fig. 11-11. The breakdown voltage is increased and the avalanche multiplication is observed in this diode as described in the next sub-section. However, the breakdown characteristic is too "soft" to obtain a large multiplication. Further improvement of the crystal quality and fabrication technology is required for the APD operation.

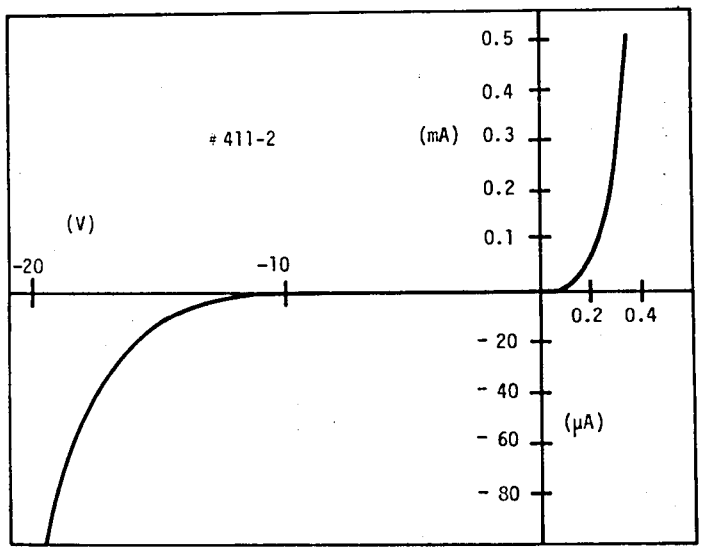

Fig. 11-11 I-V curve of a mesa-diode on the InP substrate with a low EPD.

11-3-4. Avalanche Multiplication

A multiplication *vs.* reverse voltage is shown in Fig. 11-12. Multiplication as large as 1.8 is obtained at -20 V in the diode which has the I - V curve shown in Fig. 11-11. At a higher reverse voltage, the shot noise increases so large as to disturb the measurement.

In the Si-APD and Ge-APD the multiplication of about 500[17] and 100[17] are commonly obtained at lower frequencies, respectively. In the Si-APD, the device characteristics have been shown to be degraded by the microplasmas which are induced from the dislocations in the active area[18], and thus the defect-free Si is commonly used as the substrate. Moreover, it is a conventional technique in Si- and Ge-APD to form the "guard ring" surrounding the active area in order to obtain uniform avalanche characteristics[19].

Both the reduction in EPD and the guard ring formation are required for a stable, low-noise and high-gain operation of the $In_{0.53}Ga_{0.47}As$-APD. Since InP is used as a "window layer" (which has a larger energy gap than the active layer and transparent to the incident light) for the $In_{0.53}Ga_{0.47}As$ active layer, the surface-recombination of the photo-generated carriers can be eliminated by the hetero-interface. The recombination at the lattice-matched interface is expected to be much lower compared with that at the

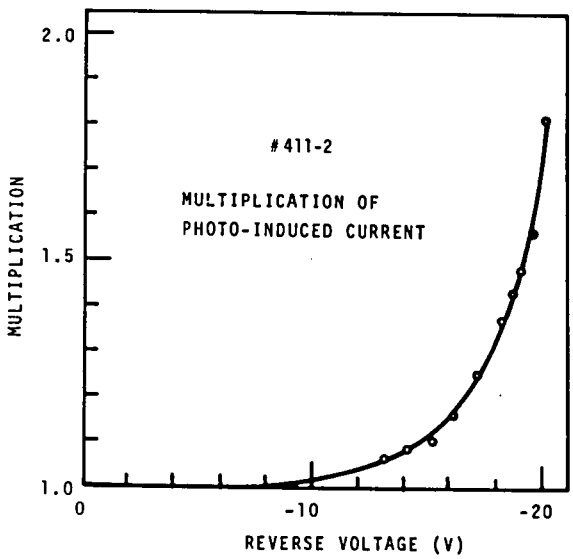

Fig. 11-12 Multiplication *vs.* reverse voltage observed in the diode shown in Fig. 11-11.

free surface of the $In_{0.53}Ga_{0.47}As$ layer.

The improvement of the $In_{0.53}Ga_{0.47}As$-APD is being vigorously made, since this detector is thought as a clue to the success of the extremely long distance (>100 km) transmission system with no repeater.

11-4. SUMMARY

1) Photodetectors and APD's have been fabricated with $In_{0.53}Ga_{0.47}As$ on InP which covers the wavelength region from 1.0 to 1.65 μm.

2) From the C - V characteristics it has been found that an abrupt junction is formed and that the built-in potential is 0.6 eV, that a slight variation of donor concentration is there in the undoped $In_{0.53}Ga_{0.47}As$ layer.

3) The photoresponse has a peak at around 1.65 μm and the diode has been found to be suited to the detector at 1.55 μm wavelength.

4) The breakdown characteristic is improved by use of low EPD InP as the substrate.

5) A multiplication of photo-current as large as 1.8 has been obtained in the $In_{0.53}Ga_{0.47}As$ - APD.

References

[1] For example, Y. Suematsu and K. Iga, *Introduction to Optical Fiber Communication* (Ohm-sha, Tokyo, 1976) (in Japanese)

[2] K. Noda (editor), *Optical Fiber Transmission* (IECE Japan, Tokyo, 1978) (in Japanese)

[3] M. Horiguchi and H. Osanai, Electron. Lett., 12, 310 (1976)

[4] D. N. Payne and W. A. Gambling, Electron. Lett., 11, 176 (1975)

[5] K. Oe, S. Ando, and K. Sugiyama, Japan. J. Appl. Phys., 16, 1273 (1977)

[6] T. Yamamoto, K. Sakai, and S. Akiba, Japan. J. Appl. Phys., 16, 1699 (1977)
S. Akiba, K. Sakai, and T. Yamamoto, Rept. Tech. Group Opto- and Quantum Electron., OQE78-112 (1978-12), IECE Japan (in Japanese)

[7] H. Melchior and W. T. Lynch, IEEE Trans. Electron Devices, ED-13, 829 (1966)

[8] For a recent development, M. Ito, T. Kaneda, H. Kanbe, and T. Mikawa, Rept. Tech. Group Electron Devices, ED78-65 (1978-10), IECE Japan (in Japanese) (1978)

[9] T. P. Pearsall and D. W. Hopson, J. Electron. Mater., 7, 133
K. J. Backman and J. L. Shag, Appl. Phys. Lett., 32, 446 (1978)
Y. Takeda and A. Sasaki, 1978 Nat. Conv. Rec., IECE Japan, S3-4, Tokyo, March 1978 (in Japanese)

[10] C. E. Hurwitz and J. J. Hsieh, Appl. Phys. Lett., 32, 487 (1978)

[11] S. J. Anderson, F. Scholl, and J. S. Harris, in *Gallium Arsenide and Related Compounds*, 1976 Conf. Series 33b (Institute of Physics, London, 1977) p. 346

[12] L. R. Tomasetta, H. D. Law, and K. Nakano, Laser Focus, December, 42 (1978)

[13] T. Miya, Y. Terunuma, T. Hosaka, and T. Miyashita, Electron. Lett., 15, 106 (1979)

[14] L. M. Terman, Solid-State Electron., 2, 1 (1961)

[15] W. C. Dash and R. Newman, Phys. Rev., 99, 1151(1955)

[16] M. S. Abrahams and C. J. Buiocchi, J. Appl. Phys., 36, 2855 (1965)

[17] P. P. Webb, R. J. McIntyre, and J. Conradi, RCA Rev., 35, 234 (1974)
For a recent review of APD in general, G. E. Stillman and C. M. Wolfe, "Avalanche Photodiodes," in *Semiconductors and Semimetals* edited by R. K. Willardson and A. C. Beer (Academic Press, New York, 1977) Vol. 12, Chap. 5

[18] K. V. Ravi, C. J. Varker, and C. F. Volk, J. Electrochem. Soc., 120, 533 (1973)

[19] L. K. Anderson, P. G. McMullin, L. A. D'Asaro, and A. Goetzberger, Appl. Phys. Lett., 6, 62 (1965)

XII. CONCLUSIONS

When we started the study on $In_{1-x}Ga_xAs$ on InP substrate, it had been uncertain that a ternary alloy can be obtained by hetero-epitaxy on a substrate which is not the constituent binary compound of the alloy, and it had been a conventional technique to grow alloys on the constituent binary-compound substrate by step-wise or continuous composition grading to obtain the alloy of a desired composition. However, in this study, it has been confirmed that such hetero-epitaxy is possible and demonstrated that a very high quality alloy is obtained at the lattice-matching composition. By eliminating the problems due to the lattice mismatch, the essential properties of the ternary alloy have been revealed and the alloy has become possible to be applied to devices.

In this thesis, liquid phase epitaxial growth of $In_{1-x}Ga_xAs$ on (111)B-oriented InP has been carried out, and optimum growth conditions have been shown to yield high quality alloys. Many characterizations have been conducted on the grown alloys and among them the electrical properties have been extensively investigated both experimentally and theoretically. High-field transport properties and p-n junction characteristics of $In_{0.53}Ga_{0.47}As$ have shown that this alloy has superior potential in the high-frequency field-effect transistors (FET's) and high switching speed devices, and in the infrared photodetectors and avalanche photodiodes (APD's).

In Chapter II, the LPE-growth system used in the experiments, careful procedures for the material preparation, the temperature cycle for the pre-baking and growth, and the phase diagram calculation based on Wu and Pearson's model have been described.

In Chapter III, it has been shown that the InP substrate surface is thermally etched during the saturation period by the

evaporation of phosphorus and that the surface morphology of the grown layer is affected both by the lattice mismatch and the roughness of the thermally etched substrate surface. The thickness of the grown layer increases with growth temperature except at 750°C, following qualitatively the temperature dependence of the As fraction in the melt. The x-ray transmission Laue pattern has shown clear evidence of the epitaxy of the alloy layer and has shown lattice distortion in a mismatched layer. The etch pit density (EPD) increases with lattice mismatch (when $x < 0.47$) and the lower limit is about 1×10^{5} cm^{-2}. The composition of the alloy has been evaluated by x-ray diffraction at high reflection angles using the InP reflection as an internal standard. The composition and crystal quality have been shown to be very homogeneous and uniform along the growth direction and over the surface. The same quality layers have been obtained at temperatures between 620° and 700°C by etching back the substrate surface with pure In just prior to growth and by matching the lattice parameter closely.

In Chapter IV, the effects of the incomplete removal of melt on the characterization of the grown layer have been revealed experimentally, taking the growth of $In_{1-x}Ga_xAs$ as an example. The remaining melt deposits the quasi-grown layer whose characteristics are much different from those of the actual layer which was intended. The quasi-grown layer has been shown to have a rough surface, lower PL intensity, and larger spectral width. In the quasi-grown layer, the composition varies along the growth direction and the EPD is high. Growth of the quasi-grown layer has been avoided by the complete removal of melt with a well-designed boat structure.

In Chapter V, $In_{1-x}Ga_xAs$($0.3\leqq x\leqq 0.65$) has been directly grown on InP and on InP with an $In_{0.53}Ga_{0.47}As$ buffer layer. In the direct growth, it has been found (1) that the composition is latched to $x=0.445\pm0.005$ with a small cooling rate and a small step-cooling interval, and (2) that the layer of composition between 0.45

and 0.50 deposits uniformly, (3) that the island growth is obtained at $x < 0.39$ and $x > 0.55$. In the growth with the buffer layer, the latching phenomenon has not been observed and a wide range of composition from 0.40 to 0.70 has been obtained. The step-wise composition grading has been shown to improve the crystal quality of the layer with $x \neq 0.47$.

In Chapter VI, with the high quality $In_{0.53}Ga_{0.47}As$ layer, the energy gap has been determined to be 0.75 eV from the photon-energy dependence of the absorption coefficient. The value has been shown to be consistent with the result in photoluminescence (PL) measurements. The infrared transmission spectrum of $In_{0.53}Ga_{0.47}As$ changes steeply near the absorption edge, indicating good crystal quality and composition homogeneity of the alloy. The intrinsic carrier concentration has been calculated to be 6.4×10^{11} cm^{-3} at room temperature.

In Chapter VII, the drift and the Hall mobility and the Hall factors of ternary alloys have been theoretically calculated by the iterative method taking the polar-optical phonon, acoustic phonon, piezoelectric, ionized impurity, and/or alloy scattering into account. Simplifying assumption such as the summation of the inverse μ limited by each scattering, the relaxation-time approximation, and the parabolic band approximation have not been used in the calculation. The Hall factors have been found to become smaller with increasing, but moderate, ionized impurity concentration. The difference between the drift and the Hall mobility cannot be neglected in a pure material. The temperature dependence of the Hall mobility and the Hall factors of n-$In_{0.53}Ga_{0.47}As$ has been shown. The donor concentration dependence of the Hall mobility of n-$In_{0.53}Ga_{0.47}As$ at 300 and 77 K has been calculated and compared with the experimental data.

In Chapter VIII, the Hall mobility of n-$In_{0.53}Ga_{0.47}As$ has been investigated experimentally. High mobility values (> 8 000

$cm^2/Vsec$) have been obtained in n-$In_{0.53}Ga_{0.47}As$ grown at 650° ∿ 750°C. The electron mobility increases on cooling from 300 to 77 K in all samples, and this is the essential property of high quality $In_{1-x}Ga_xAs$. The lattice-temperature dependence of the mobility has been found to be weaker than that of GaAs. Scattering mechanisms in $In_{0.53}Ga_{0.47}As$ have been discussed with relation to growth temperature, and it has been suggested that still better crystal can be obtained by the purification of melt materials.

In Chapter IX, a high electric field has been applied to the $In_{0.53}Ga_{0.47}As$ planar devices fabricated from the uniform and high quality crystals. The velocity - field ($v - E$) curve has been derived for n-$In_{0.53}Ga_{0.47}As$ below threshold, and agrees fairly well with that calculated by the Monte Carlo method. The transferred-electron oscillation has been observed beyond threshold and the impact ionization has been found to follow it. A model calculation of $In_{0.53}Ga_{0.47}As$ - MESFET (metal-semiconductor field-effect transistor) based on the experimentally determined parameters has shown superior characteristics to those of GaAs - MESFET.

In Chapter X, Zn-doped p-type $In_{0.53}Ga_{0.47}As$ has been grown. Zn has been found to be a useful dopant as an acceptor and found that the hole concentration is proportional to $(n_{Zn}^{\ell})^{\frac{1}{2}}$, where n_{Zn}^{ℓ} is the atomic fraction of Zn in the melt. The electrical properties have been found to be very similar to those of Zn-doped p-type GaAs and $In_{0.15}Ga_{0.85}As$. The photon energy at peak intensity and half width of the PL spectra vary with the hole concentration in the same manner as in GaAs, but the dependence is weaker. An $In_{0.53}Ga_{0.47}As$ homojunction has been formed on InP utilizing the Zn-doping. Minority carrier diffusion lengths have been derived using the EBIC (electron beam induced current) in the diode.

Finally, in Chapter XI, photodetectors and APD's have been fabricated with $In_{0.53}Ga_{0.47}As$ which covers the wavelength region from 1.0 to 1.65 μm. The photoresponse has a peak at around 1.65

μm and the diode is considered to be best suited to 1.55 μm wavelength detector. The capacitance - voltage (C - V) characteristics indicate that the junction is an abrupt one and that there is a slight variation of impurity concentration in the n-type region. The breakdown characteristics have been improved by use of the low EPD InP substrate and a multiplication of photo-current as large as 1.8 has been obtained in the $In_{0.53}Ga_{0.47}As$-APD.

Suggestions for further study are summarized as follows. It is a natural extension of this study to fabricate FET's, switching devices, and APD's. For these applications, investigation has to be extended to solve further probelms. For FET's and switching devices, the $v - E$ characteristics over a wider range of electric field and their carrier concentration and temperature dependence should be investigated. Good Schottky and ohmic contacts are necessary. The MOS structure should be studied. For APD's, the stable and high avalanche gain is required, and the crystal quality and the device structure should be simultaneously improved. $In_{0.53}Ga_{0.47}As$ with low carrier concentration (*e.g.*, $<10^{12}$ cm^{-3}) and well-controlled impurity diffusion are essential to designing the optimum device structure. Other material parameters such as the impact-ionization coefficients for electron and hole, life time of minority carrier are remained unknown. The reliability of the device is also unknown at a very high electric field.

In the crystal growth, uniform and homogeneous layers of the alloy on a larger area (as large as possible) of the substrate are desired for practical use in industry. Precise control of the layer thickness and its reproducibility are also desired. Semi-insulating and high purity layers are needed for many device applications. Growth on other crystal surfaces, *e.g.*, (100) and growth by vapor phase epitaxy are interesting.

It is possible that the electron mobility of $In_{1-x}Ga_xAs$ may increase still further. The utmost limit of the mobility both at room temperature and at lower temperatures will give a clear answer to the origin and nature of the "alloy scattering".

ADDENDUM

I. LIST OF PUBLICATION

1) "Electron Mobility and Energy Gap of $In_{0.53}Ga_{0.47}As$ on InP Substrate,"
Y. Takeda, A. Sasaki, Y. Imamura, and T. Takagi,
J. Appl. Phys., 47, 5405 (1976)

2) "Liquid Phase Epitaxial Growth, Electron Mobility, and Maximum Drift Velocity of $In_{1-x}Ga_xAs$($x \simeq 0.5$) for Microwave Devices,"
A. Sasaki, Y. Takeda, N. Shikagawa, and T. Takagi,
Proc. 8th Conf. (1976 International) on Solid State Devices, Tokyo, 1976; Japan. J. Appl. Phys., 16 (1977) Suppl. 16-1, p.239

3) "Properties of Liquid Phase Epitaxial $In_{1-x}Ga_xAs$($x \simeq 0.5$) on InP Substrate,"
Y. Takeda, A. Sasaki, Y. Imamura, and T. Takagi,
J. Electrochem. Soc., 125, 130 (1978)

4) "Composition Latching Phenomenon and Lattice Mismatch Effects in LPE-Grown $In_{1-x}Ga_xAs$ on InP Substrate,"
Y. Takeda and A. Sasaki,
Proc. 4th International Conf. on Vapour Growth and Epitaxy, Nagoya, 1978; J. Cryst. Growth, 45, 257 (1978)

5) "Quasi-Grown Layers in Liquid Phase Epitaxial Growth,"
Y. Takeda, Y. Imamura, and A. Sasaki,
J. Cryst. Growth, 46, 75 (1979)

6) "Hall Mobility and Hall Factor of $In_{0.53}Ga_{0.47}As$,"
Y. Takeda and A. Sasaki,
(submitted to Japan. J. Appl. Phys.)

7) "Properties of Zn-Doped p-Type $In_{0.53}Ga_{0.47}As$ on InP Substrate,"
Y. Takeda, M. Kuzuhara, and A. Sasaki,
(submitted to Japan. J. Appl. Phys.)

8) "Transferred-Electron Oscillation in n-$In_{0.53}Ga_{0.47}As$,"
Y. Takeda, N. Shikagawa, and A. Sasaki,
(submitted to Solid-State Electron.)

II. LIST OF LECTURES

A. International Conference

1) "Liquid Phase Epitaxial Growth, Electron Mobility, and Maximum Drift Velocity of $In_{1-x}Ga_xAs$($x \simeq 0.5$) for Microwave Devices,"
A. Sasaki, Y. Takeda, N. Shikagawa, and T. Takagi,
8th Conf. (1976 International) on Solid State Devices, Tokyo, September, 1976, A-4-4 (This has been published as 2) in List of Publication.)

2) "Composition Latching Phenomenon and Lattice Mismatch Effects in LPE-Grown $In_{1-x}Ga_xAs$ on InP Substrate,"
Y. Takeda and A. Sasaki,
4th. International Conf. on Vapour Growth and Epitaxy, Nagoya, July, 1978, 12A-p3 (This has been published as 4) in List of Publication.)

B. IECE Japan*)

1) "Electron Velocity-Field Characteristics of $In_{1-x}Ga_xAs(x\simeq0.5)$,"
A. Sasaki, N. Shikagawa, Y. Takeda, and T. Takagi,
Trans. 1976 Joint Conv. of Elect. Insts. of Kansai Section, Osaka, November, 1976, G8-18

2) "Electron Mobility and High-Field Properties of $In_{1-x}Ga_xAs$ ($x\simeq0.5$) for Microwave Devices,"
Y. Takeda, N. Shikagawa, A. Sasaki, and T. Takagi,
Rept. Tech. Group Electron Devices, ED76-65 (1976-11)

---

* The Institute of Electronics and Communication Engineers of Japan

3) "Fundamental Study on p^+-n InGaAs Photodiodes on InP,"
Y. Takeda and A. Sasaki,
1978 Nat. Conv. Rec., Tokyo, April, 1978, S3-4

4) "Fabrication and Characteristics of InGaAs Long Wavelength Photodiode on InP,"
Y. Takeda and A. Sasaki,
Rept. Tech. Group Electron Devices, ED78-63 (1978-10)

5) "$In_{0.53}Ga_{0.47}As$ Avalanche Photodiode on (111)B-InP,"
Y. Takeda and A. Sasaki,
1979 Nat. Conv. Rec., Tokyo, April, 1979, S3-19

C. Japan. Soc. Appl. Phys.

1) "Liquid Phase Epitaxial Growth of $In_{1-x}Ga_xAs$ on InP substrate,"
Y. Takeda, A. Sasaki, T. Takagi, and Y. Imamura,
Chiba Univ., April, 1975, 2a-E-9

2) "Liquid Phase Epitaxial Growth of $In_{1-x}Ga_xAs$ on InP Substrate - Electrical Properties of Layers on Cr-Doped InP,"
A. Sasaki, Y. Takeda, Y. Imamura, and T. Takagi,
Fukuoka Univ., November, 1975, 22p-K-10

3) "Liquid Phase Epitaxial Growth of $In_{1-x}Ga_xAs$ on InP Substrate - Characteristics of Layers on Undoped InP,"
Y. Takeda, Y. Imamura, A. Sasaki, and T. Takagi,
Fukuoka Univ., November, 1975, 22p-K-11

4) "Electron Mobility of $In_{0.54}Ga_{0.46}As$,"
Y. Takeda, Y. Imamura, A. Sasaki, and T. Takagi,
Waseda Univ., March, 1976, 28a-H-6

5) "Liquid Phase Epitaxial Growth of $In_{1-x}Ga_xAs$ on InP Substrate - Substrate Materials and Lattice Mismatch,"
A. Sasaki, Y. Takeda, Y. Imamura, and T. Takagi,
Waseda Univ., March, 1976, 28a-H-7

6) "Energy Gap of $In_{0.53}Ga_{0.47}As$,"
Y. Takeda, Y. Imamura, A. Sasaki, and T. Takagi,
Tohoku Univ., October, 1976, 1p-T-12

7) "Measurement of Electron Temperature in Semiconductors by Photoluminescence Spectrum,"
A. Sasaki, Y. Takeda, N. Shikagawa, and T. Takagi,
Tohoku Univ., October, 1976, 3a-V-8

8) "Drift and Hall Mobility of Ternary Semiconductor Alloys,"
Y. Takeda, A. Sasaki, and T. Takagi,
Keio Univ., March, 1977, 29a-Q-6

9) "Composition Latching Phenomenon in LPE-$In_{1-x}Ga_xAs$ on InP Substrate,"
Y. Takeda and A. Sasaki,
Okayama Univ., October, 1977, 14a-S-8

10) "$In_{1-x}Ga_xAs$ on InP Substrate,"
Y. Takeda and A. Sasaki,
Symp. on Fundamental Problems of Long Wavelength Semiconductor Optical Source, p. 19
Nagaya Univ., November, 1977

11) "Growth and Properties of Zn-Doped p-Type $In_{0.53}Ga_{0.47}As$,"
Y. Takeda and A. Sasaki,
Musashino Inst. Tech., March, 1978, 28a-K-6

12) "Precise Composition Control and Multi-layered Structure of InGaAs on InP Substrate,"
Y. Takeda and A. Sasaki,
Kinki Univ., November, 1978, 5p-L-5

13) "Electron and Hole Diffusion Length and Photoresponse of InGaAs p-n Junction on InP,"
Y. Takeda and A. Sasaki,
Kinki Univ., November, 1978, 5a-Z-4

14) "Variation of EPD Caused by Lattice Mismatch in InGaAs on InP,"
Y. Takeda, K. Noda, and A. Sasaki,
Gakushuin Univ., March, 1979, 29a-H-6

D. Japan. Asso. Cryst. Growth

1) "Properties of $In_{1-x}Ga_xAs$ Layers on InP Substrate,"
Y. Takeda, Y. Imamura, A. Sasaki, and T. Takagi,
NCCG-7*), Nagoya, November, 1975, 14pA6
J. Japan. Asso. Cryst. Growth, 2, 60 (1975) (in Japanese)

2) "Electrical Properties along Growth Direction of $In_{1-x}Ga_xAs$ Layers on InP Substrate,"
A. Sasaki, Y. Imamura, Y. Takeda, and T. Takagi,
NCCG-7, Nagoya, November, 1975, 14pA7
J. Japan. Asso. Cryst. Growth, 2, 61 (1975) (in Japanese)

3) "Growth Temperature Dependence of Crytal Quality of $In_{1-x}Ga_xAs$ Alloy on InP Substrate,"
Y. Takeda, A. Sasaki, Y. Imamura, and T. Takagi,
NCCG-8, Sendai, July, 1976, 12aB3
J. Japan. Asso. Cryst. Growth, 3, 32 (1976) (in Japanese)

4) "Quasi-Grown Layers in Liquid Phase Epitaxy,"
A. Sasaki, Y. Takeda, Y. Imamura, and T. Takagi,
NCCG-8, Sendai, July, 1976, 12aB5
J. Japan. Asso. Cryst. Growth, 3, 34 (1976) (in Japanese)

5) "LPE-Growth of $In_{1-x}Ga_xAs$ ($x > 0.47$) on InP Substrate,"
Y. Takeda and A. Sasaki,
NCCG-9, Tokyo, August, 1977, 29pA10
J. Japan. Asso. Cryst. Growth, 4, 18 (1977) (in Japanese)

6) "Selective LPE-Growth of InGaAs on InP,"
Y. Takeda and A. Sasaki,

---

* The 7th National Conference on Crystal Growth

NCCG-10, Kyoto, November, 1978, 21aA2

J. Japan. Asso. Cryst. Growth, 5, 2 (1978) (in Japanese)